

THESIS

2 (1979)



This is to certify that the

dissertation entitled

HEAVY QUARK PRODUCTION IN PERIURBATIVE QCD AT HERA

presented by

Xiaoning Wang

has been accepted towards fulfillment of the requirements for

Ph.D. degree in Physics

Wu-Ki Tung

Major professor

Date August 6, 1998

Jest in an ablance of the same

PLACE IN RETURN BOX to remove this checkout from your record.

TO AVOID FINES return on or before date due.

MAY BE RECALLED with earlier due date if requested.

DATE DUE	DATE DUE	DATE DUE

1/98 c/CIRC/DateDue.p85-p.14

HEAVY QUARK PRODUCTION IN PERTURBATIVE QCD AT HERA

By

Xiaoning Wang

A DISSERTATION

Submitted to
Michigan State University
in partial fulfillment of the requirements
for the degree of

DOCTOR OF PHILOSOPHY

Department of Physics and Astronomy

1998

ABSTRACT

HEAVY QUARK PRODUCTION IN PERTURBATIVE QCD AT HERA

By

Xiaoning Wang

Heavy quark (charm quark, bottom quark) production in deep inelastic scattering (DIS) has becomes an increasingly important area of research as new data from high energy collider experiments are available.

The conventional perturbative Quantum Chromodynamics (PQCD) calculation methods are not general enough to cover heavy quark production at all energies, because this is a "two-large-scale problem". Existing results tend to have a large QCD scale dependence and the predictions do not agree with data well in some cases.

A unified PQCD formalism that is valid for all energy range was defined. This unified scheme is often refered as the ACOT scheme, which is actually a composite of two simple renormalization schemes. For charm quark DIS production, the two simple schemes are the 3-flavor scheme and the 4-flavor scheme. The 3-flavor scheme is exactly the same as the conventional PQCD approach and applies in the quark mass threshold region. The 4-flavor scheme treats the heavy quark as an additional parton flavor inside the proton and includes new partonic scattering processes which essentially resums the large logarithmic terms $\ln \frac{Q^2}{m^2}$. This scheme applies at higher energy scales. In both schemes, charm mass is kept in the calculation. At the intermediate energy scale region, a set of matching conditions are defined to provide the transition between the two different renormalization schemes.

We implement the ACOT scheme calculation for charm productions in DIS. In this implementation, we calculate both the 3-flavor contributions and the 4-flavor contributions up to $O(\alpha_s)$. Our implementation uses the Monte Carlo method to perform the phase space integrations. Results for inclusive structure functions and differential distribution functions of charm DIS production at HERA are presented. Our results show that the ACOT scheme calculation is well behaved in the perturbative expansion and the predictions agree with experiment very well.

For My Family.

ACKNOWLEDGMENTS

First and foremost I would like to express my deepest gratitude to my thesis advisor, Wu-Ki Tung, for his constant supports and tireless guidance throughout my research. Without his inspiration and insights, I would never have finished anything nor learned so much.

I owe great thanks to Jim Amundson and Carl Schmidt, both of whom participated in this project. Without their helps in theory and programming, this work would not have been possible.

I am also very grateful to the members of my Thesis Committee: Jon Pumplin, for his time and effort in proofreading my draft and correcting my English; Harry Weerts, Tim Beers and Scott Pratt for their patient and careful evaluation of the manuscript.

I thank C.-P. Yuan and Hung-Liang Lai for many fruitful discussions in both physics and other common interests.

I also thank my colleagues in the Physics Department: Chris Glosser for correcting my English in my first draft; Tom Rockwell, Csaba Balasz, Mike Wiest, Hongjian He, Ming Lei and Jian Huang for many stimulating conversations that make these years enjoyable.

I must thank my parents for their encouragement and help over the years. Without their support, I would not be where I am today. Last, but not at all least, I express my heartfelt thanks to Ming, the love of my life. For without her support, not only would this dissertation be still incomplete, I would be incomplete as well.

Contents

L	ST (OF TABLES	viii
L	ST (OF FIGURES	ix
1	Inti	roduction to the Standard Model	1
	1.1	Strong Interaction	2
	1.2	Electroweak Interaction	4
	1.3	Higgs Sector and Spontaneous Symmetry Breaking	7
	1.4	Yukawa Interaction and the CKM Matrix	10
	1.5	Gauge Interactions	12
	1.6	Problems with the Standard Model	13
2	Dec don	ep Inelastic Scattering, QCD Parton Model and Asymptotic Freed	- 15
	2.1	Deep Inelastic Scattering	16
	2.2	The Naive Parton Model	21
	2.3	QCD and Hadron Physics	26
	2.4	Factorization and the QCD Improved Parton Model	3 0
	2.5	Other Hadronic Interactions	34
	2.6	The Global Analysis for Parton Distribution Functions	37
3	Hea	avy Quark Production Mechanisms	39
	3.1	Heavy Quark Production in Collider Physics	40
	3.2	Conventional Methods for Heavy Quark Production Calculation	46
	3.3	The Three-flavor Scheme	51
	3.4	The Four-flavor Scheme	52
	3.5	The Composite Scheme — The Unified Approach to Charm Production	56

4	Imp	plementation of the ACOT Scheme Calculation	59
	4.1	The Calculation Formalism	60
	4.2	Heavy Quark Mass Effects on the Kinematics	68
	4.3	The Next-to-Leading Order Production Mechanism	71
	4.4	Leading Order Calculations	77
	4.5	Next-to-Leading Order Calculations	78
5		ults of Inclusive and Differential Distributions of Charm Quar	k 83
	5.1	Implementation of the Calculation	84
	5.2	Inclusive Charm Structure Function	91
	5.3	Differential Distributions	95
6	Sun	nmary and Outlook	108
A		icity Amplitudes of Heavy Quark Deep Inelastic Scattering Pro tions Via Neutral Current Interactions	- 110
		$\gamma^*/Z + C \to C$	110
		$\gamma^*/Z + g \rightarrow C + \bar{C}$, HC1	
		$\gamma^*/Z + C \rightarrow C + g$, HE2	113
В	Fro	m Helicity Amplitudes to Cross Sections	117
	B.1	$\gamma^*/Z + C \rightarrow C$, HE1	120
	B.2	$\gamma^*/Z + C \rightarrow C$, HE2	121
	B.3	$\gamma^*/Z + g \rightarrow C + \overline{C}$, HC1	122
	B.4	$\gamma^*/Z + C \rightarrow C + g$, HE2	124
LI	ST (OF REFERENCES	127

THESIS

2 (1919.)



This is to certify that the

dissertation entitled

HEAVY QUARK PRODUCTION IN PERTURBATIVE QCD AT HERA

presented by

Xiaoning Wang

has been accepted towards fulfillment of the requirements for

Ph.D. degree in Physics

Wu-Ki Tung

Major professor

Date August 6, 1998

0-12771

PLACE IN RETURN BOX to remove this checkout from your record.

TO AVOID FINES return on or before date due.

MAY BE RECALLED with earlier due date if requested.

DATE DUE	DATE DUE	DATE DUE

1/98 c:/CIRC/DateDue.p65-p.14

HEAVY QUARK PRODUCTION IN PERTURBATIVE QCD AT HERA

Ву

Xiaoning Wang

A DISSERTATION

Submitted to
Michigan State University
in partial fulfillment of the requirements
for the degree of

DOCTOR OF PHILOSOPHY

Department of Physics and Astronomy

1998

ABSTRACT

HEAVY QUARK PRODUCTION IN PERTURBATIVE QCD AT HERA

By

Xiaoning Wang

Heavy quark (charm quark, bottom quark) production in deep inelastic scattering (DIS) has becomes an increasingly important area of research as new data from high energy collider experiments are available.

The conventional perturbative Quantum Chromodynamics (PQCD) calculation methods are not general enough to cover heavy quark production at all energies, because this is a "two-large-scale problem". Existing results tend to have a large QCD scale dependence and the predictions do not agree with data well in some cases.

A unified PQCD formalism that is valid for all energy range was defined. This unified scheme is often refered as the ACOT scheme, which is actually a composite of two simple renormalization schemes. For charm quark DIS production, the two simple schemes are the 3-flavor scheme and the 4-flavor scheme. The 3-flavor scheme is exactly the same as the conventional PQCD approach and applies in the quark mass threshold region. The 4-flavor scheme treats the heavy quark as an additional parton flavor inside the proton and includes new partonic scattering processes which essentially resums the large logarithmic terms $\ln \frac{Q^2}{m^2}$. This scheme applies at higher energy scales. In both schemes, charm mass is kept in the calculation. At the intermediate energy scale region, a set of matching conditions are defined to provide the transition between the two different renormalization schemes.

We implement the ACOT scheme calculation for charm productions in DIS. In this implementation, we calculate both the 3-flavor contributions and the 4-flavor contributions up to $O(\alpha_s)$. Our implementation uses the Monte Carlo method to perform the phase space integrations. Results for inclusive structure functions and differential distribution functions of charm DIS production at HERA are presented. Our results show that the ACOT scheme calculation is well behaved in the perturbative expansion and the predictions agree with experiment very well.

For My Family.

ACKNOWLEDGMENTS

First and foremost I would like to express my deepest gratitude to my thesis advisor, Wu-Ki Tung, for his constant supports and tireless guidance throughout my research. Without his inspiration and insights, I would never have finished anything nor learned so much.

I owe great thanks to Jim Amundson and Carl Schmidt, both of whom participated in this project. Without their helps in theory and programming, this work would not have been possible.

I am also very grateful to the members of my Thesis Committee: Jon Pumplin, for his time and effort in proofreading my draft and correcting my English; Harry Weerts, Tim Beers and Scott Pratt for their patient and careful evaluation of the manuscript.

I thank C.-P. Yuan and Hung-Liang Lai for many fruitful discussions in both physics and other common interests.

I also thank my colleagues in the Physics Department: Chris Glosser for correcting my English in my first draft; Tom Rockwell, Csaba Balasz, Mike Wiest, Hongjian He, Ming Lei and Jian Huang for many stimulating conversations that make these years enjoyable.

I must thank my parents for their encouragement and help over the years. Without their support, I would not be where I am today. Last, but not at all least, I express my heartfelt thanks to Ming, the love of my life. For without her support, not only would this dissertation be still incomplete, I would be incomplete as well.

Contents

L	ST (OF TABLES	viii
L	ST (OF FIGURES	ix
1	Int	roduction to the Standard Model	1
	1.1	Strong Interaction	2
	1.2	Electroweak Interaction	4
	1.3	Higgs Sector and Spontaneous Symmetry Breaking	7
	1.4	Yukawa Interaction and the CKM Matrix	10
	1.5	Gauge Interactions	12
	1.6	Problems with the Standard Model	13
2	Dec	ep Inelastic Scattering, QCD Parton Model and Asymptotic Freen	- 15
	2.1	Deep Inelastic Scattering	16
	2.2	The Naive Parton Model	21
	2.3	QCD and Hadron Physics	26
	2.4	Factorization and the QCD Improved Parton Model	3 0
	2.5	Other Hadronic Interactions	34
	2.6	The Global Analysis for Parton Distribution Functions	37
3	Hea	avy Quark Production Mechanisms	39
	3.1	Heavy Quark Production in Collider Physics	40
	3.2	Conventional Methods for Heavy Quark Production Calculation	46
	3.3	The Three-flavor Scheme	51
	3.4	The Four-flavor Scheme	52
	3.5	The Composite Scheme — The Unified Approach to Charm Production	56

4	Imp	plementation of the ACOT Scheme Calculation	59
	4.1	The Calculation Formalism	60
	4.2	Heavy Quark Mass Effects on the Kinematics	68
	4.3	The Next-to-Leading Order Production Mechanism	71
	4.4	Leading Order Calculations	77
	4.5	Next-to-Leading Order Calculations	78
5		ults of Inclusive and Differential Distributions of Charm Quar	k 83
	5.1	Implementation of the Calculation	84
	5.2	Inclusive Charm Structure Function	91
	5.3	Differential Distributions	95
6	Sun	nmary and Outlook	108
A		icity Amplitudes of Heavy Quark Deep Inelastic Scattering Pro tions Via Neutral Current Interactions	- 110
	A.1	$\gamma^*/Z + C \rightarrow C$	110
		$\gamma^*/Z + g \rightarrow C + \bar{C}$, HC1	
	A.3	$\gamma^*/Z + C \rightarrow C + g$, HE2	113
В	Fro	m Helicity Amplitudes to Cross Sections	117
	B .1	$\gamma^*/Z + C \rightarrow C$, HE1	120
	B.2	$\gamma^*/Z + C \rightarrow C$, HE2	121
	B.3	$\gamma^*/Z + g \rightarrow C + \overline{C}$, HC1	122
	B.4	$\gamma^*/Z + C \rightarrow C + g$, HE2	124
LI	ST (OF REFERENCES	127

List of Tables

1.1	Boson Masses	2
1.2	Lepton and Quark Masses	3
1.3	$SU(2)$ representation of the fermions $\ldots \ldots \ldots \ldots \ldots$	5
1.4	Quantum numbers of the fermion spectrum	5
2.1	MS renormalization parameters	28

List of Figures

1.1	Electroweak charged current and neutral current interactions	13
1.2	Gauge boson self-interactions	14
2.1	Deep inelastic scattering $l + h \rightarrow l' + X \dots \dots \dots$	17
2.2	The parton model interpretation of $e + P \rightarrow e + X$ process	23
2.3	Born level $e + q \rightarrow e + q$ scattering	24
2.4	QCD running coupling α_s with $n_f = 5$	3 0
2.5	Vector boson production $A + B \rightarrow V + X \dots \dots \dots$	34
2.6	Partonic process $q + \overline{q'} \rightarrow W^{\pm}/Z$ for vector boson production	35
2.7	Jet production	3 6
3.1	Scale dependence of the integrated b -quark p_T distribution at 630 GeV (dashed lines) and at 1800 GeV (solid lines), for different values of p_T^{min} .	42
3.2	CDF data on the integrated b -quark p_t distribution, compared to the results of NLO QCD	43
3.3	D0 data on the integrated b -quark p_T distribution, compared to the results of NLO QCD	44
3.4	Linear comparison between experimental data and theory for the integrated b -quark p_t distribution	45
3.5	Three-flavor scheme production mechanism. (a) is $\gamma^* + g \to c + \overline{c}$ process(heavy quark creation: HC), (b) is one loop $\gamma^* + g \to c + \overline{c}$ process, (c) is $\gamma^* + g \to g + c + \overline{c}$ process, (d) is $\gamma^* + a \to a + c + \overline{c}$ process. Only one diagram for each process is plotted	53
3.6	Four flavor production processes. (a) is $\gamma^* + c/\overline{c} \to c/\overline{c}$ process(heavy quark excitation: HE), (b) is one loop $\gamma^* + c/\overline{c} \to c/\overline{c}$ process, (c) is $\gamma^* + c/\overline{c} \to g + c/\overline{c}$ process. (d) is $\gamma^* + g \to c + \overline{c}$ process (heavy quark creation: HC), Only one diagram for each process is shown	54
4.1	The factorization for the deep inelastic scattering	61
4.2	The factorization of the structure functions	62
4.3	Deep inelastic scattering: vector boson and nucleon scattering	69
U	woop moreous beginning, reconstructed and mucieum beginning	v

4.4	Processes contributing to the leading ACOT scheme calculation. (a), (b), (c) only present in the 4-flavor region, (d), (e), (f), (g), (h) presents in both the 3-flavor scheme region and the 4-flavor scheme region. HC1:(d), HE1:(a), HE2:(b),(c), GF2:(e), HC2:(f),(g),(h). Only one diagram for each process is plotted	74
5.1	F_2^c for $Q^2=100$ and $m_c=1.5$ GeV from $^1(\gamma^*c\to c)+(\gamma^*c\to gc)$ processes. Solid line is this work's result. Dashed line is the calculation of Reference [69]	89
5.2	F_2^c for $x=0.1$ and $m_c=1.5$ GeV from $^1(\gamma^*c\to c)+(\gamma^*c\to gc)$ processes. Solid line is this work's result. Dashed line is the calculation of Reference [69]	90
5.3	F_2^c for $Q^2=10$ and $m_c=1.5$ GeV from $^1(\gamma^*c\to c)+(\gamma^*c\to gc)$ processes. Solid line is this work's result. Dashed line is the calculation of Reference [69]	91
5.4	F_2^c for $Q^2=10$ and $m_c=0.3$ GeV from $^1(\gamma^*c\to c)+(\gamma^*c\to gc)$ processes. Solid line is this work's result. Dashed line is the calculation of Reference [69]	92
5.5	μ -dependence of $F_2^c(x=0.01,Q=10~{\rm GeV})$ in various calculational schemes. μ_0 is defined by Equation. 5.9	99
5.6	Measured D^* cross section at Zeus [63] with experimental cuts (described in the text) compared with our calculation as a function of the pole mass m_c . The shaded band represents the $1-\sigma$ experimental errors.	100
5.7	Total F_2^c for various values of Q^2 . Solid lines: ACOT. Dashed lines: three-flavor NLO calculation of Reference [38]. Dotted lines: three-flavor LO calculation. Solid points: Zeus 95 preliminary [65]. Open points: H1 [64]	101
5.8	F_2^c at $x=0.1$, solid line: This work, dashed line: LO ACOT calculation, dotted line: LO three-flavor calculation	102
5.9	Contributions of the various subprocesses to $F_2^c(x,Q)$ at fixed $x=0.01$. The sign convention is such that the total cross section is HE1 + HC1 - HC1 _{sub} + HE2 - HE2 _{sub} + GF2	102
5.10	Contributions of the various subprocesses to $F_2^c(x,Q)$ at fixed $Q^2 = 7$ GeV. The sign convention is such that the total cross section is HE1 + HC1 - HC1 _{sub} + HE2 - HE2 _{sub} + GF2	103
5.11	p_t distribution compared with data from Zeus 95. The experimental cuts are described in the text	104
5.12	Q^2 distribution compared with data from Zeus 95. The experimental cuts are described in the text	105
5.13	W distribution compared with data from Zeus 95. The experimental cuts are described in the text.	106
5.14	η distribution compared with data from Zeus 95. The experimental cuts are described in the text.	107

A.1	$\gamma^*/Z + g \to c + \overline{c}$ in the $c\overline{c}$ center of mass frame	113
A.2	$\gamma^*/Z + c \rightarrow g + c$ in the gc center of mass frame	115

Chapter 1

Introduction to the Standard Model

The Standard Model [1, 2] is the fundamental theory behind today's high energy physics phenomenological and experimental studies. It consists of electroweak theory [3] and quantum chromodynamics (QCD) theory [4], and has been very successful in describing and predicting experimental results.

The Standard Model is a local gauge theory [5] with $SU(3)_C \times SU(2)_L \times U(1)_Y$ symmetry. Color $SU(3)_C$ symmetry is associated QCD, which describes the elementary strong color interaction. $SU(2)_L \times U(1)_Y$ is associated with electroweak theory, which describes the electromagnetic and weak interactions.

The strong and electroweak interactions are mediated by gauge bosons. Eight gluons with different color quantum numbers mediate the strong interaction, and four vector bosons, W^{\pm} , Z^0 and γ mediate the electroweak interaction. The gauge bosons and their properties are listed in Table 1.1.

Leptons and quarks are the fundamental fermonic constituents of matter. Both leptons and quarks engage in electroweak interactions through exchanges of W^{\pm} , Z and γ gauge bosons, but only quarks engage in the strong interactions as a consequence of their color-charges. There are three generations of quarks and leptons in the

Table 1.1: Boson Masses

Particle	Symbol	Mass (GeV)	Charge	Spin	Force
		_			
Photon	$oldsymbol{\gamma}$	0	0	1	Electromagnetic Force
W Boson	W^\pm	80. 33	±	1	Charged Weak Force
Z Boson	Z^0	91.187	0	1	Neutral Weak Force
Gluon	\boldsymbol{G}	0	0	1	Strong Force

Standard Model, and their masses are generated by spontaneous symmetry breaking through Yukawa interaction. The masses are listed in Table 1.2.

All the standard model particles have been discovered except the Higgs boson. The detailed properties of each particle can be found in the Particle Data Book [6].

1.1 Strong Interaction

Under SU(3) color symmetry, each quark flavor is represented by a color triplet,

$$\Psi_q = \left(egin{array}{c} q_{red} \ q_{green} \ q_{blue} \end{array}
ight),$$

and gluons are associated with $3 \times 3 - 1 = 8$ SU(3) group generators. Quarks and gluons interact with each other by exchanging gluons.

The strong interaction is described by the QCD Lagrangian:

$$L_{QCD} = -\frac{1}{4} F^{i}_{\mu\nu} F^{i\mu\nu} + \sum_{f} \overline{q}_{f\alpha} i \gamma^{\mu} D^{\alpha}_{\mu\beta} q_{f}^{\beta}, \qquad (1.1)$$

where

$$F^i_{\mu\nu} = \partial_\mu G^i_\nu - \partial_\nu G^i_\mu - g_s f_{ijk} G^j_\mu G^k_\nu \tag{1.2}$$

Table 1.2: Lepton and Quark Masses

$ u_e$	0	
\boldsymbol{e}	0.00051	First
\boldsymbol{u}	0.002 to 0.008	Generation
d	0.005 to 0.015	
$ u_{\mu}$	0	
•	0.106	Second
c	1.0 to 1.6	Generation
<i>s</i>	0.1 to 0.3	
ν_{τ}	0	
$\overset{\cdot}{oldsymbol{ au}}$	1.78	Third
t	180	Generation
b	4.1 to 4.5	
	e u d v_{μ} μ c s v_{τ} t	e 0.00051 u 0.002 to 0.008 d 0.005 to 0.015 v_{μ} 0 μ 0.106 c 1.0 to 1.6 s 0.1 to 0.3 v_{τ} 0 τ 1.78 t 180

is the field strength tensor for gluon fields G^i_{μ} , $i=1,2,\cdots,8$, and q^{α}_f is the f-th (f = 1, ..., 6) quark flavor (u,d,c,s,t,b) with color index α , $\alpha=1,2,3$.

$$D^{\alpha}_{\mu\beta} = (D_{\mu})_{\alpha\beta} = \partial_{\mu}\delta_{\alpha\beta} + ig_{s}\frac{\lambda^{i}_{\alpha\beta}}{2}G^{i}_{\mu}$$
 (1.3)

is the quark covariant derivative and g_s is QCD SU(3) running gauge coupling constant. f_{ijk} $(i,j,k=1,\cdots,8)$ are SU(3) group structure constants, and they satisfy the Lie algebra

$$[\lambda^i, \lambda^j] = 2if_{ijk}\lambda^k,$$

where $\frac{\lambda^{i}}{2}$, $i = 1, \dots, 8$, are the eight SU(3) group generators for the fundamental representation. The λ matrices are listed in Equation 1.4.

$$\lambda_{1} = \begin{pmatrix} 0 & 1 & 0 \\ 1 & 0 & 0 \\ 0 & 0 & 0 \end{pmatrix}, \quad \lambda_{2} = \begin{pmatrix} 0 & -i & 0 \\ i & 0 & 0 \\ 0 & 0 & 0 \end{pmatrix}, \quad \lambda_{3} = \begin{pmatrix} 1 & 0 & 0 \\ 0 & -1 & 0 \\ 0 & 0 & 0 \end{pmatrix}$$

$$\lambda_{4} = \begin{pmatrix} 0 & 0 & 1 \\ 0 & 0 & 0 \\ 1 & 0 & 0 \end{pmatrix}, \quad \lambda_{5} = \begin{pmatrix} 0 & 0 & -i \\ 0 & 0 & 0 \\ i & 0 & 0 \end{pmatrix}, \quad \lambda_{6} = \begin{pmatrix} 0 & 0 & 0 \\ 0 & 0 & 1 \\ 0 & 1 & 0 \end{pmatrix}$$

$$\lambda_{7} = \begin{pmatrix} 0 & 0 & 0 \\ 0 & 0 & -i \\ 0 & i & 0 \end{pmatrix}, \quad \lambda_{8} = \frac{1}{\sqrt{3}} \begin{pmatrix} 1 & 0 & 0 \\ 0 & 1 & 0 \\ 0 & 0 & -2 \end{pmatrix}.$$

$$(1.4)$$

It is easy to see from the QCD Lagrangian that the color interactions are diagonal in the flavor indices, but in general change the quark colors. There are no mass terms in Equation 1.1, as they will be generated later by spontaneous symmetry breaking.

1.2 Electroweak Interaction

 $SU(2)_L$ and $U(2)_Y$ represent weak isospin and weak hypercharge symmetries respectively. The weak hypercharge Y is specified according to the formula

$$Q=T_3+\frac{1}{2}Y$$

in electroweak theory to incorporate the electric charge Q and unify the electromagnetic force and weak force.

The SU(2) symmetry is chiral, which means the left-handed fermion field ($\psi_L = \frac{1-\gamma_5}{2}\psi$) transforms differently from the right-handed fermion field ($\psi_R = \frac{1+\gamma_5}{2}\psi$). Under SU(2) symmetry, the left-handed fermions behave as SU(2) doublets while the right-handed fermions behave as singlets. There is no right-handed neutrino in the Standard Model. The SU(2) representation of fermions are listed in Table 1.3.

Table 1.3: SU(2) representation of the fermions

quarks:	$\binom{u}{d}_L$	$\binom{c}{s}_L$,	$\binom{t}{b}_L$;	u_R ,	d_R ,	c_R ,	s_R ,	t_R ,	b_R
leptons:	$\binom{\nu_e}{e}_L$	$\begin{pmatrix} u_{\mu} \\ \mu \end{pmatrix}_{L}$	$\binom{\nu_{\tau}}{\tau}_{L};$		e_R ,		μ_R ,		$ au_R$

Table 1.4: Quantum numbers of the fermion spectrum

Chirality	Q	T	T_3	Y	C
$ u_{eL} $ $ e_L $		•	1/2 -1/2		0 0
$egin{aligned} oldsymbol{u}_L \ oldsymbol{d}_L \end{aligned}$	2/3 -1/3	•	1/2 -1/2	1/3 1/3	$egin{aligned} oldsymbol{r}, g, b \ oldsymbol{r}, g, b \end{aligned}$
e_R	-1	0	0	-2	0
u_R	2/3	0	0	4/3	r, g, b
d_R	-1/3	0	0	-2/3	r, g, b

The quantum numbers of the first generation of fermions are listed in Table 1.4, where T is the weak isospin, and T_3 is the third component of T. The other two generations of fermions have exactly the same quantum numbers as those listed in Table 1.4.

The electroweak interaction is described by Lagrangian:

$$L_{electroweak} = L_{fermion} + L_{gauge} + L_{Higgs} + L_{Yukawa} . \tag{1.5}$$

The fermion part is

$$L_{fermion} = \sum_{m=1}^{3} (\overline{q}_{mL} i \gamma^{\mu} D_{\mu} q_{mL} + \overline{l}_{mL} i \gamma^{\mu} D_{\mu} l_{mL} + \overline{q}_{mR} i \gamma^{\mu} D_{\mu} q_{mR} + \overline{l}_{mR} i \gamma^{\mu} D_{\mu} l_{mR}), \quad (1.6)$$

where m is the family index. Since the right-handed fermions do not couple to weak isospin, their covariant derivative is

$$D_{\mu}=\partial_{\mu}+i\frac{g_1}{2}YB_{\mu},$$

where g_1 is the U(1) gauge coupling constant, and B_{μ} is the U(1) gauge field. The corresponding covariant derivative for the left-handed fermions is

$$D_{\mu} = \partial_{\mu} + i \frac{g_1}{2} Y B_{\mu} + i g_2 \frac{\tau^j}{2} W_{\mu}^j,$$

where g_2 is the $SU(2)_L$ gauge coupling constant, and W^j_{μ} , j=1, ..., 3 are the $SU(2)_L$ gauge fields. τ^i are the Pauli matrices and shown in Equation 1.7.

$$\tau_1 = \begin{pmatrix} 0 & 1 \\ 1 & 0 \end{pmatrix}, \quad \tau_2 = \begin{pmatrix} 0 & -i \\ i & 0 \end{pmatrix}, \quad \tau_3 = \begin{pmatrix} 1 & 0 \\ 0 & -1 \end{pmatrix}$$
 (1.7)

The gauge Lagrangian is

$$L_{gauge} = -\frac{1}{4} F^{i}_{\mu\nu} F^{i\mu\nu} - \frac{1}{4} B_{\mu\nu} B^{\mu\nu}$$
 (1.8)

where

$$B_{\mu\nu} = \partial_{\mu}B_{\nu} - \partial_{\nu}B_{\mu}$$

$$F^i_{\mu\nu} = \partial_\mu W^i_\nu - \partial_\nu W^i_\mu - g_2 \epsilon^{ijk} W^j_\mu W^k_\nu$$

The gauge bosons will gain their masses through the spontaneous symmetry breaking mechanism. The discovery of their mass eigenstates, the W^{\pm} and Z bosons, at CERN by the UA1 [7] and UA2 [8] groups in 1983 confirmed the electroweak theory.

1.3 Higgs Sector and Spontaneous Symmetry Breaking

The Lagrangian we discussed so far only contains massless gauge bosons and fermions. Explicit mass terms in the Lagrangian are not allowed because if there were such bare mass terms, the electroweak gauge invariance would be violated. On the other hand, massless gauge bosons are not acceptable for the weak interactions since these are known to be short-ranged. Hence, to have a sensible theory of massive elementary particles and to be able to explain the short-ranged weak interactions, the gauge invariance must be broken somehow. In the Standard Model, the Higgs mechanism was introduced to account for the spontaneous symmetry breaking. The idea is that instead of the Lagrangian, it is the vacuum that does not respect gauge invariance, which induces effective masses for the propagating particles.

The Higgs Lagrangian is

$$L_{Higgs} = (D^{\mu}\phi)^{\dagger}D_{\mu}\phi - V(\phi), \tag{1.9}$$

where $\phi = \begin{pmatrix} \phi^+ \\ \phi^0 \end{pmatrix}$ is the complex Higgs scalar. The Higgs scalar field is a doublet under SU(2) and has U(1) charge $Y_{\phi} = 1$. The gauge covariant derivative is

$$D_{\mu} = \partial_{\mu} + i \frac{g_1}{2} B_{\mu} + i g_2 \frac{\tau^i}{2} W_{\mu}^i.$$

 $V(\phi)$ is the Higgs potential and takes the form of

$$V(\phi) = \mu^2 \phi^{\dagger} \phi + \lambda (\phi^{\dagger} \phi)^2, \quad \lambda > 0, \ \mu^2 < 0.$$

When $\lambda > 0$, $\mu^2 < 0$, it is easy to see that the ground state of the Higgs potential can be produced when vacuum expectation value, $<\phi^{\dagger}\phi>_0=\frac{v^2}{2}$, with $v=\sqrt{\frac{-\mu^2}{\lambda}}$. When the Higgs field approaches its classical ground state, *i.e.*, classical vacuum

state, $\phi_0 = \begin{pmatrix} 0 \\ \frac{v}{\sqrt{2}} \end{pmatrix}$, the generator L_1, L_2 and $L_3 - Y$ are spontaneously broken,

i.e. L_1 $\phi_0 \neq 0$, L_2 $\phi_0 \neq 0$, $(L_3 - Y/2)$ $\phi_0 \neq 0$. On the other hand, the electric charge $Q = L^3 + \frac{Y}{2}$ is still conserved, that is, $Q\phi_0 = (L_3 + Y/2)$ $\phi_0 = 0$. Thus after introducing the Higgs mechanism, the electroweak $SU(2)_L \times U(1)_Y$ symmetry is spontaneously broken down to $U(1)_Q$.

Using the Kibble transformation, Higgs scalar can be rewritten as

$$\phi = \begin{pmatrix} \phi^+ \\ \phi^0 \end{pmatrix} = \frac{1}{\sqrt{2}} e^{i \sum_{i=1}^3 \psi^i L^i} \begin{pmatrix} 0 \\ v+H \end{pmatrix}$$
 (1.10)

where H is a neutral Hermitian field which will eventually turn out to be the physical Higgs field. The three ψ fields are Goldstone bosons and will disappear from the physical spectrum in the unitary gauge where

$$\phi = \frac{1}{\sqrt{2}} \begin{pmatrix} 0 \\ v + H \end{pmatrix} \,, \tag{1.11}$$

but the Goldstone bosons essentially reappear as the longitudinal degree of freedom of the gauge boson after the symmetry breaking.

In the unitary gauge, the covariant kinetic energy for the scalar field becomes:

$$(D_{\mu}\phi)^{\dagger}(D^{\mu}\phi) = \frac{1}{2}(0, v + H) \left[\frac{g_{2}}{2}\tau^{i}W_{\mu}^{i} + \frac{g_{1}}{2}B_{\mu}\right]^{2} \begin{pmatrix} 0\\ v + H \end{pmatrix}$$

$$= \frac{1}{2}(0, v + H) \left[\frac{g_{2}}{2}\begin{pmatrix} W_{\mu}^{3} & \sqrt{2}W^{-}\\ \sqrt{2}W^{+} & W_{\mu}^{3} \end{pmatrix} + \frac{g_{1}}{2}B_{\mu}\right]^{2} \begin{pmatrix} 0\\ v + H \end{pmatrix}$$
(1.12)

Working out the kinetic energy term for the gauge bosons, we have

$$(D_{\mu}\phi)^{\dagger}(D^{\mu}\phi) \to (\frac{g_{2}v}{2})^{2} W_{\mu}^{+}W^{-\mu} + \frac{1}{8}v^{2}(W_{\mu}^{3}, B_{\mu}) \begin{pmatrix} g_{2}^{2} & -g_{1}g_{2} \\ -g_{1}g_{2} & g_{1}^{2} \end{pmatrix} \begin{pmatrix} W^{3\mu} \\ B^{\mu} \end{pmatrix} + H \text{ terms.}$$

$$(1.13)$$

This essentially generates the mass terms for the gauge bosons. The H terms in Equation 1.13 includes the kinetic energy terms for the Higgs boson which we will not discuss here.

In Equation 1.13, the neutral gauge boson masses are not diagonal in the basis of W^3 and the weak hypercharge B field, so a diagonalizing transformation is performed. As the results of the transformation, two new fields, Z boson and photon γ field, are defined by the mixing of W^3 and B.

$$Z = -\sin\theta_W B + \cos\theta_W W^3, \tag{1.14}$$

$$A = \cos \theta_W B + \sin \theta_W W^3, \tag{1.15}$$

where θ_W is called the weak angle and defined by $\tan \theta_W = \frac{g_1}{g_2}$. W^{\pm} is defined as

$$W^{\pm} = \frac{1}{\sqrt{2}}(W^1 \mp iW^2). \tag{1.16}$$

After the redefinition of the gauge boson fields, the kinetic energy term becomes

$$(D_{\mu}\phi)^{\dagger}(D^{\mu}\phi) \to M_W^2 W^{+\mu} W_{\mu}^- + \frac{M_Z^2}{2} Z^{\mu} Z_{\mu} + H \ terms,$$
 (1.17)

from which the masses of the W and Z bosons can be easily obtained.

The masses of the four gauge bosons are

$$M_W = \frac{g_2 v}{2} \tag{1.18}$$

$$M_Z = \frac{v}{2} \sqrt{g_1^2 + g_2^2} = \frac{M_W}{\cos \theta_W}$$
 (1.19)

$$M_{\gamma} = 0 \tag{1.20}$$

The W and Z bosons were discovered at CERN by UA1 [7] and UA2 [8] in 1983, and their masses and properties are in very good agreement with the standard model predications.

The Higgs mass is not predicted by the Standard Model because the λ parameter in Higgs potential term is unknown. Although various theoretical and experimental limits seem to suggest that 60 GeV $< M_H < O(600)$ GeV, Higgs remains the last particle in the Standard Model to be found.

1.4 Yukawa Interaction and the CKM Matrix

The fermions gain their masses through Yukawa interaction by coupling with the Higgs doublet. In the unitary gauge, the Yukawa Lagrangian is

$$-L_{Yukawa} = \sum_{m,n=1}^{3} \overline{q}_{m,L}^{0} \Gamma_{m,n}^{u} (\frac{v+H}{\sqrt{2}}) u_{n,R}^{0} + \overline{q}_{m,L}^{0} \Gamma_{m,n}^{d} (\frac{v+H}{\sqrt{2}}) d_{n,R}^{0}$$
$$+ \overline{l}_{m,L}^{0} \Gamma_{m,n}^{e} (\frac{v+H}{\sqrt{2}}) e_{n,R}^{0} + H.C.$$
(1.21)

after the spontaneous symmetry breaking. In Equation 1.21, m, n = 1, 2, 3 are the generation indices, and

$$q_{L} = \begin{pmatrix} \begin{pmatrix} u_{L} \\ d_{L} \end{pmatrix}, \begin{pmatrix} c_{L} \\ s_{L} \end{pmatrix}, \begin{pmatrix} t_{L} \\ b_{L} \end{pmatrix} \end{pmatrix},$$

$$l_{L} = \begin{pmatrix} \begin{pmatrix} \nu_{eL} \\ e_{L} \end{pmatrix}, \begin{pmatrix} \nu_{\mu L} \\ \mu_{L} \end{pmatrix}, \begin{pmatrix} \nu_{\tau L} \\ \tau_{L} \end{pmatrix} \end{pmatrix},$$

$$u_{R} = u_{R}, c_{R}, t_{R}$$

$$d_{R} = d_{R}, s_{R}, b_{R}$$

$$e_{R} = e_{R}, \mu_{R}, \tau_{R}.$$

$$(1.22)$$

In Equation 1.21 and Equation 1.22, we have used fermion weak eigenstates in the Lagrangian, and since $\Gamma_{m,n}$ is a 3 × 3 matrix and generally not diagonal, it means there are possible mixings among different families in Yukawa interaction. Alternatively, we can perform unitary transformations on the left-handed and right-handed fermion

fields separately and rewrite the Yukawa Lagrangian as

$$L_{Yukawa} = \sum_{i=1}^{3} \overline{q'}_{iL} (-m_i - \frac{gm_i}{2M_W} H) u'_{iR} + \overline{q'}_{iL} (-m_i - \frac{gm_i}{2M_W} H) d'_{iR}$$

$$+ \overline{l'}_{iL} (-m_i - \frac{gm_i}{2M_W} H) e'_{iR} + H.C.$$

$$= \sum_{i=1}^{3} \overline{\psi}_i (-m_i - \frac{gm_i}{2M_W} H) \psi_i, \qquad (1.23)$$

where ψ_i can be identified as mass eigenstates of the fermions and $m_i = \frac{v}{\sqrt{2}} f_i$ as the corresponding masses. However, since f_i is not predicated by the Standard Model, the measured fermion masses are used as parameters in the Lagrangian instead.

From Equation 1.21 and 1.23, we can see that generally the electroweak eigenstates of fermions are different from the mass eigenstates. However, this does not affect the lepton sector since the neutrinos are massless and their fields can be redefined without affecting the Lagrangian. In the quark sector, the charged quark current, taking u_L as the gauge basis and u'_L as the mass basis, is

$$J^{\mu}_{charge} = \overline{u}_L \gamma^{\mu} d_L = \overline{u}'_L \gamma^{\mu} S^{u\dagger}_L S^d_L d'_L$$

and there is a mixing between different generations of quarks. By convention, the three charge 2/3 quarks u, c and t are unmixed:

$$\begin{pmatrix} u \\ c \\ t \end{pmatrix}_{\text{Weak}} = \begin{pmatrix} u \\ c \\ t \end{pmatrix}_{\text{Mass}}.$$

All the mixing is therefore expressed in terms of a (3×3) unitary matrix $V = S_L^{u\dagger} S_L^d$ which operates on the charge (-1/3) quarks d, s and b:

$$\begin{pmatrix} d \\ s \\ b \end{pmatrix}_{\text{Weak}} \equiv \begin{pmatrix} V_{ud} & V_{us} & V_{ub} \\ V_{cd} & V_{cs} & V_{cb} \\ V_{td} & V_{ts} & V_{tb} \end{pmatrix} \begin{pmatrix} d \\ s \\ b \end{pmatrix}_{\text{Mass}}$$
(1.24)

The quark mixing matrix V is called Cabibbo-Kobayashi-Maskawa (CKM) [9, 10, 11] matrix and can be parameterized by four parameters, θ_{12} , θ_{13} , θ_{23} and δ_{13} .

$$V = \begin{pmatrix} c_{12}c_{13} & s_{12}c_{13} & s_{13}e^{-i\delta_{13}} \\ -s_{12}c_{23} - c_{12}s_{23}s_{13}e^{-i\delta_{13}} & c_{12}c_{23} - s_{12}s_{23}s_{13}e^{-i\delta_{13}} & s_{23}c_{13} \\ s_{12}s_{23} - c_{12}c_{23}s_{13}e^{-i\delta_{13}} & -c_{12}s_{23} - s_{12}c_{23}s_{13}e^{-i\delta_{13}} & c_{23}c_{13} \end{pmatrix}.$$
(1.25)

Here $c_{ij} = \cos \theta_{ij}$ and $s_{ij} = \sin \theta_{ij}$, with i, j = 1, 2, 3 being the family label. The complex phase introduced by δ_{13} in the CKM matrix signals the existence of CP violation in the Standard Model. In the limit of $\theta_{23} = \theta_{13} = 0$, the third generation decouples, and the CKM matrix reduces to the usual Cabbibo matrix in GIM mechanism [10].

1.5 Gauge Interactions

The major tests of the electroweak theory involve gauge interactions mediated by γ , W^{\pm} and Z bosons. The charged current weak interaction mediated by W boson is incorporated into the Standard Model from the original four-fermi interaction, and the γ mediated electromagnetic interaction is incorporated from quantum electrodynamics. From the Standard Model SU(2) \times U(1) local gauge theory, the neutral current weak interaction mediated by Z boson was successfully predicted and confirmed in the experiments.

The charged current interaction Lagrangian is given by

$$L = -\frac{g_2}{2\sqrt{2}} \left(J_W^{\mu} W_{\mu}^{-} + J_W^{\mu\dagger} W_{\mu}^{+} \right), \tag{1.26}$$

where J_W^μ is the weak current. The charged current weak interaction has been successfully tested in a large variety of weak decays, and it has been used to measure CKM matrix elements. The neutrino-hadron scattering processes such as $\nu_\mu N \to \mu^- X$ as shown in Figure 1.1 have been used as a probe the structure of the hadrons and QCD as well.

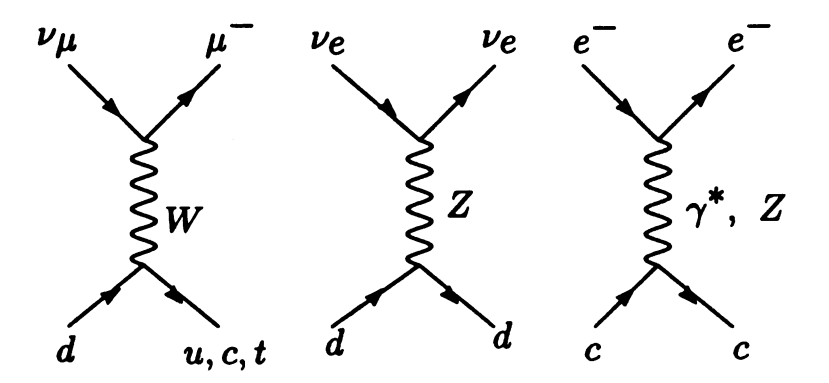


Figure 1.1: Electroweak charged current and neutral current interactions

The neutral current interaction Lagrangian is given by

$$L = -\frac{\sqrt{g_1^2 + g_2^2}}{2} J_Z^{\mu} \left(-\sin \theta_W B_{\mu} + \cos \theta_W W W_{\mu}^3 \right), \tag{1.27}$$

where J_Z^{μ} is the weak neutral current. Since there was no evidences for flavor-changing neutral currents in early experiments, GIM mechanism was introduced along with the prediction of the charm quark. The weak neutral current was discovered at CERN in 1973 and at Fermilab shortly after, and in 1974 J/ψ was discovered at Brookhaven and SLAC as the lowest energy bound states of the charm quark. Since then, the neutral weak current has been extensively studied in many different interactions such as $\nu_e N \to \nu_e X$ as shown in Figure 1.1, and these have been the primary quantitative test of the unification part of the Standard Model.

The self-interactions of the gauge bosons have not been extensively tested. Some typical interactions predicted by the Standard Model are shown in Figure 1.2. These tests will be very important for the Standard Model study and the Higgs search.

1.6 Problems with the Standard Model

The Standard Model is a very successful theory and its predictions have been consistent with all experimental results so far. However, because it has too many arbitrary

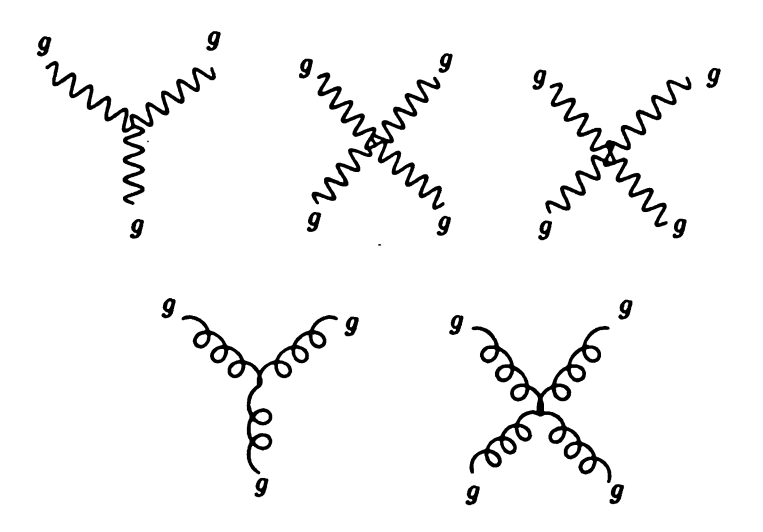


Figure 1.2: Gauge boson self-interactions

parameters, few believe it is the final fundamental theory. Not counting the assumption that neutrinos are massless, there are 18 free parameters in the minimal Standard Model Lagrangian, nine of which are fermion masses $(m_u, m_d, m_c, m_s, m_t, m_b, m_e, m_\mu, m_\tau)$, four are CKM matrix parameters $(\theta_{12}, \theta_{13}, \theta_{23}, \delta_{13})$, four are electroweak parameters (e, M_W, θ_W, M_H) , and the last one is the QCD strong coupling constant α_s . In addition, there is no explanation in the theory why there are three generations of fermions, or what is the origin of the CKM flavor mixing. Also, the Standard Model is a complicated direct product of three sub-groups SU(3) × SU(2) × U(1) with separate gauge couplings, and there is no explanation why only the electroweak interaction is chiral.

Various new theories have been proposed to extend the Standard Model, for example, SUSY, GUT, superstring theory, etc. But so far, there is no concrete experimental evidence to support any of these new models, and despite its shortcomings, the Standard Model seems to agree with experiments amazingly well.

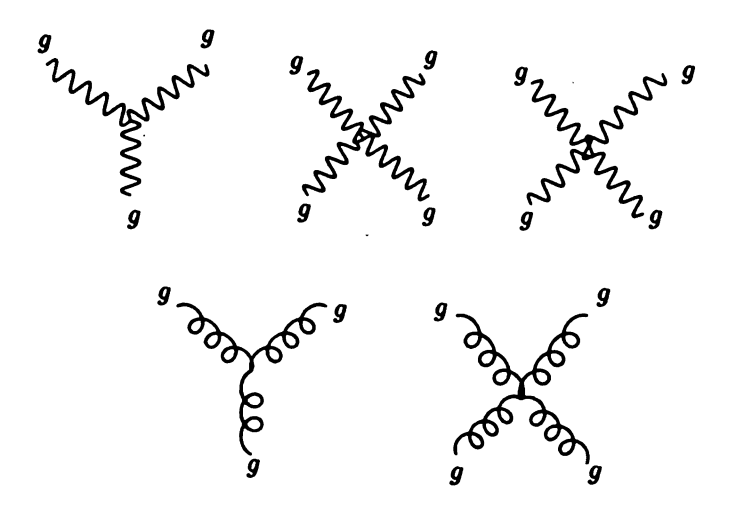


Figure 1.2: Gauge boson self-interactions

parameters, few believe it is the final fundamental theory. Not counting the assumption that neutrinos are massless, there are 18 free parameters in the minimal Standard Model Lagrangian, nine of which are fermion masses $(m_u, m_d, m_c, m_s, m_t, m_b, m_e, m_\mu, m_\tau)$, four are CKM matrix parameters $(\theta_{12}, \theta_{13}, \theta_{23}, \delta_{13})$, four are electroweak parameters (e, M_W, θ_W, M_H) , and the last one is the QCD strong coupling constant α_s . In addition, there is no explanation in the theory why there are three generations of fermions, or what is the origin of the CKM flavor mixing. Also, the Standard Model is a complicated direct product of three sub-groups SU(3) × SU(2) × U(1) with separate gauge couplings, and there is no explanation why only the electroweak interaction is chiral.

Various new theories have been proposed to extend the Standard Model, for example, SUSY, GUT, superstring theory, etc. But so far, there is no concrete experimental evidence to support any of these new models, and despite its shortcomings, the Standard Model seems to agree with experiments amazingly well.

Chapter 2

Deep Inelastic Scattering, QCD Parton Model and Asymptotic Freedom

That QCD is the theory of hadrons and the strong interaction has been universally accepted today, and in virtually every experimental analysis and theoretical calculation, QCD plays an important role. However, in the early sixties, because of the bewildering spectrum of baryons, mesons and their resonances, it was by no means obvious that a theory of strong interaction would succeed at all. Douglas B. Lenat, one of the foremost computer scientists today, in describing the reason of artificial intelligence as his career choice in the Sixties, once said [12], "I got far enough along in mathematics to realize I would not be one of the world's great mathematicians... I got far enough along in physics to realize that in some sense it was all built on sand ... People would walk around with ever-growing chest pocket cards of elementary particles which really means resonances that were found but not understood. Things were just happening that divorced themselves from physical reality."

While a systematic basic theory for the strong interaction seemed out of reach at that time, much progress was still made in hadron physics, for example, Gell-Mann's constitute quark model successfully explained hadron and meson resonances. However, it was not until the SLAC-MIT [13] experiment in the late sixties that strong interaction theory and hadron physics really began their exciting development. The experiments clearly showed that the proton possessed charge substructure of a spatial size much smaller that proton itself, and suggested an incoherent scattering process between the lepton and the constituent substructure. The "Bjorken scaling" [14] observed in the experiment was successfully explained by the naive parton model. Since a "color" quantum number for the quark was required in the constituent-quark model, it was quickly recognized the theory could be a SU(3)_C color Yang-Mills gauge theory. The theory was later found to possess a number of important properties, one of the most crucial one being asymptotic freedom, which means the coupling decreases with an increase in the measured energy scale. With asymptotic freedom, the separation of long distance physics and short distance physics, that is, factorization, is verified, and the QCD parton model is established in the context of quantum field theory.

2.1 Deep Inelastic Scattering

Deep inelastic scattering (DIS) plays a crucial role in our understanding of the hadron structures. In sixties, the SLAC-MIT experiment of electron-nucleon scattering gave us the first evidence that strong interactions become weak at short distances, and today, the structure function results from DIS give us the most precise tests of the theory and most accurate data used to determine the momentum distributions of partons inside hadrons.

Consider the process

$$l(k) + h(p) \to l'(k') + X$$
, (2.1)

as illustrated in Figure 2.1, where we label the initial-state lepton of momentum k^{μ} by l(k), the initial-state hadron of momentum p^{μ} by h(p), the final-state lepton of

momentum k'^{μ} by l'(k'), and the inclusive hadronic final state by X. The lepton l and the hadron h interact through the exchange of vector boson V which can be a γ , W^{\pm} , or Z boson. The momentum of the exchanged vector boson is labeled as

$$q^{\mu} = k^{'\mu} - k^{\mu} \ . \tag{2.2}$$

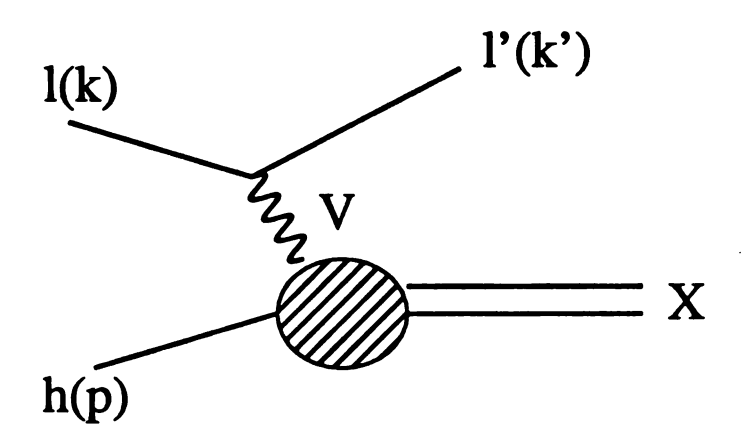


Figure 2.1: Deep inelastic scattering $l+h \rightarrow l'+X$

Because of the point-like electroweak interaction between the vector boson and the lepton, the cross section for this process can be written in term of hadron structure functions,

$$d\sigma^{(lh)} = \frac{d^3k'}{2s|k'|} \frac{c_V^4}{4\pi^2(q^2 - m_V^2)^2} L_{lV}^{\mu\nu}(k, q) W_{\mu\nu}^{Vh}(p, q) , \qquad (2.3)$$

where c_V is the coupling constant, $L_{lV}^{\mu\nu}$ is the leptonic tensor and $W_{\mu\nu}^{Vh}$ is the hadronic tensor. Notice that the leptonic part and the hadronic part are separated in Equation 2.3 and the only connection is vector boson of momentum transfer q. So lepton-hadron scattering can also be viewed as a vector boson scattering on a hadron with center of mass energy $W = (q + p)^2$. Note that W equals the square of the final hadronic state invariance mass.

 $L_{IV}^{\mu\nu}$ can be easily calculated from electroweak theory:

$$L_{lV}^{\mu\nu}(k,q) = nTr[\not k \Gamma_{Vl}^{\mu}(\not k - \not q)\Gamma_{Vl}^{\nu}], \qquad (2.4)$$

where Γ_{Vl} is the electroweak vertex connecting lepton l to vector V and the outgoing lepton l', but with the factor c_V^2 removed. To average over lepton spin, we set n equal to 1/2 for unpolarized e^{\pm} or μ^{\pm} , and 1 for $\nu(\bar{\nu})$. For example, for photon exchange at $e + p \rightarrow e + X$,

$$L^{\mu\nu}(k,q) = 2(2k^{\mu}k^{\nu} - k^{\mu}q^{\nu} - q^{\mu}k^{\nu} + k \cdot q g^{\mu\nu})$$
 (2.5)

The hadronic tensor is defined in term of the electroweak current operators,

$$W_{\mu\nu}^{(Vh)}(p,q) = \frac{1}{8\pi} \sum_{X} \left\langle h(p) | j_{\mu}^{V\dagger}(0) | X \right\rangle \left\langle X | j_{\nu}^{V}(0) | h(p) \right\rangle \times (2\pi)^{4} \delta^{4}(p+q-p_{X}), \quad (2.6)$$

where sum is done on the final inclusive hadronic state. Unlike leptonic sector, $\langle X|j_{\nu}^{V}(0)|h(p)\rangle$ is not calculable and $W^{\mu\nu}$ is usually defined in term of several structure functions or form factors.

The scattering process is deeply inelastic provided the magnitude of momentum transfer $Q^2 = -q^2$ and $p \cdot q$ are both large while their ratio $x = \frac{Q^2}{2p \cdot q}$ is fixed. On the other hand, when the invariant mass of the inclusive final hadronic state $W = -Q^2 + 2p \cdot q + M_P^2 \to M_P^2$, taking electron-proton scattering as an example, the proton is mostly probed by long-wavelength photons with modest values of Q^2 , and as a result, the proton may be excited to various resonances and quickly decay into different baryons and mesons afterwards. In elastic scattering, proton will not be broken into other hadrons, and the process could be described by $e(E_1) + P \to e(E_2) + P$ with $W = M_P^2$. In this case, $W^{\mu\nu}$ can be expressed in term of two form factors, F_1 and F_2 , which are related to the proton charge and magnetic moment distributions. Contracting the tensor indices in $L^{\mu\nu}$ and $W_{\mu\nu}$, we can derive the Rosenbluth Formula:

$$\frac{d\sigma}{d\Omega}|_{lab} = \left(\frac{\alpha^2}{4E_1^2 \sin^4 \frac{\theta}{2}}\right) \frac{E_2}{E_1} \left\{ \left(F_1^2 - \frac{\kappa^2 q^2}{4M_P^2} F_2^2\right) \cos^2 \frac{\theta}{2} - \frac{q^2}{2M_P^2} (F_1 + \kappa F_2)^2 \sin^2 \frac{\theta}{2} \right\}$$
(2.7)

Rosebluth Formula describes the elastic scattering between the electron and the proton. F_1 and F_2 in Equation 2.7 only depend on the scattering angle θ , and E_2 is fixed by the elastic scattering kinematics as $\frac{E_1}{1 + (2E_1/M_P)\sin^2(\theta/2)}$.

However, when Q^2 becomes large enough, the proton is bombarded by short-wavelength, energetic photons (or W, Z bosons when Q^2 reaches their mass threshold) and will break up. To describe this more complicated deep inelastic scattering interaction, a set of six independent basis tensors is needed. So, in deep inelastic scattering, $W_{\mu\nu}^{Vh}$ can be written as

$$W_{\mu\nu}^{Vh} = -g_{\mu\nu}W_1 + \frac{p_{\mu}p_{\nu}}{M_h^2}W_2 - i\frac{\epsilon_{\alpha\beta\mu\nu}p^{\alpha}q^{\beta}}{2M_h^2}W_3 + \frac{q_{\mu}q_{\nu}}{M_h^2}W_4 + \frac{p_{\mu}q_{\nu} + q_{\mu}p_{\nu}}{2M_h^2}W_5 + \frac{p_{\mu}q_{\nu} - q_{\mu}p_{\nu}}{2M_h^2}W_6 , \qquad (2.8)$$

where the scalar coefficient functions W_i are the invariant hadron structure functions.

In photon (γ^*) and proton deep inelastic scattering, due to parity conservation and electromagnetic current conservation,

$$q^{\mu}W_{\mu\nu}^{em} = q^{\nu}W_{\mu\nu}^{em} = 0$$

it can be shown that

$$W_3 = 0 (2.9)$$

$$W_4 = \left(\frac{p \cdot q}{q^2}\right)^2 W_2 + \frac{m^2}{q^2} W_1 \tag{2.10}$$

$$W_5 = -\frac{2p \cdot q}{q^2} W_2 \tag{2.11}$$

$$W_6 = 0 (2.12)$$

and hadron tensor $W^{em}_{\mu\nu}$ can be simplified as

$$W_{\mu\nu}^{em} = -(g^{\mu\nu} - \frac{q^{\mu}q^{\nu}}{q^2})W_1 + \frac{1}{M_h^2}(p^{\mu} - \frac{p \cdot q}{q^2}q^{\mu})(p^{\nu} - \frac{p \cdot q}{q^2}q^{\nu})W_2$$
 (2.13)

in this special case.

In deep inelastic scattering, several standard kinetic variables are usually used,

$$p^{2} = M_{h}^{2}$$

$$\nu = \frac{p \cdot q}{\sqrt{p \cdot p}} = E_{1} - E_{2}$$

$$x = \frac{Q^{2}}{2p \cdot q} = \frac{Q^{2}}{2M_{h}(E_{1} - E_{2})}$$

$$y = \frac{q \cdot p}{k \cdot p} = 1 - \frac{E_{2}}{E_{1}}$$

$$s = (k+p)^{2} = M_{h}^{2} + \frac{Q^{2}}{xy}$$

$$W = (q+p)^{2} = M_{h}^{2} + Q^{2} \frac{1-x}{x}$$
(2.14)

where E_1 and E_2 are energies of the incoming and outgoing lepton respectively in the rest frame of the proton.

In Equation 2.8, $\{W_4, W_5, W_6\}$ terms are usually ignored because their contribution to the cross section are proportional to $O(m_i^2/Q^2)$ after contracting with the leptonic tensor. Also, the proton structure functions $\{W_i\}$ are usually replaced by three dimensionless structure functions $\{F_i\}$, where

$$F_1(x,Q^2) = W_1(x,Q^2), (2.15)$$

$$F_2(x,Q^2) = \frac{\nu}{M_h} W_2(x,Q^2), \qquad (2.16)$$

$$F_3(x,Q^2) = \frac{\nu}{M_h} W_3(x,Q^2).$$
 (2.17)

Contracting the leptonic tensor and hadronic tensor in Equation 2.3, the differential cross section for DIS can be expressed in terms of the dimensionless variables x and y and the structure functions $\{F_i\}$,

$$\frac{d\sigma}{dxdy} = N^{IV} \left[xy^2 F_1 + (1 - y - \frac{M_h xy}{2E}) F_2 + \delta^V (y - \frac{y^2}{2}) x F_3 \right] , \qquad (2.18)$$

where δ^V is ± 1 for W^{\pm} exchange and zero for the photon exchange, and

$$N^{\gamma} = 8\pi\alpha^2 \frac{M_h E}{Q^4},\tag{2.19}$$

$$N^{W^{\pm}} = \pi \alpha^2 \frac{M_h E}{2 \sin^4 \theta_W (Q^2 + M_W^2)^2} . \tag{2.20}$$

Or alternatively, the cross section in the hadron target rest frame is

$$\frac{d\sigma}{dE_2 d\cos\theta} = N^{lV} \left[2W_1^{(Vh)}(x, q^2) \sin^2(\theta/2) + W_2^{(Vh)}(x, q^2) \cos^2(\theta/2) + \delta^V W_3^{(Vh)}(x, q^2) \frac{E_1 + E_2}{M_h} \sin^2(\theta/2) \right]$$
(2.21)

Comparing with Rosebluth Formula in Equation 2.7, W_1, W_2 and W_3 are functions of x, q^2 , or equivalently, θ, q^2 . In Equation 2.21, E_2 is not kinematically fixed by E_1 and the scattering angle θ as in Equation 2.7.

The striking feature of early deep inelastic scattering experiments results was that for $Q^2 \geq 2 \text{ GeV}^2$, the structure function $F_i(x, Q^2)$ become functions of x only, nearly independent of Q^2 . This property is called "Bjorken scaling" [14]. It was originally postulated by Bjorken and later dramatically confirmed by the SLAC-MIT experiment. The "Bjorken scaling" is nicely explained by the Naive Parton Model.

2.2 The Naive Parton Model

The naive parton model [17, 18] assumes that a hadron is made of point-like onshell particles which are called partons. Each of these partons carries some fraction ξ of the proton momenta. In deep inelastic scattering, the striking vector boson interacts incoherently with the partons one at a time, which means during the short distance interaction, the other partons are present merely as spectators and there is no interference with the scattering mechanism. The parton model does not make predictions about the distributions of the partons inside hadrons, nor does it explain how the partons eventually hadronize into baryons and mesons. That information must be extracted from experimental data.

Mathematically, the fundamental relation of the parton for deep inelastic scattering can be written as

$$d\sigma^{lN}(p,q) = \sum_{f} \int_{0}^{1} d\xi \ d\sigma^{(lf)}_{Born}(\xi p, q) \ \phi_{f/N}(\xi), \tag{2.22}$$

where $d\sigma^{lN}(p,q)$ is the inclusive cross section for lepton-hadron scattering, and $d\sigma^{(lf)}_{Born}$ is the Born level, elastic lepton-parton scattering cross section. $d\sigma^{(lf)}_{Born}(\xi p,q)$ is calculable in perturbative QCD theory. The functions $\phi_{f/N}(\xi)$ are the parton distribution functions (PDF), which describe the probability of finding a parton of flavor f with momentum fraction ξ in the hadron. These parton distribution functions are not calculable at the present time because they involve non-perturbative physics and must be extracted from experimental data. Obviously the parameter ξ in $\phi_{f/N}(\xi)$ is between zero and one, and because of the total momentum conservation, the patron distribution functions must satisfy

$$\sum_{f} \int_{0}^{1} d\xi \, \xi \, \phi_{f/N}(\xi) = 1. \tag{2.23}$$

Early deep inelastic scattering experiments also confirmed the Callan-Gross relation which states that the scaling functions are related by $2xF_1(x) = F_2(x)$. This relation reflects the fact that the charged partons inside the proton carry spin 1/2, which are exactly the quark constitutes of the proton in the Gell-Mann quark model [19]. Hence by summing over all contributing partons in the proton, the quantum numbers of the proton should be recovered. It follows that

$$\int_0^1 (u(x) - \overline{u}(x)) dx = 2, \qquad (2.24)$$

and

$$\int_0^1 \left(d(x) - \overline{d}(x) \right) dx = 1 \tag{2.25}$$

number sum rules must be satisfied by the parton distribution functions.

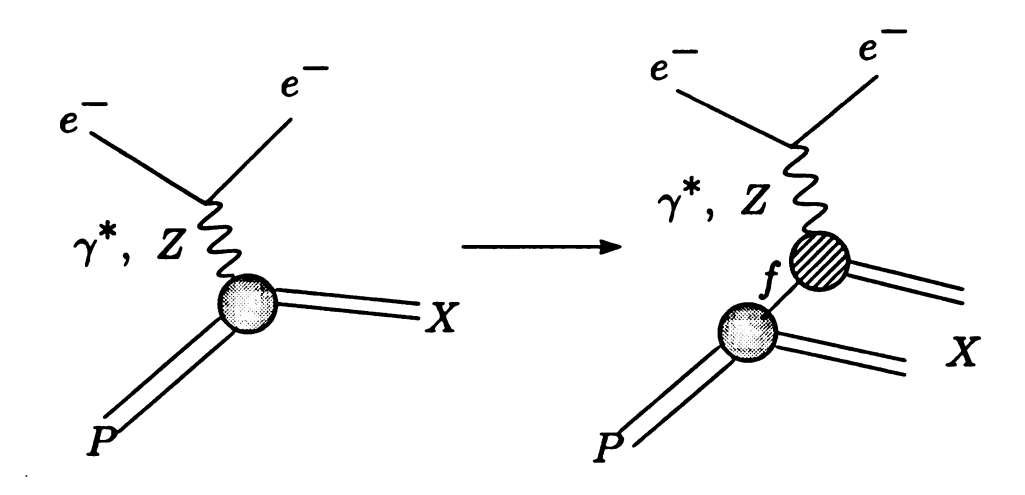


Figure 2.2: The parton model interpretation of $e + P \rightarrow e + X$ process

The parton model interpretation of the deep inelastic scattering can be pictured as Figure 2.2. Notice in Equation 2.22, there is no interference between different flavors and different momentum fractions ξ , and the total cross section is just an incoherent sum of the cross sections of all the available partons and momentum fractions. This "incoherence" feature implies that parton distribution functions are universal and independent of short distance scattering processes. There is no explanation for this in the naive parton model, and it is invoked as an assumption. In QCD improved parton mode, it is proved order by order in the context of perturbative QCD.

To calculate σ^{lN} using Equation 2.22, we need to calculate the lepton-parton scattering σ^{lf} first. The lepton-parton scattering process is shown in Figure 2.3. $d\sigma^{(lf)}$ can be calculated easily for this $2 \to 2$ scattering process since the electroweak couplings between the vector boson and the quark are point-like couplings. Similar to Equation 2.3 where $d\sigma^{(lh)}$ was written in term of hadronic tensor $W^{\mu\nu}$, we can factor

out the lepton sector and write $d\sigma^{(lf)}$ as

$$d\sigma^{(lf)} = \frac{d^3k'}{2\xi s |k'|} \frac{c_V^4}{4\pi^2(q^2 - m_V^2)^2} L_{lV}^{\mu\nu}(k, q) w_{\mu\nu}^{Vf}(\xi p, q) , \qquad (2.26)$$

where $w^{\mu\nu}$ is the partonic tensor. Upon factoring out the lepton tensor in Equation 2.3 and 2.26, we can get the parton model relation between hadronic tensor and partonic tensor,

$$W_{\mu\nu}^{(lN)} = \sum_{f} \int_{0}^{1} \frac{d\xi}{\xi} \ w_{\mu\nu}^{(lf)} \ \phi_{f/N}(\xi) \tag{2.27}$$

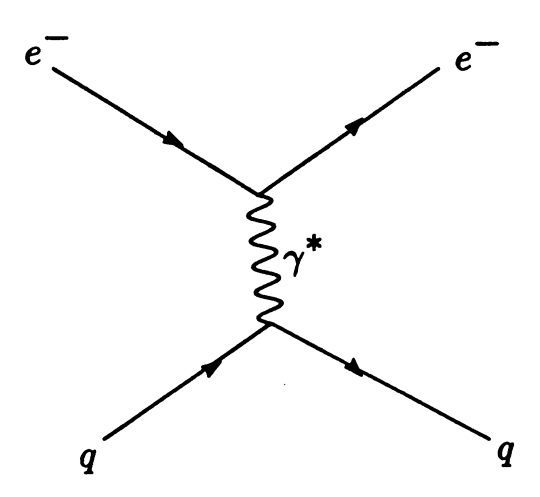


Figure 2.3: Born level $e + q \rightarrow e + q$ scattering

For photon mediated electron-proton deep inelastic scattering process, similar to Equation 2.13,

$$w_{\mu\nu}^{em} = -(g^{\mu\nu} - \frac{q^{\mu}q^{\nu}}{q^2})w_1 + \frac{1}{m^2}(p^{\mu} - \frac{p \cdot q}{q^2}q^{\mu})(p^{\nu} - \frac{p \cdot q}{q^2}q^{\nu})w_2. \tag{2.28}$$

A calculation of the Born level photon parton elastic scattering process Figure 2.3 gives the results for $w_{\mu\nu}^{(lf)}$,

$$w_{\mu\nu}^{(em)} = \frac{1}{8\pi} \int \frac{d^3p'}{(2\pi)^3 2E_{p'}} e_f^2 tr(\gamma_\mu \not p' \gamma_\nu \not p) (2\pi)^4 \delta^4(p' - p - q)$$

$$= -\frac{1}{2} (g_{\mu\nu} - \frac{q_\mu q_\nu}{q^2}) e_f^2 \delta(1 - x)$$

$$+ (p_\mu - q_\nu \frac{p \cdot q}{q^2}) (p_\nu - q_\mu \frac{p \cdot q}{q^2}) e_f^2 \frac{1}{\nu} \delta(1 - x)$$
(2.29)

where e_f is the fractional charge of the parton. We then have, from Equation 2.28,

$$w_1^{(f)} = \frac{1}{2}e_f^2\delta(1-x) , \ w_2^{(f)} = e_f^2\delta(1-x)\frac{m_h^2}{\nu}.$$
 (2.30)

Or using dimensionless structure function,

$$F_1^{(f)} = \frac{1}{2}e_f^2\delta(1-x) , \ F_2^{(f)} = e_f^2\delta(1-x)$$
 (2.31)

Substitute $w_i^{(f)}$ or $F_i^{(f)}$ into Equation 2.27, it is easy to find

$$2xF_1^{(N)}(x) = F_2^{(N)}(x) = \sum_f Q_f^2 x \phi_{f/N}(x)$$
 (2.32)

Despite of its success in explaining the "Bjorken scaling" of the proton structure functions, the naive parton model can not be accepted as a complete theory of hadron physics. First, more accurate experimental data show that DIS structure functions only scale approximately instead of the naive parton model's perfect scaling prediction, and the naive parton model can't explain this scaling violation. Furthermore, its assumption of free partons inside hadron can not be confirmed either experimentally or theoretically, and the naive parton model itself does not give any insight about why the assumption is true either. A calculation [20] based on the measured structure function data reveals that

$$\int_0^1 dx \ x \ (u(x) + d(x) + \overline{u}(x) + \overline{d}(x) \) \simeq 0.54$$
 (2.33)

instead of 1. The other 46% momentum of the proton is carried by neutral particles, that is, the gauge boson of the SU(3) theory, gluons. With the discovery of asymptotic freedom in SU(3) theory, QCD became the candidate for the strong interaction. Later, the factorization theorem was proved in the context of the perturbative theory, and QCD not only provides a theoretical basis for the naive parton model, but also improves on it in many aspects. Today, the QCD improved parton model has become

the cornerstone of most applications of perturbative QCD to observable phenomena. In the next two sections, we will first discuss QCD asymptotic freedom and then the factorization theorem.

2.3 QCD and Hadron Physics

The QCD Lagrangian, including the mass terms, is

$$\tilde{L}_{QCD} = -\frac{1}{4} F_{\mu\nu}^{(a)} F^{(a)\mu\nu} + \sum_{q} \overline{\psi_{i}}^{q} (i \gamma^{\mu} (D_{\mu})_{ij} - m_{q} \delta_{ij}) \psi_{j}^{q}
F_{\mu\nu}^{(a)} = \partial_{\mu} G_{\nu}^{a} - \partial_{\nu} G_{\mu}^{a} - g_{s} f_{abc} G_{\mu}^{b} G_{\nu}^{c}
(D_{\mu})_{ij} = \delta_{ij} \partial_{\mu} + i g_{s} \frac{\lambda_{ij}^{a}}{2} G_{\mu}^{a}$$
(2.34)

as described in Chapter One. However, in quantum field theory [15], we need an extra gauge fixing term to quantize the Lagrangian since the part of the Lagrangian quadratic in the gauge field has no inverse. This, depending on the gauge fixing term chosen, may necessitate a ghost term to satisfy the unitary requirement. Conventional gauge fixing terms choices can be one of the following:

$$L_{covariant} = -\frac{1}{2\lambda} (\partial^{\alpha} G_{\alpha})^2 \qquad (2.35)$$

$$L_{axial} = -\frac{1}{2\lambda}(n \cdot G)^2 \tag{2.36}$$

where λ is the gauge parameter. When $\lambda = 1$, the covariant gauge becomes the familiar Feynman gauge. When $\lambda = 0$, $n^2 = 0$, the axial gauge is called the light-cone gauge. Covariant gauge fixing term requires a ghost Lagrangian which is given by

$$L_{ghost} = \partial_{\mu} \eta^{a\dagger} (D^{\mu}_{ab} \eta^{a}), \tag{2.37}$$

where η^A is a complex scalar ghost field that obeys Fermi statistics. From the complete QCD Lagrangian,

$$L_{QCD} = \tilde{L}_{QCD} + L_{gauge-fixing} + L_{ghost}$$
 (2.38)

the Feynman rules for QCD can be derived.

The theory, of course, must be renormalized [16]. Using dimensional regularization, the integration of the two, three and four point functions of the quark, gluon and ghost fields can be carried out in d dimensions in which the integrals become finite and the singularities are exhibited as poles in $\epsilon = (4 - d)/2$. Denoting Z_i 's as the renormalization factors, the renormalized fields G, q, η and the renormalized parameters g, m can be written as

$$g(\mu)^i = \mu^{-\epsilon} Z_1^{-1} Z_3^{3/2} g^{(0)}(\epsilon),$$
 (2.39)

$$m = Z_m^{-1} m^{(0)}, (2.40)$$

$$G^{i} = Z_{3}^{-1/2}G^{(0)}, (2.41)$$

$$q_a = Z_2^{-1/2} q_a^{(0)}, (2.42)$$

$$\eta_a = \tilde{Z}_3^{-1/2} \eta_a^{(0)}, \tag{2.43}$$

$$\lambda = Z_3^{-1} \lambda^{(0)} \tag{2.44}$$

where μ is a mass scale parameter introduced in dimensional regularization to keep the Lagrangian dimension correct in d dimension.

Renormalization requires the ultraviolet divergence terms (the pole terms in ϵ) to be absorbed into theoretical bare quantities, and different ways to do this result in different renormalization schemes. In QCD calculations, $\overline{\text{MS}}$ renormalization scheme is usually chosen. In this scheme, one chooses various Z_i in such a way that the $\frac{1}{\epsilon}$ terms are subtracted along with a fixed finite constant term. Some of the Z_i to one loop order are listed in Table 2.1.

One of the most crucial features of QCD is that it is an asymptotically free theory, which means the strength of the strong coupling decreases as the momentum scale at which it is defined increases. Asymptotic freedom can be derived from renormal-

Table 2.1: MS renormalization parameters

ization group equations (RGE), which originate from the fact that the S-matrix is independent of the scale μ and can be computed in terms of either bare quantities or renormalized quantities. In $\overline{\rm MS}$ scheme, the relation between the bare and the renormalized coupling constant is

$$g(\mu) = \mu^{-\epsilon} Z_g^{-1} g_0, \tag{2.45}$$

where $Z_g = Z_1^{-1} Z_3^{3/2}$. The beta function $\beta(g)$ is defined as

$$\beta(g) = \frac{\partial}{\partial \ln \mu} g(\mu)|_{g_0}. \tag{2.46}$$

From Equation 2.45 and

$$\mu \frac{\partial}{\partial \mu} Z_{\mathbf{g}}(g(g_0, \mu)) = \beta(g) \frac{\partial}{\partial g} Z_{\mathbf{g}}, \qquad (2.47)$$

 $\beta(g)$ can easily be solved. Using Table 2.1, to the one loop order,

$$\beta(g_{(\mu)}) = -\frac{g^3}{16\pi^2} (\frac{11}{3}N_C - \frac{2}{3}n_f). \tag{2.48}$$

For QCD, $N_C = 3$, $n_f = 6$, therefore, $\beta(g)$ is negative. A negative β function means the renormalized coupling will decrease with the increase of the renormalization scale,

and thus QCD is an asymptotically free theory. In the case of QED, on the contrary, the coupling will increase as the renormalization scale increases since the β function is positive as shown in Equation 2.49.

$$\beta(e_{(\mu)}) = \frac{e^3}{12\pi^2}. (2.49)$$

To two loop order, a more complicated calculation yields

$$\beta(g_{\mu}) = -\frac{g^3}{16\pi^2} \left(\frac{11N_C - 2n_f}{3}\right) - \frac{g^5}{64\pi^3} \left(\frac{153 - 19n_f}{6\pi}\right) + O(g^7)$$
 (2.50)

$$\alpha_s(\mu^2) = \alpha_{S0}(\mu^2) \left[1 - \alpha_{S0}(\mu^2) \frac{\beta_2 lnln(\mu^2/\Lambda_{QCD}^2)}{4\pi\beta_1} + O(\alpha_{S0}^2(\mu^2)) \right]$$
 (2.51)

where

$$\alpha_{S0}(\mu^2) = \frac{4\pi}{\beta_1 ln(\mu^2/\Lambda_{QCD}^2)}$$
, (2.52)

and

$$\beta_1 = (11N_c - 2n_f)/3$$
 , $\beta_2 = 102 - 38n_f/3$; (2.53)

In Figure 2.4, we plot the two loop order strong coupling α_s as a function of the energy scale μ with different choices of Λ_{QCD} . The plots clearly show that as energy scale μ increases, the strong coupling α_s decreases: $\alpha_s \to 0$ as $\mu \to \infty$. This property is called asymptotic freedom, and it is with asymptotic freedom that everything begins. Without it, there will be no natural explanation in the quantum field theory for the parton model.

 Λ_{QCD} in Equation 2.51 and 2.52 is introduced to cut off the integration when solving the differential equations. For $Q^2 \gg \Lambda_{QCD}^2$, α_s is small and perturbative QCD can be applied. For $Q^2 \sim \Lambda_{QCD}^2$, α_s is large, which means the gluons and quarks are strongly coupled together and order by order perturbative QCD expansions will not work in this situation.

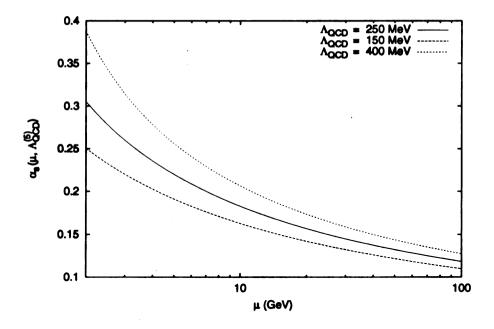


Figure 2.4: QCD running coupling α_s with $n_f = 5$.

2.4 Factorization and the QCD Improved Parton Model

Although the naive parton model can not be accepted as a complete theory of hadron physics, much of its structure remains in perturbation theory. This has to be attributed to the property of factorization [21].

Factorization permits cross sections of high energy scattering processes to be written as a convolution of a hard scattering cross section and a remainder which contains the low energy physics. The former contains only the high energy and momentum components, and because of asymptotic freedom, it can be calculated order by order in perturbation theory. The latter piece describes non-perturbative physics, and is described by the process independent, universal parton distribution function. For deep inelastic scattering, factorization theorem can be written as

$$d\sigma^{lN}(p,q) = \sum_{a=q,q} \int_0^1 d\xi \ d\sigma^{(la)}(\xi p, q, \mu^2, \alpha_s(\mu), \cdots) \ \phi_{a/N}(\xi, \mu^2), \tag{2.54}$$

where $d\sigma^{la}$ is the hard scattering piece, $\phi_{a/N}$ is the parton distribution function, and a includes quarks and gluons. Comparing with Equation 2.22 of the naive parton model, QCD scale μ dependency is introduced after the renormalization and factorization are carried out, α_s dependence originates from the order by order perturbative expansions. As before, ξ is the momentum fraction of the hadron that a parton carries. Parton distribution functions $\phi_{a/N}(\xi, \mu^2)$ depend on both ξ and energy scale μ . The energy scale dependency in $\phi_{a/N}(\xi, \mu^2)$ originates from the factorization scale introduced when long distance physics is separated from the short distance physics. The proofs of factorization theorem require a detailed examination of all the dangerous regions of phase space in Feynman diagrams and is beyond the scope of this thesis.

A remarkable result of factorization is that measuring parton distribution functions at one value of μ^2 allows us to predict their values at all other values of μ^2 , as long as the μ^2 are large enough so that the perturbation theory is applicable. This ability is related to the freedom in choosing the renormalization and factorization scales in the proofs of the factorization theorem. In order to perform the factorization, we have to introduce the artificial scale μ^2 which separate the high energy physics and low energy physics. However, no physical quantity can depend on the particular value chosen for this scale. In Equation 2.54, we notice the left side of the equation has no QCD scale μ^2 dependence, which is exactly the way a physical observable should be, so

$$\frac{d}{d\mu}\sigma^{lN} = \frac{d}{d\mu} \left(\sigma^{(la)} \otimes \phi \right) = 0. \tag{2.55}$$

Thus, the μ dependence in hard scattering cross section $\sigma^{(la)}$ and parton distribution functions $\phi_{a/N}$ must compensate each other. Although $\phi_{a/N}$ can not be calculated in perturbation theory, however, the perturbative partonic distribution functions, $\phi_{a/b}(\xi,\mu^2)$, which represents the probability of finding a parton a in a parton b with

a momentum fraction ξ of the longitudinal momentum of the parent parton, can be calculated order by order. The $\phi_{a/b}$ functions are not physical quantities like $\phi_{a/N}$, but they essentially represent the evolutions of the parton distribution functions due to the parton splittings in the parton-parton collinear configuration. In QCD, which graphs contain these collinear singularities depend on the gauge choice. In the light cone gauge, the graphs responsible are the "ladder" diagrams. Systematically calculating all the "ladder" diagrams in the light cone gauge, the variations of the parton distributions with the changes of scale μ can be obtained,

$$\frac{d}{d\mu^2}q_i(x,\mu^2) = \frac{\alpha_S(\mu^2)}{2\pi} \int_x^1 \frac{d\xi}{\xi} \left[q_i(\xi,\mu^2) P_{qq}(\frac{x}{\xi}) + G(\xi,\mu) P_{qG}(\frac{x}{\xi}) \right]$$
(2.56)

for quark (or antiquark) distributions q_i , and

$$\frac{d}{d\mu^2}G(x,\mu^2) = \frac{\alpha_S(\mu^2)}{2\pi} \int_x^1 \frac{d\xi}{\xi} \left[\sum_i q_i(\xi,\mu^2) P_{Gq}(\frac{x}{\xi}) + G(\xi,\mu) P_{GG}(\frac{x}{\xi}) \right]$$
(2.57)

for gluon distribution G. These are known as Gribov-Lipatov-Altarelli-Parisi (GLAP) evolution equations [22, 23, 24], and the evolution kernel $P_{qG}(x)$, $P_{Gq}(x)$, and $P_{GG}(x)$ are called splitting functions. The splitting functions can be calculated order by order in perturbation theory, for example,

$$P_{qq}(z,\alpha_s) = P_{qq}^{(0)}(z) + \frac{\alpha_s}{2\pi} P_{qq}^{(1)}(z) + \cdots$$
 (2.58)

Based on quark number conservation and momentum conservation in the splittings of quarks and gluons, the splitting functions must satisfy,

$$P_{qq} = P_{\overline{qq}}, \quad P_{qG} = P_{\overline{q}G}, \tag{2.59}$$

$$\int_0^1 dz \ P_{qq}(z) = 0, \tag{2.60}$$

$$\int_0^1 dz \ z \left[P_{qq}(z) + P_{Gq}(z) \right] = 0, \tag{2.61}$$

$$\int_0^1 dz \ z \left[2n_f P_{qG}(z) + P_{GG}(x) \right] = 0 \tag{2.62}$$

The lowest order approximations to the evolution kernel are,

$$P_{qq}^{(0)}(z) = C_F \left[\frac{1+x^2}{(1-x)_+} + \frac{3}{2}\delta(1-x) \right], \qquad (2.63)$$

$$P_{qG}^{(0)}(z) = T_R \left[x^2 + (1-x)^2 \right] \tag{2.64}$$

$$P_{Gq}^{(0)}(z) = C_F \left[\frac{1 + (1-x)^2}{x} \right], \tag{2.65}$$

$$P_{GG}^{(0)}(z) = 2N_c \left[\frac{x}{(1-x)_+} + \frac{1-x}{x} + x(1-x) \right] + \delta(1-x) \frac{(11N_c - 4n_f T_R)}{6}, \qquad (2.66)$$

where

$$C_F = \frac{N_c^2 - 1}{2N_c},$$
$$T_R = \frac{n_f}{2}.$$

The methods of QCD improved parton model can also be applied to the fragmentation process, which describes the decay of a parton into hadrons. In this case, fragmentation function $D_{H/i}(\xi, \mu^2)$ is defined as the probability of a parton *i* decaying into hadron *H* which carries a fraction ξ of the parton momentum. The evolution function for fragmentation functions can be derived similar to the GLAP equation,

$$\frac{d}{d\mu^2}D_q^H(x,\mu^2) = \frac{\alpha_S(\mu^2)}{2\pi} \int_x^1 \frac{d\xi}{\xi} \left[D_q^H(\xi,\mu^2) P_{qq}(\frac{x}{\xi}) + D_g^H(\xi,\mu) P_{gq}(\frac{x}{\xi}) \right]$$
(2.67)

$$\frac{d}{d\mu^2}D_g^H(x,\mu^2) = \frac{\alpha_S(\mu^2)}{2\pi} \int_x^1 \frac{d\xi}{\xi} \left[\sum_i D_q^H(\xi,\mu^2) P_{qg}(\frac{x}{\xi}) + D_g^H(\xi,\mu) P_{gg}(\frac{x}{\xi}) \right] (2.68)$$

Currently, the fragmentation functions are mostly extracted from e^+e^- annihilation data.

2.5 Other Hadronic Interactions

Besides the deep inelastic scattering, QCD parton model has been successfully applied to other processes such as vector boson production, jet production, and direct photon productions etc. For each of these processes, theoretical calculations are performed using the factorization theorem, and the results so far are in good agreement with experimental data.

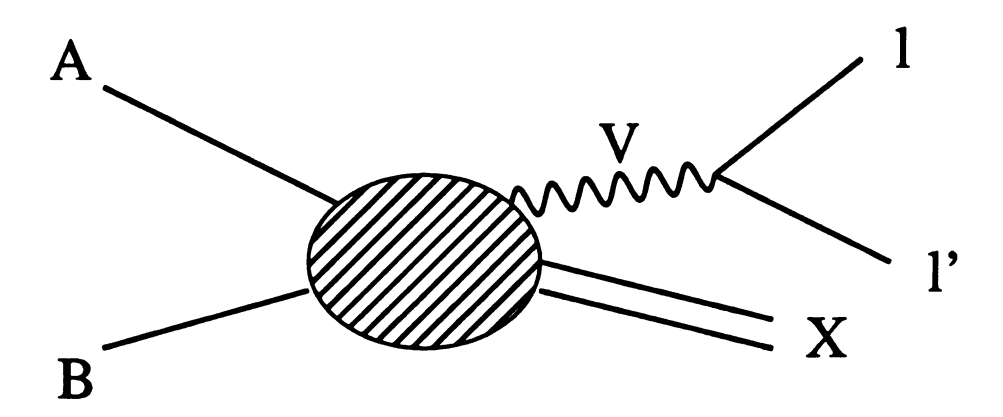


Figure 2.5: Vector boson production $A + B \rightarrow V + X$

Vector Boson production (VBP) in hadron A hadron B collision

$$A(p) + B(p') \to V(q) + X \to l(k) + l'(k') + X,$$
 (2.69)

as shown in Figure 2.5, is the simplest process for large transverse momentum reactions with two colliding hadrons in the initial state. The vector boson generated during the hard scattering, γ , W^{\pm} , or Z, is usually detected through its leptonic decay products.

The factorization for inclusive vector boson production can be written as,

$$\frac{d\sigma_{AB}^{V}}{dq^{2}}(p,p',q) = \sum_{ab} \int_{0}^{1} d\xi \int_{0}^{1} d\xi' \phi_{a/A}(\xi,\mu^{2}) \phi_{b/B}(\xi',\mu^{2}) \frac{d\hat{\sigma}_{ab}^{V}(\xi p,\xi' p',q,\mu)}{dq^{2}} . \quad (2.70)$$

where a, b are the two partons from the two colliding hadrons and ξ , ξ' are their momentum fractions respectively. From Equation 2.70, we see that the hard scattering can be calculated in $d\hat{\sigma}_{a+b->V+X}$, and the universal parton distribution functions, just as in deep inelastic scattering, describe the long distance physics and are factored out from the hard scattering. The lowest order contribution to the hard scattering in vector boson production is the process $q + \overline{q'} \to W$, Z or γ^* , as shown in Figure 2.6. Vector Boson Production was first analyzed by Drell and Yan, so it is also called Drell-Yan(DY) [25] process sometimes.

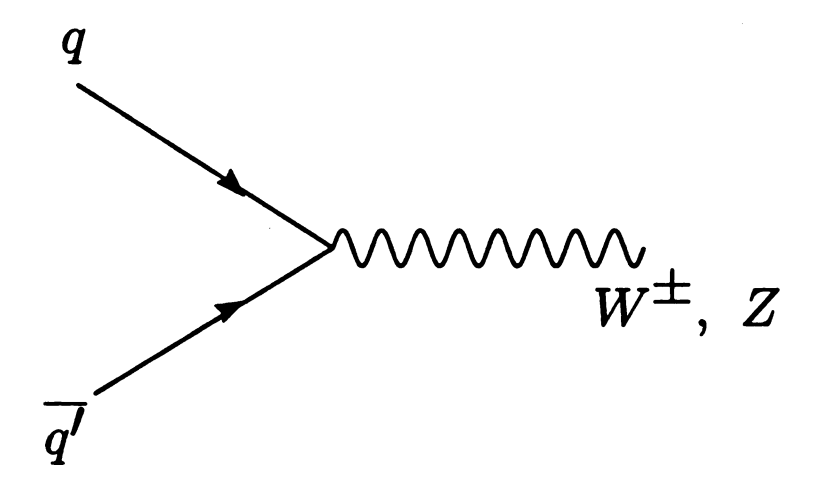


Figure 2.6: Partonic process $q + \overline{q'} \rightarrow W^{\pm}/Z$ for vector boson production

Vector Boson Production is a complimentary process to deep inelastic scattering and it provides a lot of useful information needed in the parton distribution function analysis. Recently, it has been used as a precision test for electroweak theory in W and Z boson productions [26].

Another important application of the QCD improved parton is the jet production in hadron collisions. Jet production is the dominant hard scattering activity in hadron collisions because of the strong coupling between quarks and gluons. Jets are formed when the colored final state quarks and gluons in the hard scattering hadronize to the observable color neutral particles. The validity of the QCD improved parton

model for the description of large transverse momentum hadron-hadron interaction got dramatic qualitative confirmation when the clear jet events were found by the UA1 and UA2 experiments [27, 28].

For single jet inclusive process, the jet production cross section can be written as

$$\frac{d\sigma}{dp_t^2}(AB \to jets) = \sum_{abcd} \int dx_a dx_b \phi_{a/A}(x_a, \mu^2) \phi_{b/B}(x_b, \mu^2) \frac{d\hat{\sigma}}{dp_t^2}(ab \to cd), \qquad (2.71)$$

where p_t is the transverse momentum relative to the beam axis of the scattered partons, and it is given by

$$p_t^2 = \frac{\hat{u}\hat{t}}{\hat{s}}.\tag{2.72}$$

 $\hat{s} = (p_a + p_b)^2$ is the squared center of mass energy of the parton subprocess, $\hat{t} = (p_a - p_c)^2$ is the t-channel energy exchange $\hat{u} = (p_a - p_d)^2$ is the u-channel energy exchange. A list of the lowest order partonic scattering processes between quarks and gluons in jet production is shown in Figure 2.7.

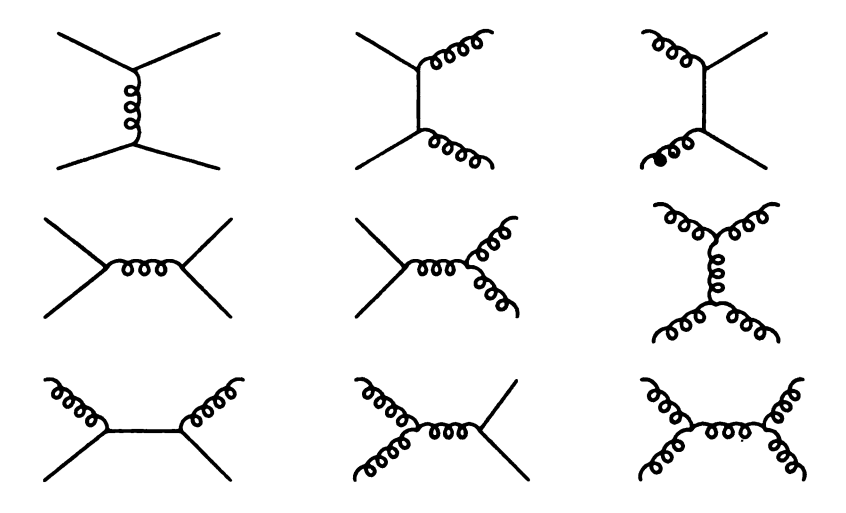


Figure 2.7: Jet production

QCD improved parton model has also been applied into direct photon production, e^+e^- jet production etc. Furthermore, not only are inclusive quantities calculated through the factorization theorem, differential distributions have also been calculated

for various scattering processes. The results usually are in good agreement with the experimental data.

2.6 The Global Analysis for Parton Distribution Functions

The factorization theorem, based on the QCD parton model described before provides the foundation for analyzing high energy hard scattering processes. There are two basic ingredients of calculations used for comparing theoretical predictions with experiments: (1) the perturbatively calculated scattering cross sections involving the fundamental partons, leptons, and gauge bosons; and (2) the parton distributions inside the incoming hadrons. The universal, i.e. process independent, parton distributions functions (PDF's) are derived from the analysis of data in a variety of hard scattering processes, but governed by the renormalization group equations.

With the wealth of data and corresponding theoretical calculations from various processes, global QCD analyses have become possible. In such an analysis there are two main goals. The first is to determine the parton distribution functions as precisely as possible, and the second is to explore whether or not the parton level theoretical calculations in perturbative QCD constitute a consistent theoretical framework to account for all the available experimental data. Here we briefly lay out the essential elements of performing a global QCD analysis used by the CTEQ collaboration.

 A well-defined physical measurable can be written in terms of the convolution of parton distributions and the hard cross sections by the factorization theorem;

$$\sigma_{phy} = f \otimes \hat{\sigma} . \tag{2.73}$$

• The hard cross sections can be calculated order by order in α_s :

$$\hat{\sigma} = \sum_{n} \alpha_s^n \hat{\sigma_n} . \tag{2.74}$$

Parton distributions evolve in μ according to the renormalization group equations;

$$\frac{d}{d\mu^2}\phi = \frac{\alpha_s}{2\pi}P\otimes\phi , \qquad (2.75)$$

where the splitting function P is calculable order by order in α_s .

- Since the initial parton distributions are in a non-perturbative physics regime and not calculable, their initial conditions are parameterized at the scale $\mu = Q_0$ with certain functional forms: $\phi(\mu = Q_0, x) = \phi_0(x)$.
- Λ_{QCD} is needed for the calculation of α_s

With experiments on the one hand and parameter space (e.g. initial parton distribution parameters and Λ_{QCD}) on the other, based on QCD theory, CTEQ performs a least χ^2 fit by adjusting parameters to obtain parton distributions and the corresponding α_s in consistency with data. Most of the modern global analyses [29, 30, 31, 32, 33] use both the hard cross section $\hat{\sigma}$ and the splitting function P in NLO.

Chapter 3

Heavy Quark Production Mechanisms

The QCD parton model we discussed in Chapter 2 allows one to relate the non-calculable hadronic structure functions to the calculable partonic structure functions involving only elementary particles. This is achieved through the factorization theorem which separates the long distance physics from the short distance physics. The conventional QCD factorization theorem works well in one large scale problems such as inclusive deep inelastic scattering where Q^2 of the probing vector boson is the only large scale. However, in the case of heavy quark production, there exists an additional scale — quark mass. For multiple-scale [34] problems like heavy quark production, the conventional approaches are often plagued by large logarithmic terms in the calculations. These large logarithmic terms are the results of ratios among the multiple energy scales associated with the collision process. Since these scales can vary significantly, the logarithmic terms can be very large in some kinematic region. The existence of the large logarithmic terms in calculations often signals a breakdown in the perturbative expansion.

In this chapter, we will discuss various approaches in the heavy quark production calculation and introduce the ACOT scheme [41]. The ACOT scheme is a composite

renormalization scheme applicable over all energy range, and it is an example of resummation methods which have been successfully used to handle the multiple scale problems.

3.1 Heavy Quark Production in Collider Physics

The study of heavy quark production has become an increasingly important area of theoretical and experimental research. It not only provides us with critical new tests of perturbative QCD, but also gives us a tool to probe new physics beyond the Standard Model. By heavy quark, here we mean the quark whose mass m_H is significantly larger than Λ_{QCD} so that perturbative QCD is applicable at its mass scale. In the Standard Model, this includes the charm ($m_c \simeq 1.5 \text{ GeV}$), bottom ($m_b \simeq 5 \text{ GeV}$) and top quarks ($m_t \simeq 175 \text{ GeV}$). The existence of heavy quarks with different masses allows us to probe perturbative QCD in regions of different energy scales, where the relative impact of radiative corrections and non-perturbative effects are very different.

The top quark was discovered by CDF and DØ at the Fermilab Tevatron collider in 1995 [35, 36]. It is the heaviest of the known heavy quarks. The top quark production cross section has roughly the predicted magnitude at Tevatron, and the existing study of the kinematic distributions show qualitative agreements with QCD predictions. More studies are being pursued in top quark physics to further test the underlying strong interaction dynamics and possible new physics. However, in this work, we will not discuss the top quark because its mass is too high for our formalism to make any practical differences from the conventional method.

While there are only a few top quark events found until now, there are plenty of bottom and charm quarks produced at Tevatron and LEP. The electron-proton collider HERA has also begun to produce data on charm photo-production and electroproduction. These experiments provide us an invaluable tool for quantitative QCD study. They can be very useful either as a probe of the nucleon structure, or as a test of perturbative QCD itself at different energy scales. Furthermore, these experiments will help us to search for signals of new physics, or study backgrounds to new physics. For example:

- Charm productions in charged-current interactions in lepton-hadron scattering have been used to probe the strange quark content of the proton and measure the CKM matrix parameter V_{cs} .
- Bottom production cross sections at Tevatron are being extensively studied to improve the reliability of estimations of the b rates at the LHC, where b's can be used to measure CP violation and probe possible b-meson rare decays predicted by several theories beyond the Standard Model.
- Inclusive b production in high energy hadronic collisions are critical to the searches for Higgs at hadronic colliders because the QCD process $gg \to b\bar{b}$ are the main background events to the $H \to b\bar{b}$ process.

Although perturbative QCD theory has been successfully applied to many hard scattering processes at collider energies and most calculations agree well with experimental data, the theoretical results for heavy quark production are not very satisfying [37]. First, the next-to-leading order corrections to the leading order results are very large, in the case of bottom hadroproductions, often up to 50% to 100%. Second, the theoretical results show a strong dependence on the renormalization and factorization scales. The scale dependence for the next-to-leading order (NLO) calculation of the bottom hadroproduction is plotted in Figure 3.1. The dependences are far from being

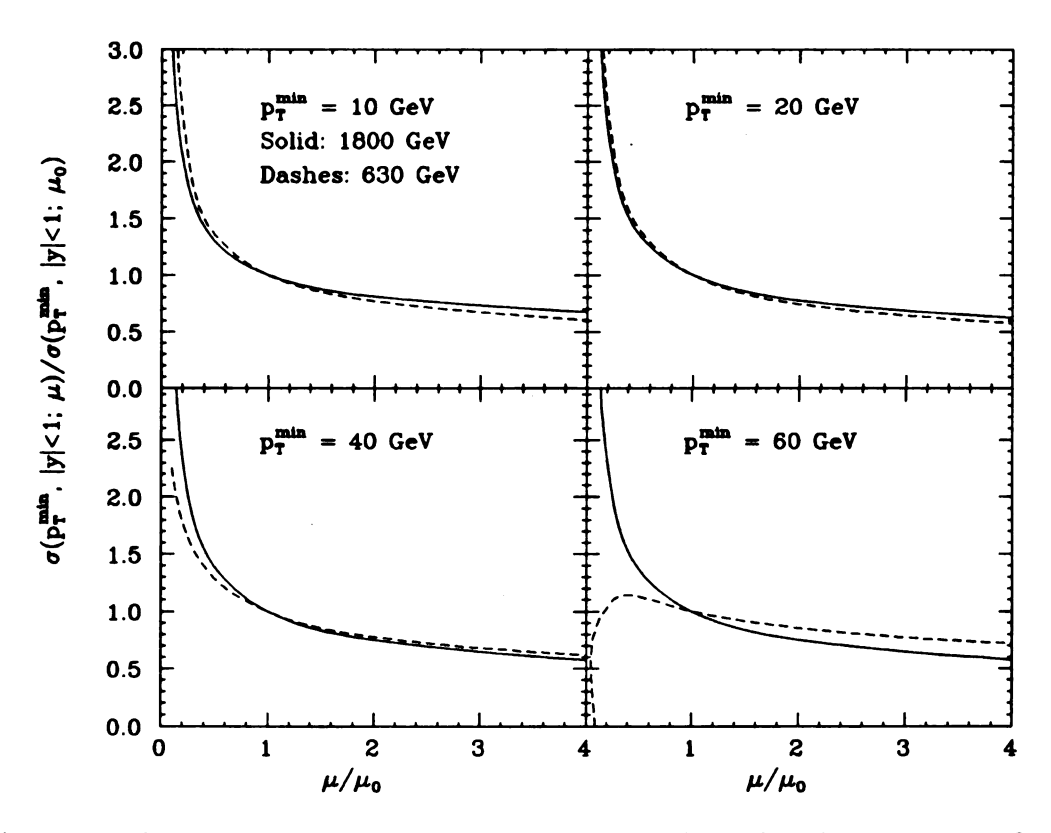


Figure 3.1: Scale dependence of the integrated b-quark p_T distribution at 630 GeV (dashed lines) and at 1800 GeV (solid lines), for different values of p_T^{min} .

flat. Also, the NLO is not flatter than the LO. Third, the experimental data tend to lie on the upper side of the theoretical predications. This can be seen in Figure 3.2 and Figure 3.3 where bottom productions at Tevatron are plotted. Notice the y-axis is in logarithmic scale.

For an easier comparison of the results, the NLO theoretical results and experimental data can be present on a linear scale plot [37] in the form of $\frac{Data}{Theory}$ as in Figure 3.4. In Figure 3.4, we also include the UA1 data. The central line in the figure is the central theoretical prediction result where QCD scale μ is chosen as $\mu_0 = \sqrt{m^2 + p_t^2}$. The upper and lower lines are the upper theory with $\mu = \mu_0/2$ and the lower theory with $\mu = 2\mu_0$ respectively. The dot-dashed straight lines are constant fits to the ratios, weighed by the inverse of the experimental uncertainties.

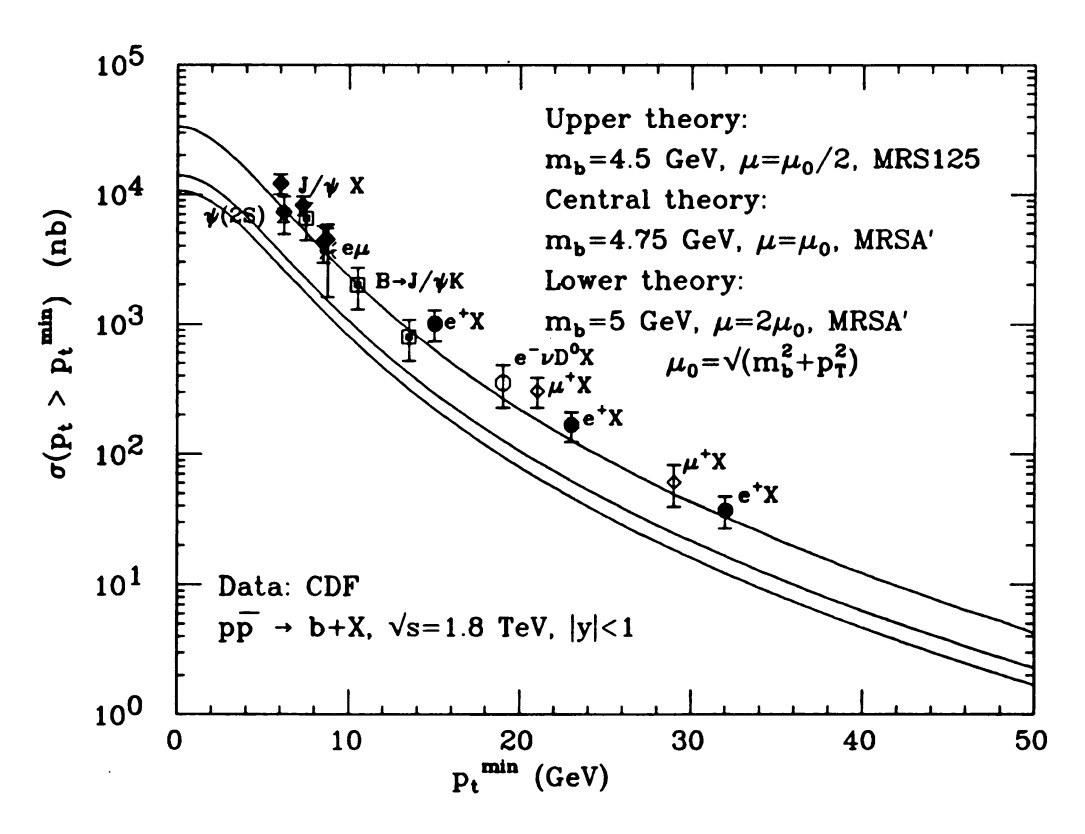


Figure 3.2: CDF data on the integrated b-quark p_t distribution, compared to the results of NLO QCD.

It is easy to see that independently of the beam energy, the data are higher by a factor of about 2 than the default prediction based on $\mu = \mu_o$.

The large next-to-leading order corrections and the significant scale dependence of the NLO results for bottom hadroproductions are symptoms of uncertainties due to neglected large contributions from even higher order processes. The possible existence of large corrections from higher order contributions results in bad convergence of the perturbative expansion and casts doubts on the NLO calculation formalism. In the case of the charm electroproduction where the same conventional perturbative QCD formalism has been used to carry out the NLO calculations, the same kind of problems also exist [37, 38, 39, 40], although the results at the current experimental range are somewhat better behaved than those of bottom hadroproduction shown above.

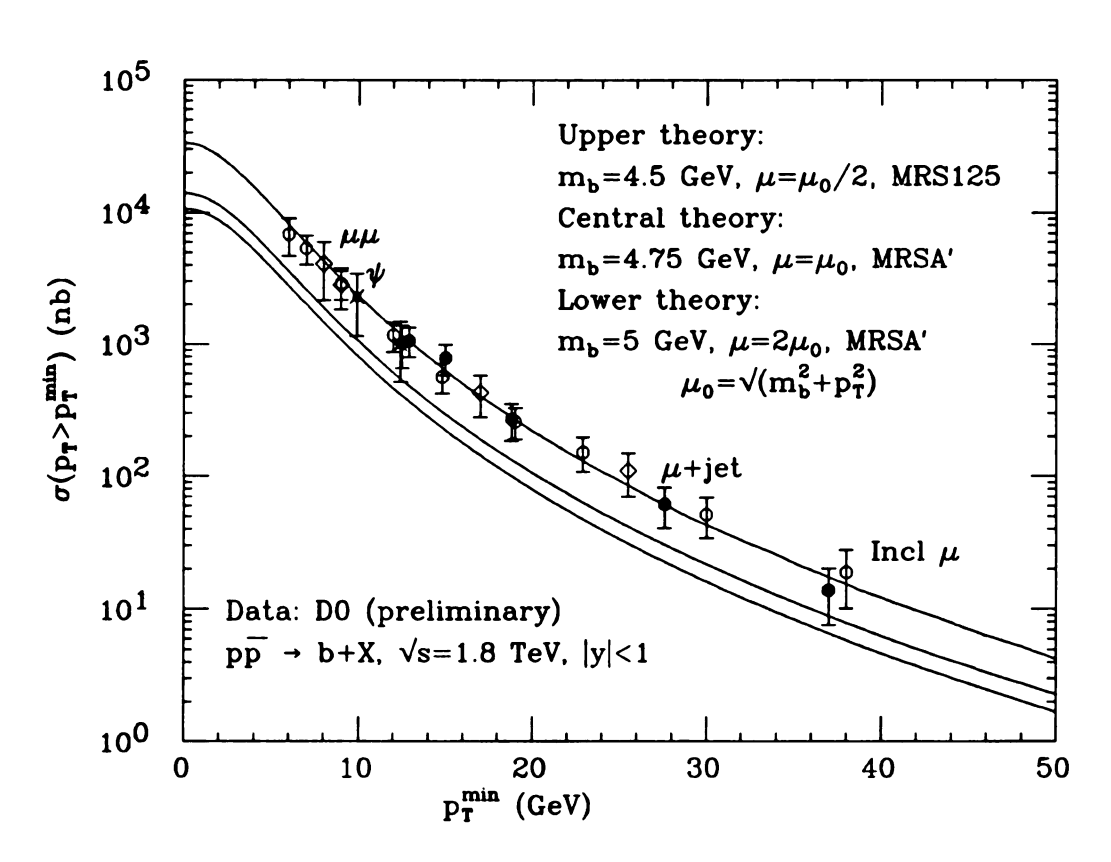


Figure 3.3: D0 data on the integrated b-quark p_T distribution, compared to the results of NLO QCD.

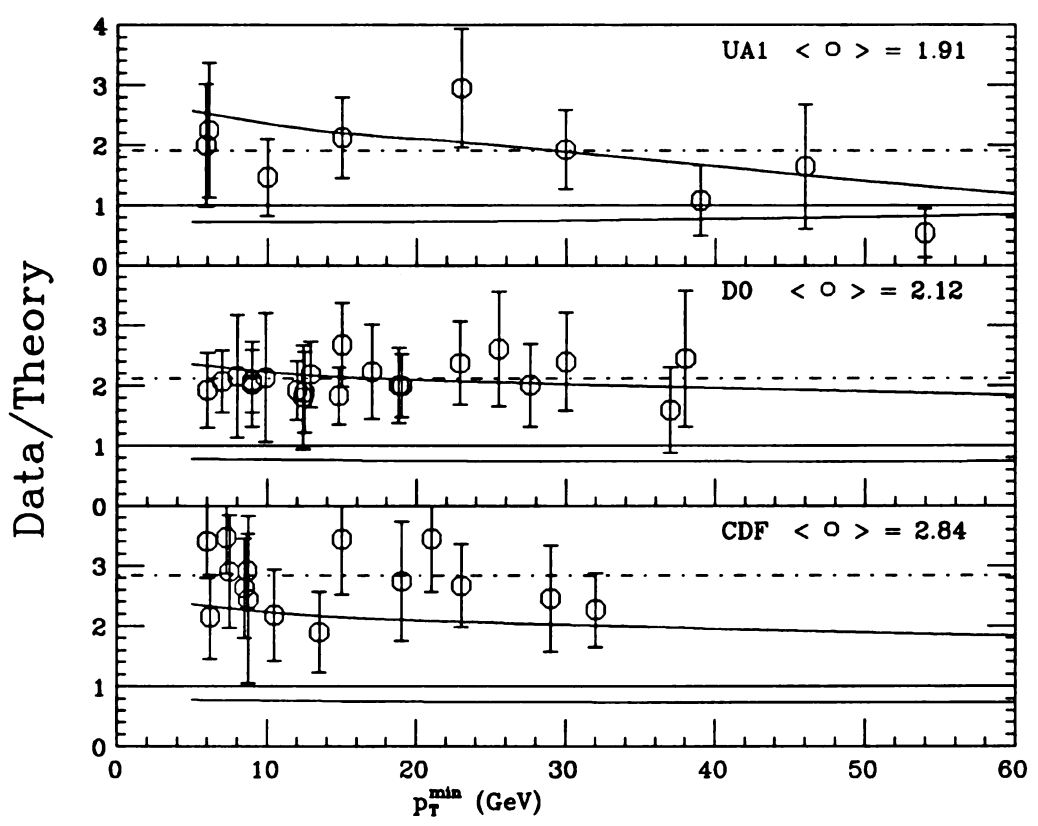


Figure 3.4: Linear comparison between experimental data and theory for the integrated b-quark p_t distribution.

Recent measurements of charm production in the deep inelastic scattering at HERA [43, 44] has shown that charm final states account for up to 25% of the total cross section in the small x region. To study the details of the charm production mechanisms in deep inelastic scattering and extract useful information on the charm and gluon contents of the proton, we must have a more reliable theoretical formalism and calculation than the currently existing conventional QCD results so that we can effectively explore HERA's wide kinematical range. Clearly, the formalism and calculation methods of the conventional perturbative QCD for the heavy quark production must be carefully reexamined [41, 42].

3.2 Conventional Methods for Heavy Quark Production Calculation

For heavy quark production, the existence of the quark mass m_H makes the problem considerably more subtle than that of light parton(jet) production. Conventional perturbative QCD (PQCD) theory is formulated in terms of zero-mass quark-partons. For processes depending on one hard scale such as Q or P_t , the well-known factorization theorem then provides a straightforward procedure for order-by-order perturbative calculations, as well as an associated intuitive parton picture interpretation of the perturbation series. Heavy quark production represents a challenge in PQCD because the heavy quark mass, m_H (H = c, b), provides an additional hard scale which complicates the perturbative series.

The two conventional methods for PQCD calculation of heavy quark processes effectively treat these multiple-scale problems as if they are one-scale problems: (i) in the parton model approach, the zero-mass parton approximation is applied to a heavy quark calculation as soon as the typical energy scale of the physical process (Q) is above the mass threshold m_H , leaving Q as the only hard scale in the problem; and (ii) in the heavy quark approach, the quark H is always treated as a "heavy" particle, the mass parameter m_H is explicitly kept along with Q (as if they are of the same order) and H is never considered as a parton. Clearly, these two treatments represents two diametrically opposite ways of reducing the two-scale problem to a one-scale problem.

In the parton model approach, the cross section for heavy quark production in deep inelastic scattering can be written as

$$\sigma_{lN\to HX} = \sum_{a=active\ partons} \phi_N^a(x,\mu) \otimes \hat{\sigma}_{la\to HX}(\hat{s},Q,\mu)|_{m_a=0}^{\overline{\rm MS}} . \tag{3.1}$$

In Equation 3.1, μ is the factorization and renormalization scale, and Q is the hard

scattering scale set by the probing vector boson. $\hat{\sigma}_{la\to HX}$ is the perturbatively calculable hard cross section for the $l + a \rightarrow H + X$ hard scattering process where lis the incoming lepton, a is the initial parton, H is the final state heavy quark and X represents anything else in the final state. The parton label a is summed over all possible active parton species. In the parton model approach, whether the heavy quark H is included in the sum or not depends on the energy scale μ . For example, in charm quark production, the active partons are u, d, s and g when μ is below the charm mass threshold, however, when μ is above this threshold, charm quark becomes an active parton and the active parton species then include u, d, s, g and c. The masses of the partons in this approach are all set equal to zero, including the heavy quark mass m_H . The advantage of the parton model approach is that it is quite easy to implement. The hard cross section $\hat{\sigma}_{la\to HX}$ is calculated in the limit of zero mass for all the partons, and it is made infra-red safe by dimensional regularization in the $\overline{\rm MS}$ scheme. The parton distribution functions $\phi_N^a(x,\mu)$ are extracted from global analyses. Their μ -dependence is determined by QCD renormalization group equations.

The parton model approach is routinely used in most high energy calculations such as global analysis of parton distributions in EHLQ [46], MRS [45] and CTEQ [31], as well as in all analytic or Monte Carlo programs for generating Standard Model and new physics cross sections. For the light partons $a = \{g, u, d, s\}, m_a \to 0$ is a valid approximation for all hard scale Q (since, by definition, $Q \gg m_a$). However, for a heavy quark H, it is a reasonable approximation only in the high energy regime $\mu \sim Q \gg m_H$; and it clearly becomes unreliable in the intermediate region $Q \sim \mathcal{O}(m_H)$. So this approach can only be reliably applied when $\mu \gg m_H$. In the threshold region, the effects of heavy quark mass cannot be ignored and the zero quark mass approximation becomes questionable. It is because of this reason that for the study of

heavy quark production where the quark mass effects are very important, this method is seldomly used.

The heavy quark approach, on the other hand, treats the heavy quark as a real "heavy" particle that only appears in the final state — much in the same way as top quark is treated. In this approach, only light partons are included in the initial state and the number of parton flavors n_a is kept at a fixed value regardless of the energy scales involved. An important feature of the heavy quark approach is that the heavy quark mass m_H is kept exactly in the hard cross section $\hat{\sigma}_{la\to HX}$. Comparing with Equation 3.1, the cross section for inclusive heavy quark production using this approach can be written as

$$\sigma_{lN\to HX} = \sum_{a=light \ partons \ only} \phi_N^a(x,\mu) \otimes \hat{\sigma}_{la\to HX}(\hat{s},Q, \ m_H,\mu), \tag{3.2}$$

where the sum over parton a only includes light massless partons. For charm production in deep inelastic scattering, no matter what the energy scale is, the partons a only include u, d, s and g and the number of flavor n_a is fixed at 3.

The heavy quark approach is conceptually simple and well defined. The hard cross section $\hat{\sigma}_{ab\to HX}(\hat{s}, Q, m_H, \mu)$ can be calculated order by order with appropriate prescriptions for subtracting various divergences. Broadly speaking, divergences due to the light parton are removed using the $\overline{\text{MS}}$ counter terms, whereas those due to the charm quark are removed using the BPHZ zero-momentum subtraction counter terms. The NLO calculations using the heavy quark approach requires considerable amount of work, but they have been carried out for both electroproduction [38, 39, 40] and hadroproduction [47, 48].

Since the heavy quark approach has played a dominant role in the NLO calculations of the production of heavy quarks, it has been routinely used in most recent heavy quark production phenomenological studies. As expected, this approach works

well when $Q \sim m_H$ because in the mass threshold region, we effectively have a one scale problem. Typically, the perturbative hard cross section $\hat{\sigma}_{la\to HX}$ calculated using the heavy quark approach will contains logarithm factors of the form $\alpha_s^n(\mu) \log^m(\frac{\mu}{m_H})$. When $\mu \sim m_H$, these terms are under control and the perturbative expansion is well behaved. However, when $\mu \gg m_H$, these logarithmic terms become quite large and the perturbative expansion is no longer consistent because the truncated perturbative series in the heavy quark approach has left out important physics effects. Therefore, its predictions should only be reliable over some range of Q^2 . Unfortunately, we do not know a priori how large that range is. Recent estimates [49, 50] comparing the differences between calculations carried out in different schemes, suggest that $Q \sim 20$ GeV marks the limit of this range for electro-production of charm quarks. However, the criterion used is not definitive; the boundary depends necessarily on the process (e.g., charged/neutral current leptoproduction, hadroproduction, etc.) as well as on the variable x. In this situation, the validity of the perturbative expansion using the heavy quark approach becomes questionable. In fact, this has been known since the next-to-leading order (NLO) calculations in the heavy quark approach were completed. As we have seen in Section 3.1 where the NLO results for bottom hadroproductions calculated using the heavy quark approach were quoted, the next-to-leading order corrections are often of the same numerical magnitude as the leading order result, and the uncertainty of the theoretical calculation, as measured by the dependence of the calculated cross section on the unphysical scale parameter μ , is as large in NLO as in LO — contrary to what is expected from a good perturbation expansion. Experimentally, comparisons also show that the measured charm and bottom production cross sections do not agree with the NLO theoretical predictions very well.

A more careful study reveal that the results may not be all that surprising after all. For charm quark and bottom quark production, the condition $\mu \sim m_H$ is not well satisfied in most collider experiments. In fact, the current experimental range for the lepto- and hadro-production of those heavy quarks mostly lie in a region between those appropriate for the parton model approach $(\mu \gg m_H)$ and the heavy quark approach $(\mu \sim m_H)$. To make reliable predictions and study the QCD mechanisms about heavy quark productions in detail, a well defined theory which can be applied over the full energy scale is needed.

The clue for solving this problem can be obtained from examining the conventional massless QCD theory. In the heavy quark approach, when $Q\gg m_H$, the logarithmic terms in $\hat{\sigma}$ become large and are infra-red unsafe. The "mass singular" term as $\frac{Q}{m_H}\to\infty$ for heavy quark is equivalent to $m_H\to 0$ in the massless QCD theory. In massless QCD theory, these infra-red unsafe terms are resumed into parton distribution functions [22, 23, 24]. The same method of resummation can also be applied in heavy quark production: The large logarithms of the form $\alpha_s^n \ln^m(\frac{\mu}{m_H})$ can be resumed to all orders in α_s into the parton distribution function $\phi_N^H(x,\mu)$ for the heavy quark H. After the resummation, the H parton should be included in the sum over parton flavors — it participates in the hard scattering on the same footing as the other partons. Also, the infra-red unsafe large logarithmic terms are subtracted from the hard scatter cross section $\hat{\sigma}$ and the remaining hard cross section becomes infra-red safe as $\frac{Q}{m_H}\to\infty$. This observation leads to a natural solution of heavy quark production problem over the full energy range — the ACOT scheme [41].

In the following sections, we will focus the discussion on charm neutral current production in deep inelastic scattering, although the discussion and method apply to other heavy quark productions as well. We will use γ^* to refer γ^* and Z boson generically. First, we will define two simple renormalization schemes for charm electroproduction, the three-flavor scheme and the four-flavor scheme. Then, we will define the ACOT scheme, which is actually a composite scheme composed of the

three-flavor scheme and the four-flavor scheme.

3.3 The Three-flavor Scheme

The 3-flavor scheme is an example of the application of the heavy quark approach to the problems of charm quark production. This scheme is the one used in Reference [38, 39, 40, 51] to calculate charm production to NLO, i.e. $\mathcal{O}(\alpha_s^2)$. It is precisely defined by choosing to work with only 3 active quark flavors, consisting of the light quarks, and using the subtraction procedure of Reference [52]. The prescription for subtracting ultra-violet divergences encountered in the calculation of the partonic structure functions and distribution functions depends on the particle that produces the divergence. Divergences involving the light partons a are removed using the $\overline{\text{MS}}$ counter terms, whereas those involving the charm quark c are removed by the BPHZ zero-momentum subtraction counter terms. This ultra-violet subtraction scheme has the nice feature that the charm quark explicitly decouples as its mass becomes large. In particular, the operators which make up the charm quark distribution function are suppressed by powers of order Λ^2/m_c^2 . Since these terms are power-suppressed in the "heavy quark" mass, they are usually excluded from the 3-flavor scheme parton picture, which usually represents leading-twist dynamics.

In practice then the partonic calculations in this scheme are done by considering only diagrams with the massive charm quark in the final state and no charm quark distribution functions in the initial state. The light parton distributions always evolve according to the 3-flavor GLAP equation, irrespective of the renormalization scale μ . The parton distribution functions defined in this scheme will be restricted to the light parton a, $(a, a' = g, q, \bar{q})$, sector, and they will be denoted by ${}^3\phi_N^a$. In the perturbative calculation, the perturbative partonic distribution functions ${}^3\tilde{\phi}_a^{a'}$ contain ϵ^{-1} pole

terms which are due to collinear singularities. The lowest order (LO, $\mathcal{O}(\alpha_s^1)$) process contributing to the calculation of the partonic structure functions in this scheme, to be denoted by $\sigma_g^{c\bar{c}}$, is the $\gamma^*g \to c\bar{c}$ "heavy-flavor creation" (HC) process (also known as boson-gluon fusion), corresponding to the diagrams of Fig.(3.5a). It is finite. The next-to-leading order (NLO) contribution consists of the 1-loop virtual corrections to $\gamma^*g \to c\bar{c}$ (cf. Fig.(3.5b)), plus the real partonic HC processes $\gamma^*g \to c\bar{c}g$ (cf. Fig.(3.5c)) and $\gamma^*a \to c\bar{c}a$ (cf. Fig.(3.5d)). The collinear divergences which appear in the calculation of the $\mathcal{O}(\alpha_s^2)$ partonic structure functions ${}^3\sigma_g^{c\bar{c}}g$ and ${}^3\sigma_a^{c\bar{c}a}$ arise from splitting of massless light partons in the collinear configuration, and take the form of ϵ^{-1} pole terms, precisely corresponding to those appearing in ${}^3\tilde{\phi}_a^{c'}$ mentioned above. That is, the partonic structure functions have the factorized structure shown in Equation 3.2, and the hard cross section functions $\hat{\sigma}_a$ will be free from ϵ^{-1} collinear singularities.

As mentioned in the last section, hard cross sections calculated in this scheme contain powers of $\ln(Q^2/m_c^2)$. The perturbative expansion should be accurate at energy scales not too far above threshold, or $Q^2 \sim m_c^2$, where $\ln(Q^2/m_c^2)$ is of order 1. However, at high $Q^2 \gg m_c$ the perturbative expansion parameter is effectively $\alpha_s \ln(Q^2/m_c^2)$, and the large logarithm factor spoils the convergence of the perturbative series. In other words, the "hard cross sections" $\hat{\sigma}_a$ defined in this scheme are finite, but not infra-red safe in the limit $\frac{m_c}{Q} \to 0$ — they contain "mass singularities" in this sense.

3.4 The Four-flavor Scheme

In order to better deal with the large logarithms at high energies associated with mass singularities, it is more useful to use the 4-flavor scheme. In this scheme the

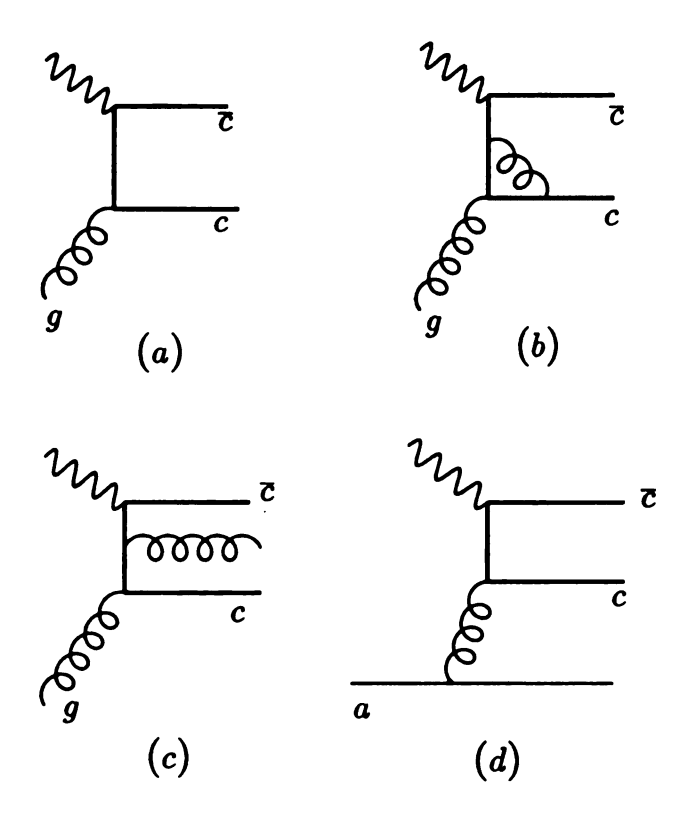


Figure 3.5: Three-flavor scheme production mechanism. (a) is $\gamma^* + g \to c + \overline{c}$ process(heavy quark creation: HC), (b) is one loop $\gamma^* + g \to c + \overline{c}$ process, (c) is $\gamma^* + g \to g + c + \overline{c}$ process, (d) is $\gamma^* + a \to a + c + \overline{c}$ process. Only one diagram for each process is plotted.

renormalization of σ_a and the perturbative partonic function $\tilde{\phi}_a^b$, $(a,b=g,q,\bar{q},c)$ is carried out using dimensional regularization and the $\overline{\rm MS}$ counter terms for all Feynman diagrams, while keeping the full quark mass dependence in the Lagrangian.

Charm distribution functions calculated in this scheme, ${}^4\tilde{\phi}^c_a$ are not suppressed as in the 3-flavor scheme, but contain powers of $\ln(m_c/\mu)$, along with possible ϵ^{-1} poles. Because of the different subtraction procedures used in the two schemes, even the light parton distributions ${}^4\tilde{\phi}'_l$, $l,l'=q,\bar{q},g$ will differ from ${}^3\tilde{\phi}'_l$ by a finite renormalization in general. Because renormalization constants in the $\overline{\rm MS}$ subtraction procedure are independent of mass, the evolution kernels for the ${}^4\tilde{\phi}^b_a$ parton distributions will be the same as the corresponding ones in the familiar zero-mass 4-flavor case. This is

a significant convenience. The perturbative parton distribution functions ${}^4\tilde{\phi}^b_a$ have been calculated to NLO in Reference [50].

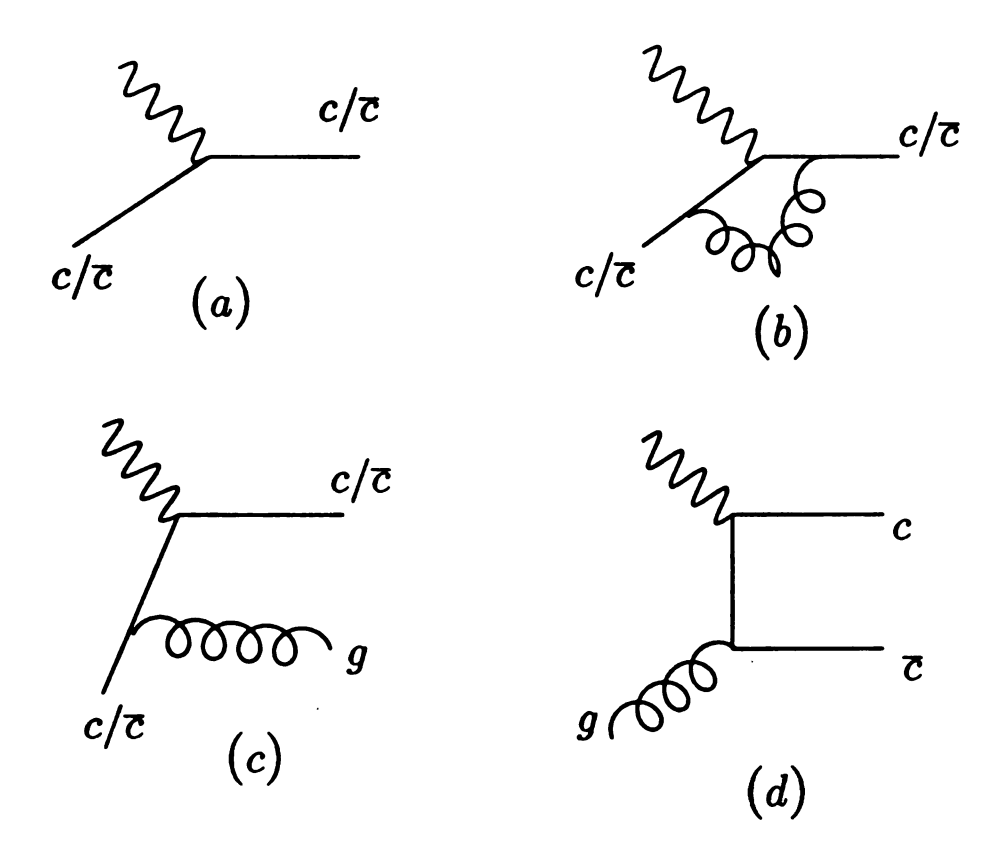


Figure 3.6: Four flavor production processes. (a) is $\gamma^* + c/\overline{c} \to c/\overline{c}$ process(heavy quark excitation: HE), (b) is one loop $\gamma^* + c/\overline{c} \to c/\overline{c}$ process, (c) is $\gamma^* + c/\overline{c} \to g + c/\overline{c}$ process. (d) is $\gamma^* + g \to c + \overline{c}$ process (heavy quark creation: HC), Only one diagram for each process is shown.

Since charm also has a parton interpretation in this scheme, the set of partonic processes are expanded to include those involving charm initial states. The LO partonic process in the 4-flavor scheme is the $\gamma^*c \to c$ "heavy-quark excitation" (HE) process (Fig.(3.6a)). NLO contributions to charm production in the 4-flavor scheme come from the 1-loop virtual corrections to HE $\gamma^*c \to c$ (Fig.(3.6b)), and from the real HE $\gamma^*c \to gc$ and HC $\gamma^*g \to c\bar{c}$ processes (Fig.(3.6c,d)). Partonic cross sections σ_a calculated beyond LO in this subtraction scheme will contain, as in the 3-flavor scheme, both ϵ^{-1} poles due to collinear singularities associated with light degrees

of freedom and powers of $\ln(Q/m_c)$ due to collinear configurations associated with the heavy degree of freedom. The important difference compared to the 3-flavor case, is: these potentially large logarithm terms also appear in the 4-flavor parton distributions ${}^4\tilde{\phi}_a^b$. Hence, they will be systematically subtracted out from σ_a when we evaluate the hard cross sections $\hat{\sigma}_a$ As a result, $\hat{\sigma}_a$ will be free from both types of collinear "singularities" (in quotes since the logarithms become singular only in the zero-mass limit). In effect, all logarithmic factors $\ln(Q/m_c)$ in σ_a will be replaced by $\ln(Q/\mu)$ in $\hat{\sigma}_a$ (with accompanying finite subtractions), and the latter is infra-red safe in the $\frac{m_c}{Q} \to 0$ limit. Thus, the 4-flavor scheme has a well-defined high energy limit, and is expected to give a much more reliable description of the physics of charm production at large Q than the 3-flavor scheme.

As formulated above, the hard cross sections still contain finite charm-mass dependence, i.e. $\hat{\sigma}_a = \hat{\sigma}_a(x, \frac{Q}{\mu}, \frac{m_c}{Q}, \mu)$. Being infra-red safe, the limit $\hat{\sigma}_a(x, Q, m_c, \mu) \rightarrow \hat{\sigma}_a^{m_c=0}(x, Q, \mu)$ as $m_c/Q \rightarrow 0$ is well defined. In this limit, the 4-flavor scheme with non-zero charm mass reduces to the conventional parton model scheme. As emphasized in Reference [41], however, the factorization of potentially dangerous $\ln(m_c)$ terms does not require taking the $m_c \rightarrow 0$ limit in the infra-red safe coefficient functions. The conventional practice of always setting $m_c = 0$ in the hard cross section $\hat{\sigma}_a(x,Q,\mu)$ is a convenience, not a necessity; it results from the use of dimensional regularization of the zero-mass theory as a simple way to classify and to remove the collinear singularities. For a "heavy quark" with non-zero mass m_c , this convenient method of achieving infra-red safety is not a natural one (as it is for light flavors), since m_c itself already provides a natural cutoff. In other words, the theory has no real collinear "singularities" associated with the charm quark, and the universal (i.e. process-independent) and potentially large mass-logarithms can be factorized systematically as outlined above. In fact, by keeping the charm quark mass dependence,

this scheme can be extended down to lower values of Q with much more reliable results than in the zero-mass case—it has the built-in characteristics to approximate the 3-flavor calculation in the region above threshold [41, 53].

Since the charm quark distributions are explicitly included in the 4-flavor scheme, and since m_c is not much larger than a typical non-perturbative scale such as the nucleon mass, one can allow for the existence of a possible nonperturbative ("intrinsic") charm component inside a hadron at a low energy scale, say Q_0 — as the boundary condition for evolution to higher scales, just like the other light flavors. This is a possibility not permitted in the 3-flavor scheme by assumption.

3.5 The Composite Scheme — The Unified Approach to Charm Production

Both the 3-flavor and the 4-flavor schemes described above are valid schemes for defining the perturbative series of charm production in principle. They are equivalent if both are carried out to all orders in the perturbation series. At a given finite order, they differ by a finite renormalization of the parton distribution functions, as well as the strong coupling α_s . From the physics point of view, the 3-flavor scheme provides a more natural and accurate description of the production mechanism near the threshold $(Q^2 \sim m_c^2)$, whereas the 4-flavor scheme does the same in the high energy regime $(Q^2 \gg m_c^2)$.

It becomes obvious then that a unified program to calculate charm production must involve a composite scheme consisting of: (i) the 3-flavor scheme, applied in the threshold region; (ii) the 4-flavor scheme, applied at higher energy scales; and (iii) a set of matching conditions to effect the transition between the two schemes at an intermediate scale (say, μ_c) where they are comparable to each other. The existence

of an appropriate transition region, where the difference between the two schemes is small (i.e. it is of a higher order in α_s with no large logarithms), is important. As demonstrated in Reference [41] and mentioned above, the 4-flavor scheme has the required feature of approximating the 3-flavor scheme results as $Q \to m_c$ from above; whereas the conventional parton model approach does not. The transition from the 3-flavor to the 4-flavor scheme involves performing the requisite finite renormalization ("matching") on α_s and ϕ_N^a at some scale $\mu = \mu_c$, and using the appropriate α_s , ϕ_N^a and $\hat{\sigma}_a$ in the cross section calculation in the two respective regions.

This composite scheme described above constitutes the ACOT scheme [41]. It was implemented at the order α_s^1 level in Reference [41], and now rigorously established in Reference [53]. It is a more precise formulation of the commonly accepted zero-mass parton picture with effective quark flavor number increasing with the energy scale—hence the often used term "variable-flavor-number" scheme. As emphasized above, it is more precisely a composite scheme, consisting of two simple schemes with different numbers of active quark flavors, and a set of appropriate matching conditions.

Formally, the ACOT procedure is based on the CWZ renormalization scheme [52] which provides a natural transition from the mass threshold region $\mu \sim O(m_H)$ to the high energy region $\mu \gg m_H$. To switch from one region to another across the threshold, finite renormalization matching conditions are needed to make the schemes equivalent in the domain of overlap $\mu \sim m_H$ region where they are equally valid for practical low order calculations. The transition between two schemes can, in principle, be carried out at any scale $\mu \sim m_H$. The explicit formulas of the finite renormalization coefficients [54, 55, 50] are:

$${}^{4}\alpha_{s}(\mu) = {}^{3}\alpha_{s}(\mu) \left[1 - \frac{{}^{3}\alpha_{s}(\mu)}{6\pi} \ln \frac{m_{c}^{2}}{\mu^{2}} + \mathcal{O}(\alpha_{s}^{2}) \right]$$
(3.3)

and

$${}^{4}\phi_{N}^{q}(x,\mu) = {}^{3}\phi_{N}^{q}(x,\mu) + 0 + \mathcal{O}(\alpha_{s}^{2})$$

$${}^{4}\phi_{N}^{g}(x,\mu) = {}^{3}\phi_{N}^{g}(x,\mu) + \frac{{}^{3}\alpha_{s}(\mu)}{6\pi} \ln \frac{m_{c}^{2}}{\mu^{2}} {}^{3}\phi_{N}^{g}(x,\mu) + \mathcal{O}(\alpha_{s}^{2})$$

$${}^{4}\phi_{N}^{c}(x,\mu) = 0 + \frac{{}^{3}\alpha_{s}(\mu)}{4\pi} \ln \frac{\mu^{2}}{m_{c}^{2}} \int \frac{dz}{z} (z^{2} + (1-z)^{2}) {}^{3}\phi_{N}^{g}(\frac{x}{z},\mu) + \mathcal{O}(\alpha_{s}^{2})$$

$$(3.4)$$

The ACOT scheme is defined to keep all infra-red safe m_H -dependent effects in the hard cross sections so that there is no loss of accuracy when $\mu \sim m_H$. This is accomplished by defining $\hat{\sigma}_{la\to HX}(\hat{s},Q,m_H,\mu)$ as the full $\sigma_{la\to HX}(\hat{s},Q,m_H,\mu)$ with mass m_H singularities subtracted.

The ACOT scheme is designed to be applicable over all energy range. It coincides with those of the three-flavor scheme in its region of applicability, $\mu \sim m_H$, and reduces to those of the four-flavor scheme model in the asymptotic energy regime $\mu \gg m_H$. In the middle region where μ is larger but not far larger than m_H , the quark mass effects are kept in a consistent manner and the ACOT scheme provides a good approximation to the physical cross section. Furthermore, when the finite terms in the logarithmic resummation are properly calculated, the ACOT scheme will agree with the zero-mass parton approach in the limit of $m_H \to 0$. We will present the detailed implementation of the ACOT scheme and its applications in the next two chapters.

Chapter 4

Implementation of the ACOT Scheme Calculation

In this chapter, we will apply the ACOT scheme to the problem of charm quark production in deep inelastic scattering. This scheme has been applied, at leading order, to the total inclusive structure functions by M. Aivazis et. al. [56, 41]. To effectively study heavy quark production mechanisms and extract useful informations about the charm and gluon contents of the proton from experimental data, both higher order calculations and some differential distributions are needed. Higher order calculations are necessary because these contributions can not only give us better theoretical predictions to compare with experiments, but also give us an indication how well the perturbative expansion converges in the theory, which will be an important self-consistency test. Differential cross section distributions are important because these results will help us to further study and differentiate different heavy quark production mechanisms and probe possible intrinsic charm contents inside the proton.

In this work, we will implement the next logical extension of the ACOT scheme calculation — we will extend the calculation to include all contributions at order $O(\alpha_s)$. We will also extend the calculation to include differential distributions. This

is done by using the phase-space splicing method to separate different kinematic regions, and the Monte Carlo numerical integration method to handle the phase space integration. Also to compare with experimental data, fragmentation functions for the final state charm quark will be introduced to evolve the quarks into mesons. While the formalism is applicable to both charged current interactions and neutral current interactions, we will focus on charm deep inelastic scattering production in neutral current interactions, especially at HERA.

4.1 The Calculation Formalism

For the calculations of heavy quark production in the deep inelastic scattering

$$l_1(k) + N(P) \to l_2(k') + H(p') + X(P_X)$$
, (4.1)

the factorization theorem [57, 53] states that the dominant contributions to the hadronic cross section have the factorized form of Figure 4.1 with

$$d\sigma^{l_1N \to l_2HX}(q, P, m_H, \cdots) = \phi_N^a \otimes d\hat{\sigma}^{l_1a \to l_2HX}$$

$$= \int_0^1 d\xi \phi_N^a(\xi, \mu) \ d\hat{\sigma}^{l_1a \to l_2HX}(k, q, \mu^2, \alpha_s(\mu), m_H, \cdots)$$

$$= \frac{1}{2\Delta(s, M_N^2, 0)} \int \frac{d\xi}{\xi} \phi_N^a(\xi, \mu^2) |M_a|^2 d\Gamma, \tag{4.2}$$

In Equation 4.2, M_a is the hard scattering matrix element and $2\Delta(s, M_N, 0)$ is the flux factor with $\Delta(a, b, c) = \sqrt{(a^2 + b^2 + c^2 - 2ab - 2bc - 2ac)}$. The label 'a' is summed implicitly over all active parton species. In the ACOT scheme, whether the heavy quark H is included or not depends on the energy scale μ — In the three-flavor scheme region where $\mu < \mu_{threshold}$, a includes u, d, s and g, whereas in the four-flavor scheme region where $\mu > \mu_{threshold}$, a includes u, d, s, c and g. The threshold parameter $\mu_{threshold}$ should be in the region where both the three-flavor scheme and

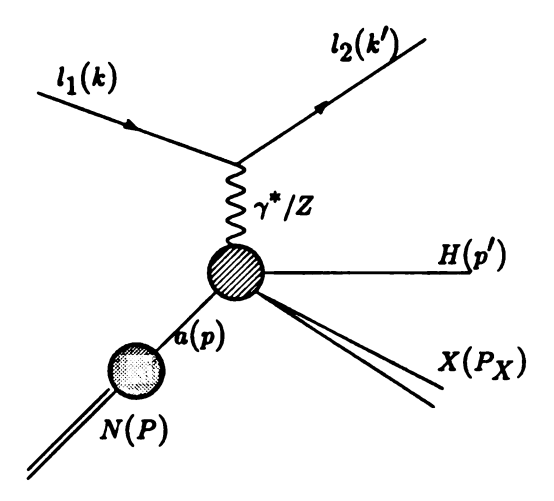


Figure 4.1: The factorization for the deep inelastic scattering

the four-flavor scheme are valid for practical calculations. The heavy quark mass dependence is kept in $d\hat{\sigma}$ after the factorization of the large logarithmic terms.

In Equation 4.2, the phase space factor $d\Gamma$ is

$$d\Gamma = (2\pi)^4 \delta^4(p + k - k' - p' - \sum p'_x) \frac{d^3k'}{(2\pi)^3 2k'_0} \frac{d^3p'}{(2\pi)^3 2E'} \Pi \frac{d^3p'_x}{(2\pi)^3 2E'_x} . \tag{4.3}$$

Using the kinematic variables defined in Equation 2.14, we can simplify the lepton phase space factor $\frac{d^3k'}{(2\pi)^32k'_0}$. Then the cross section becomes

$$d\sigma = \frac{y}{32\pi^2} dx dy \frac{d\phi}{2\pi} \int \frac{d\xi}{\xi} \phi_N^a(\xi) |M_a|^2 d\Gamma', \qquad (4.4)$$

where

$$d\Gamma' = (2\pi)^4 \delta^4(p + q - p' - \sum p_x') \frac{d^3 p'}{(2\pi)^3 2E'} \Pi \frac{d^3 p_x'}{(2\pi)^3 2E_x'} . \tag{4.5}$$

As described in Chapter Two, the leptonic factor can be factored out from the cross section $d\hat{\sigma}^{l_1N\to l_2HX}$ and $d\hat{\sigma}^{l_1a\to l_2HX}$. The factorization theorem for heavy quark production in the deep inelastic scattering can then be written in terms of hadronic tensor structure function

$$W^{VN o HX}_{\mu
u}(q, P, m_H, \cdots) = \sum_a \phi^a_N \otimes \hat{\omega}^{Va o HX}_{\mu
u}$$

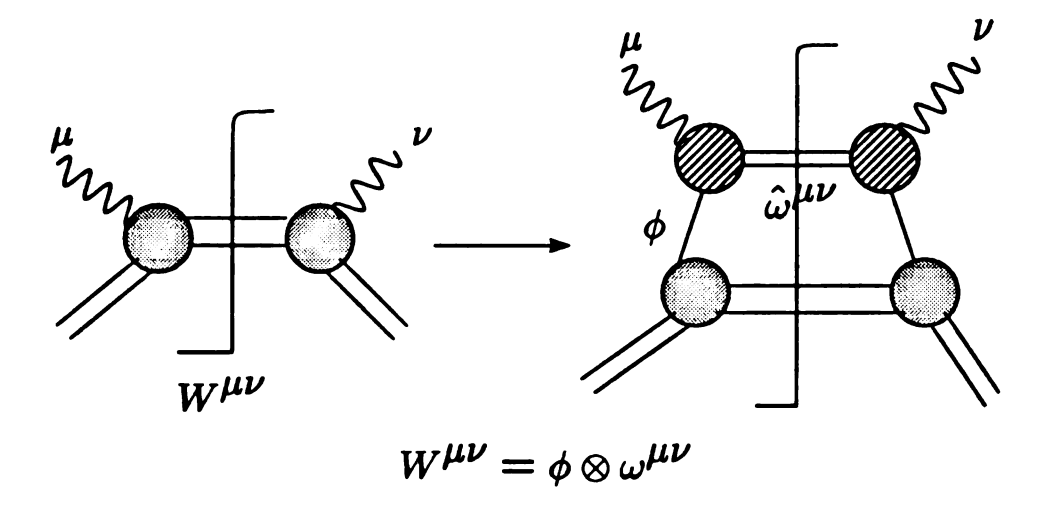


Figure 4.2: The factorization of the structure functions

$$= \sum_{a} \int_{0}^{1} \frac{d\xi}{\xi} \phi_{N}^{a}(\xi, \mu) \, \hat{\omega}_{\mu\nu}^{Va \to HX}(k_{1}, q, \mu^{2}, \alpha_{s}(\mu), m_{H}, \cdots)$$
(4.6)

as depicted in Figure 4.2.

Writing the hadronic tensor $W^{\mu\nu}$ and the partonic tensor $\omega^{\mu\nu}$ in terms of the structure functions as in Equation 2.8 and substituting them into Equation 4.6, we can obtain the relations between the hadronic invariant functions W_i and the partonic invariant functions ω_i based on the relation between the hadronic momentum P^{μ} and the partonic momentum p^{μ} . In the case of massless parton and massless hadron target, $p^{\mu} = \xi P^{\mu}$, and the relations between W_i and ω_i are simply

$$W_{i}^{VN\to HX}(q, P, \cdots) = \sum_{a} \int_{0}^{1} \frac{d\xi}{\xi} \phi_{N}^{a}(\xi, \mu) \omega_{i}^{Va\to HX}(p, q, m, \mu, \alpha_{s}(\mu), \cdots), \quad i = 1, 2, 3$$
(4.7)

However, because of the existence of the quark mass in heavy quark production, when the initial state parton a is a heavy quark, its four-momentum p^{μ} is not proportional to the proton momentum P^{μ} . Thus, equation 4.7 is not applicable. In this case, since the vectors P, p and q are collinear, p can be parameterized as

$$p^{\mu} = \xi_P P^{\mu} + \xi_q q^{\mu} , \qquad (4.8)$$

where ξ_P and ξ_q are rather complicated functions of the masses and the convolution variable ξ . As a result of this heavy quark mass effect, the relation between the W_i and the ω_i is rather complicated and it has a general form of

$$W_{i}^{VN\to HX}(q, P, ...) = \sum_{a} \int_{0}^{1} \frac{d\xi}{\xi} \phi_{N}^{a}(\xi, \mu) \times c_{j}^{i} \times \omega_{j}^{Va\to HX}(p, q, m, \mu, \cdots) \quad i = 1, 2, 3$$
(4.9)

where c_j^i are complicated coefficient functions of relevant kinematic variables [56].

A much better way to express the hadronic and partonic tensors in the presence of non-zero mass quarks is to use the helicity structure functions, which are defined as

$$F_{\lambda} = \epsilon_{\lambda}^{\mu*}(P, q) W_{\mu\nu}(P, q, \cdots) \epsilon_{\lambda}^{\nu}(P, q) \tag{4.10}$$

and

$$f_{\lambda} = \epsilon_{\lambda}^{\mu*}(p, q)\omega_{\mu\nu}(p, q, \cdots)\epsilon_{\lambda}^{\nu}(p, q), \tag{4.11}$$

for the hadron and parton respectively. ϵ^{λ} , $\lambda = +, 0, -$, is the polarization vector of the probing vector boson.

To relate F_{λ} with f_{λ} , the relations between the $\epsilon_{\lambda}^{\mu}(P,q)$ and $\epsilon_{\lambda}^{\mu}(p,q)$ must be obtained first. This is where the simplification of the helicity approach comes from — the two sets of polarization vectors $\epsilon_{\lambda}^{\mu}(P,q)$ and $\epsilon_{\lambda}^{\mu}(p,q)$ are identical even in the presence of nucleon and parton masses. The reason for this equivalence is that the polarization vectors for a vector boson with momentum q only depends on the plane defined by q and a reference momentum, which in this case can be either p or p. Since p and p and p and p and p define the same plane, p and p

$$\epsilon_{\lambda}^{\mu*}(P,q) \cdot W_{\mu\nu}^{VN \to HX} \cdot \epsilon_{\lambda}^{\nu(P,q)} = \sum_{a} \phi_{N}^{a} \otimes \left(\epsilon_{\lambda}^{\mu*}(p,q) \cdot \hat{\omega}_{\mu\nu}^{Va \to HX} \cdot \epsilon_{\lambda}^{\nu}(p,q) \right) \tag{4.12}$$

or,

$$F_{\lambda}(P,q,\ldots) = \sum_{a} \int_{0}^{1} \frac{d\xi}{\xi} \phi_{N}^{a}(\xi,\mu) f_{\lambda}(p,q,\ldots)$$
 (4.13)

As shown in Equation 4.13, the helicity structure functions have a much simpler factorization form than the invariant structure functions.

Using the helicity method will not only enable us to use the simple factorization formula, but also simplify the calculation of the scattering matrix elements. In the hadron sector, the helicity method is able to take full advantage of the basic chiral coupling between the vector boson and the quark and utilize the symmetries among different helicity scattering amplitudes. In the lepton sector, the helicity approach results in a very simple form of the lepton current because of the simple lepton vertex function and the helicity conservation of massless leptons. For neutral current interactions, considering the two possible helicities of the incoming lepton (L, R for electron, L for neutrino, and R for anti-neutrino) separately enables us to separate the lepton sector and parton sector at the amplitude level and add the contributions of the photon and the Z boson coherently. For charged current interactions, the separation is natural because the W boson only couples to the left chiral currents.

Upon the separation of the left and right handed incoming lepton currents and extraction of a factor of $\frac{e^2}{Q^4}$ from the matrix element, the chiral coupling of the vector bosons (γ^*, Z) to the quark in neutral current interactions can be written as $-ie\gamma^{\mu}g_a^b$ where a=qL,qR labels the left and right chiral couplings of the quark to the neutral bosons and b=eL,eR labels the left and right handed incoming lepton currents. g_a^b can be obtained as the following:

$$g_{qL}^{eL} = Q_q - \left(\frac{-\frac{1}{2} + \sin^2 \theta_W}{\sin \theta_W \cos \theta_W}\right) \left(\frac{Q^2}{Q^2 + M_Z^2}\right) \left(\frac{T_{3q} - Q_q \sin^2 \theta_W}{\sin \theta_W \cos \theta_W}\right)$$

$$g_{qR}^{eL} = Q_q - \left(\frac{-\frac{1}{2} + \sin^2 \theta_W}{\sin \theta_W \cos \theta_W}\right) \left(\frac{Q^2}{Q^2 + M_Z^2}\right) \left(\frac{-Q_q \sin^2 \theta_W}{\sin \theta_W \cos \theta_W}\right)$$

$$g_{qL}^{eR} = Q_q - \left(\frac{\sin^2 \theta_W}{\sin \theta_W \cos \theta_W}\right) \left(\frac{Q^2}{Q^2 + M_Z^2}\right) \left(\frac{T_{3q} - Q_q \sin^2 \theta_W}{\sin \theta_W \cos \theta_W}\right)$$

$$g_{qR}^{eR} = Q_q - \left(\frac{\sin^2 \theta_W}{\sin \theta_W \cos \theta_W}\right) \left(\frac{Q^2}{Q^2 + M_Z^2}\right) \left(\frac{-Q_q \sin^2 \theta_W}{\sin \theta_W \cos \theta_W}\right) . \tag{4.14}$$

In Equation 4.14, Q_q is the fraction charge of the quark, T_{3q} is the quark's third component of the weak isospin, and θ_W is the weak angle. The coupling g_a^b effectively adds the photon and Z boson contributions to the hadron current at the amplitude level after the lepton currents are factored out.

For a polarized incoming lepton beam with left and right polarization p_L and p_R $(p_L + p_R = 1)$ respectively, the cross section 4.4 can be reorganized into

$$d\sigma = \frac{e^2 y}{32\pi^2 Q^4} dx dy \frac{d\phi}{2\pi} \int \frac{d\xi}{\xi} \phi_N^a(\xi)$$

$$\left(p_L * |j_L^{\mu} J_{a\mu}^L|^2 + p_R * |j_R^{\mu} J_{a\mu}^R|^2 \right) d\Gamma', \tag{4.15}$$

where the lepton currents are

$$j_L^{\mu} = \langle k' - | \gamma^{\mu} | k - \rangle$$

 $j_R^{\mu} = \langle k' + | \gamma^{\mu} | k + \rangle$ (4.16)

and L, R denotes the lepton's left and right handed helicity.

The lepton current can be expanded directly in terms of the vector boson polarization vectors if they are defined in the same plane. However, in this work, we will define the polarization vectors ϵ_i^{μ} of the vector boson in the boson and proton collinear frame with either (q, P) or (q, p) as the reference momenta. Generally, we assume the hadron sector is in x-z plane and the angle between the hadron current plane and the lepton current plane is $\tilde{\phi}$. Then the polarization vectors defined in the hadron plane can be rotated to the lepton sector plane and becomes

$$\epsilon_0^{\mu}(P,q) = \frac{(-q^2)P^{\mu} + (P \cdot q)q^{\mu}}{\sqrt{(-q^2)[(P \cdot q)^2 - q^2P^2]}}$$

$$\epsilon_{q}^{\mu}(P,q) = \frac{q^{\mu}}{\sqrt{-q^{2}}}$$

$$\epsilon_{+}^{\mu}(P,q) = \frac{e^{-i\tilde{\phi}}}{\sqrt{2}}(0,+1,-i,0)$$

$$\epsilon_{-}^{\mu}(P,q) = \frac{e^{+i\tilde{\phi}}}{\sqrt{2}}(0,+1,+i,0). \tag{4.17}$$

The lepton current can then be expanded in terms of these polarization vectors as

$$j_{\epsilon L}^{\mu} = \sqrt{2Q^{2}} \left[\frac{\sinh \psi}{\sqrt{2}} \epsilon_{0}^{\mu} - (\frac{\cosh \psi - 1}{\sqrt{2}}) \epsilon_{+}^{\mu} - (\frac{\cosh \psi + 1}{\sqrt{2}}) \epsilon_{-}^{\mu} \right]$$

$$= \sqrt{2Q^{2}} D_{i}^{L} \epsilon_{i}^{\mu}, \quad i = +, -, 0$$

$$j_{\epsilon R}^{\mu} = \sqrt{2Q^{2}} \left[\frac{\sinh \psi}{\sqrt{2}} \epsilon_{0}^{\mu} - (\frac{\cosh \psi + 1}{\sqrt{2}}) \epsilon_{+}^{\mu} - (\frac{\cosh \psi - 1}{\sqrt{2}}) \epsilon_{-}^{\mu} \right]$$

$$= \sqrt{2Q^{2}} D_{i}^{R} \epsilon_{i}^{\mu}, \quad i = +, -, 0$$
(4.18)

The hyperbolic functions originate from a rotation inside the lepton plane when the reference momentum is changed from (q, P) to (q, l_1) . The rotation is actually a Lorentz boost since it is carried out in the x-t plane. It is easy to get that $\cosh \psi = \frac{2P \cdot (k+k')}{\Delta[-Q^2, P^2, P_x^2]}$ from the kinematics. In the laboratory frame, $\cosh \psi$ simplifies to $\frac{E_{l_1} + E_{l_2}}{\sqrt{Q^2 + \nu^2}}$.

Defining helicity partonic structure functions w^{ij} as

$$w^{ij} = \epsilon^{i}_{\mu} w_{\mu\nu} \epsilon^{j*}_{\nu} = \frac{1}{4\pi} \int J^{i} J^{j*} d\Gamma', \quad i, j = +, -, 0,$$
 (4.19)

where $J^i = \epsilon^i_\mu J^\mu$ and substituting Equation 4.18 into Equation 4.15, the cross section can now be written as

$$d\sigma = \frac{e^2 y}{4\pi Q^2} dx dy \frac{d\phi}{2\pi} \int \frac{d\xi}{\xi} \phi_N^a(\xi, \mu^2) \left(p_L * D_i^L D_j^L w_{L,a}^{ij} + p_R * D_i^R D_j^R w_{R,a}^{ij} \right)$$
(4.20)

Implicitly included in w^{ij} of Equation 4.19 and 4.20 are the sums of all possible partonic helicity scattering contributions. The diagonal helicity structures w^{ii} are the usual helicity helicity functions f_i , i = +1, -1, 0, as defined in Equation 4.11. The factorization formula for the hadron helicity structure function F_{λ} is

$$F_{\lambda}(x,Q^{2}) = \int_{0}^{1} \frac{d\xi}{\xi} \phi(\xi,\mu^{2}) \left(p_{L} * f_{\lambda}^{L}(\xi,\mu^{2},Q^{2},\alpha_{s}) + p_{R} * f_{\lambda}^{R}(\xi,\mu^{2},Q^{2},\alpha_{s}) \right) . \quad (4.21)$$

Remember that this factorization formula is much simpler in helicity basis than in invariant basis.

For heavy quark production at HERA where unpolarized electron beam scattering on proton, $p_L = p_R = \frac{1}{2}$, so the cross section and the structure functions simplify to

$$d\sigma = \frac{e^2 y}{8\pi Q^2} dx dy \frac{d\phi}{2\pi} \int_0^1 \frac{d\xi}{\xi} \phi_N^a(\xi, \mu^2) \left(D_i^L D_j^L w_{L,a}^{ij} + D_i^R D_j^R w_{R,a}^{ij} \right)$$
(4.22)

and

$$F_{\lambda}(x,Q^2) = \frac{1}{2} \int_0^1 \frac{d\xi}{\xi} \phi(\xi,\mu^2) \left(f_{\lambda}^L(\xi,\mu^2,Q^2,\alpha_s) + f_{\lambda}^R(\xi,\mu^2,Q^2,\alpha_s) \right)$$
(4.23)

respectively.

For the experimental results, the invariant structure functions $F_{1,2,3}$ are usually published instead of the helicity structure functions $F_{+,-,0}$. However, it is easy to convert between helicity basis and invariant basis once the vector boson polarision vectors are defined. Applying Equation 4.17 to equation 4.10, we obtain

$$F_{+} = W_{1} + \frac{\nu}{2M} \sqrt{1 + \frac{Q^{2}}{\nu^{2}}} W_{3}$$

$$F_{-} = W_{1} - \frac{\nu}{2M} \sqrt{1 + \frac{Q^{2}}{\nu^{2}}} W_{3}$$

$$F_{0} = -W_{1} + (1 + \frac{Q^{2}}{\nu^{2}}) W_{3}$$

$$(4.24)$$

or equivalently,

$$F_{1} = \frac{1}{2}(F_{+} + F_{-})$$

$$F_{2} = \frac{2x}{1 + \frac{Q^{2}}{\nu^{2}}}(F_{0} + \frac{F_{+} + F_{-}}{2})$$

$$F_{3} = (\frac{\nu^{2}}{Q^{2} + \nu^{2}})(F_{+} - F_{-}), \qquad (4.25)$$

where
$$\nu = \frac{P \cdot q}{\sqrt{P \cdot P}}$$
.

In this work, we will focus on charm quark production in deep inelastic scattering, especially in the H1 and ZEUS experiments at HERA. Equation 4.22 and 4.23 are the basic formulas we will use to calculate the cross sections and structure functions. The ACOT scheme will be used to maintain an accurate description of heavy quark production mechanisms from the mass threshold to the asymptotic energy region. For each subprocess, all possible helicity amplitudes J^i will be calculated to obtain the helicity structure functions w^{ij} and the various differential cross section distributions.

4.2 Heavy Quark Mass Effects on the Kinematics

In this section, we will briefly discuss some kinematic effects resulting from the heavy quark mass and the hadron target mass.

For the heavy quark production in lepton-hadron deep inelastic scattering process

$$l_1(k) + N(P) \to l_2(k') + H(p') + X(P_X),$$
 (4.26)

the actual underlying scattering process is

$$V(q) + N(P) \to H(p') + X(P_X),$$
 (4.27)

where a space-like vector boson V strikes a nucleon N, as shown in Figure 4.3. Since

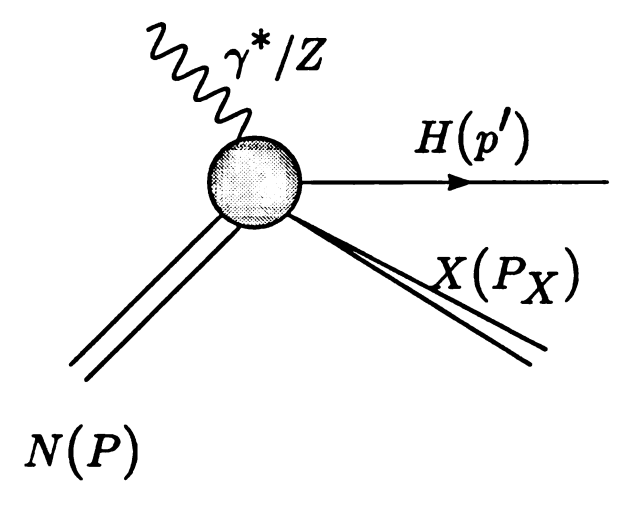


Figure 4.3: Deep inelastic scattering: vector boson and nucleon scattering

the scattering really occurs between the vector boson V(q) and the nucleon N(P), it is more natural to use the collinear coordinate frame where q and P are collinear in the z-axis and the t-z plane is defined by 4 vectors (q,P) instead of (k,P). Following the modern formulation of the factorization theorem, we specify the particles' four momenta by their light-cone coordinate components (x^+, x_1, x_2, x^-) , where $x^{\pm} = \frac{x^0 \pm x^3}{\sqrt{2}}$ instead of the usual (x_0, x_1, x_2, x_3) . Thus in this q, P collinear frame, we have

$$P^{\mu} = (P^{+}, \vec{0}, \frac{M^{2}}{2P^{+}})$$

$$q^{\mu} = (-\eta P^{+}, \vec{0}, \frac{Q^{2}}{2\eta P^{+}})$$
(4.28)

where P^+ is arbitrary and η is specified by the equation:

$$2q \cdot P = \frac{Q^2}{\eta} - \eta M^2.$$

Since $x = \frac{Q^2}{2P \cdot q}$, the relation between η and x can be solved as:

$$\frac{1}{x} = \frac{1}{\eta} - \eta \frac{M^2}{Q^2} \tag{4.29}$$

or equivalently,

$$\frac{1}{\eta} = \frac{1}{2x} + \sqrt{\frac{1}{4x^2} + \frac{M^2}{Q^2}} \tag{4.30}$$

It is easy to see η is the generalization of the usual Bjorken x with the presence of target mass M.

In the class of collinear reference frames where t-z plane is defined by (q, P), a specific frame is specified by a given choice of P^+ . For instance, setting $P^+ = M/\sqrt{2}$, we obtain the laboratory frame with the z axis along \vec{q} . Setting $P^+ \to \infty$, we get the infinite momentum frame which is often used to derive QCD factorization theorem.

In the QCD parton model, the initial parton a carries a fraction ξ of the nucleon momentum.

$$p^{\mu} = \left(\xi P^{+}, \vec{0}, \frac{m_{1}^{2}}{2\xi P^{+}}\right) \tag{4.31}$$

where $\xi = \frac{p_{parton}^+}{P_{Proton}^+}$ and m_1 is the initial state parton mass. Assume the final state threshold is \hat{s}_{th} due to the final state heavy quarks, then

$$\hat{s} = (p+q)^2 = (Q^2 + \frac{\eta}{\xi} m_1^2)(\frac{\xi}{\eta} - 1) \ge \hat{s}_{th}. \tag{4.32}$$

It is easy to find the threshold value for ξ from the above equation,

$$\xi_{th} = \eta \frac{(Q^2 - m_1^2 + \hat{s}_{th}) + \Delta(-Q^2, m_1^2, \hat{s}_{th})}{2Q^2}, \tag{4.33}$$

where

$$\Delta(a,b,c) = \sqrt{(a^2 + b^2 + c^2 - 2ab - 2bc - 2ac)}.$$
 (4.34)

So due to the heavy quark mass effect, the initial parton momentum fraction ξ 's range is $1 \geq \xi \geq \xi_{th}$ instead of $1 \geq \xi \geq 0$. For the leading order charm production partonic process $q + k_1(m_1) \rightarrow k_2(m_2)$, $\hat{s}_{th} = m_2^2$ and

$$\xi_{th} = \eta \frac{(Q^2 - m_1^2 + m_2^2) + \Delta [-Q^2, m_1^2, m_2^2]}{2Q^2}.$$

$$\rightarrow \frac{\eta}{2} \left(1 + \sqrt{(1 + \frac{4m_1^2}{Q^2})}\right), \text{ when } m_1 = m_2. \tag{4.35}$$

4.3 The Next-to-Leading Order Production Mechanism

Experiments observe baryons and mesons instead of quarks and gluons in the detectors. Sometimes the data are converted into theoretical quantities which have less dependence on the non-perturbative physics. For example, the deep inelastic scattering inclusive $D^{*\pm}$ meson cross sections σ^D data are almost always converted into a charm production cross section σ^c . On the other hand, results for the final state hadrons are also often published. For example, the differential cross section distribution $\frac{1}{\sigma^D} \frac{d\sigma^D}{dp_l^D}$. To compare with experimental data, the theoretical calculation of

 $\frac{1}{\sigma^c} \frac{d\sigma^c}{dp_i^c}$ needs to be convolved with the $c \to D^*$ fragmentation functions. Including the fragmentation function, the cross section formula Equation 4.22 becomes

$$d\sigma^{D} = \frac{e^{2}y}{8\pi Q^{2}} dx dy \frac{d\phi}{2\pi} \int_{\xi_{i,k}}^{1} \frac{d\xi}{\xi} \phi_{N}^{a}(\xi,\mu^{2}) \left(D_{i}^{L} D_{j}^{L} w_{L,a}^{ij} + D_{i}^{R} D_{j}^{R} w_{R,a}^{ij} \right) D_{c}^{D}(z,\mu^{2}) dz.$$

$$(4.36)$$

Notice that for total inclusive quantities such as σ^{D^*} , we can use

$$\sigma^{D^{\bullet}} = \sigma^{c} \cdot P_{c \to D^{\bullet}}, \tag{4.37}$$

where $P_{c\to D^*}$ is the charm fragmentation probability into D^* meson, to convert inclusive charm results to inclusive meson results. So in total inclusive cases, the difference

between the meson cross section and quark cross section is only a trivial constant factor. As a result, the fragmentation function is often omitted in the theoretical presentation. However, to make the following discussions clear, we will have the fragmentation functions explicit in the formulas in this section, although we will often refer to both parton distribution functions and fragmentation functions generically as parton distribution functions. Also we will use H to denote the final state hadron and c to denote the charm quark.

For charmed meson H production in deep inelastic scattering,

$$\sigma^{VN\to H}(x, Q^2, ...) = \sum_{a,b} \phi_N^a \otimes \hat{\sigma}^{Va\to b} \otimes d_b^H. \tag{4.38}$$

The exact nature of the factorization of the physical cross section into the three pieces on the right-hand side of Equation 4.38 depends on the scheme used to define the parton distributions. The physical cross section is independent of any calculation scheme; therefore, the subtraction scheme which is used to define the parton distributions ϕ_N^a also uniquely defines the hard cross sections $\hat{\sigma}$. Since the ACOT scheme is a composite scheme based on the CWZ renormalization, different subtraction procedures are used in the different energy regions. Within a given scheme, the hard cross sections $\hat{\sigma}^{Va \to b}$ are obtained as follows: (i) Start with cross section $\sigma^{Va \to b}$ similar to the left-hand side of Equation 4.38 but with parton targets and calculate them in perturbative theory in the given renormalization scheme (i.e. with specific counter-terms); (ii) Independently, calculate the set of process-independent perturbative partonic distribution functions $\tilde{\phi}_a^b$ in the same renormalization scheme, using either the (moment space) operator-product expansion or, equivalently, the (x-space) bi-local operator definition of the distribution functions; (iii) Verify that all divergences and potentially large logarithms appearing in $\sigma^{Va \to b}$ can be factorized into the

universal $\tilde{\phi}_a^b$ functions, in the manner of Equation 4.38,

$$\sigma^{Va\to c}(Q^2, x, m_c) = \sum_{a,d} \tilde{\phi}_a^b \otimes \hat{\sigma}^{Vb\to d} \otimes \tilde{d}_d^c ; \qquad (4.39)$$

(iv) Systematically invert Equation 4.39 to solve for the finite hard cross section $\hat{\sigma}^{Vb\to d}$, which is then used in Equation 4.38 for calculating the physical cross section. There are two points to note: (i) The inversion of Equation 4.39 order-by-order in the perturbation series is equivalent to subtracting the singularities contained in $\tilde{\phi}_a^b$ from $\sigma^{Va\to c}$; (ii) There is no need to set the quark mass(es) to zero anywhere in the above procedure.

For the ACOT scheme, the leading contributions to heavy quark production in leptoproduction are depicted diagrammatically in Figure 4.4.

The relevant hard scattering processes (with the associated fragmentation) are listed below.

$$V + G \rightarrow c + \bar{c} \qquad ; \quad c \rightarrow H \qquad : \quad \text{HC1}$$

$$V + c \rightarrow c \qquad ; \quad c \rightarrow H \qquad : \quad \text{HE1}$$

$$V + c \rightarrow c + G \qquad ; \quad c \rightarrow H \qquad : \quad \text{HE2}$$

$$V + q \rightarrow q + G \qquad ; \quad G \rightarrow H \qquad : \quad \text{GF2}$$

$$V + G \rightarrow c + \bar{c} + G \qquad ; \quad c \rightarrow H \qquad : \quad \text{HC2}$$

$$V + q \rightarrow c + \bar{c} + q \qquad : \quad c \rightarrow H \qquad : \quad \text{HC2}$$

where

- HC1 corresponds to the $(2 \rightarrow 2)$ heavy-flavor creation process;
- HE1 corresponds to the $(2 \rightarrow 1)$ heavy-flavor excitation process;
- HE2 corresponds to the $(2 \rightarrow 2)$ HE process;
- GF2 corresponds to the $(2 \rightarrow 2)$ light parton scattering process, followed by gluon fragmentation into H;
- HC2 corresponds to the $(2 \rightarrow 3)$ HC process;

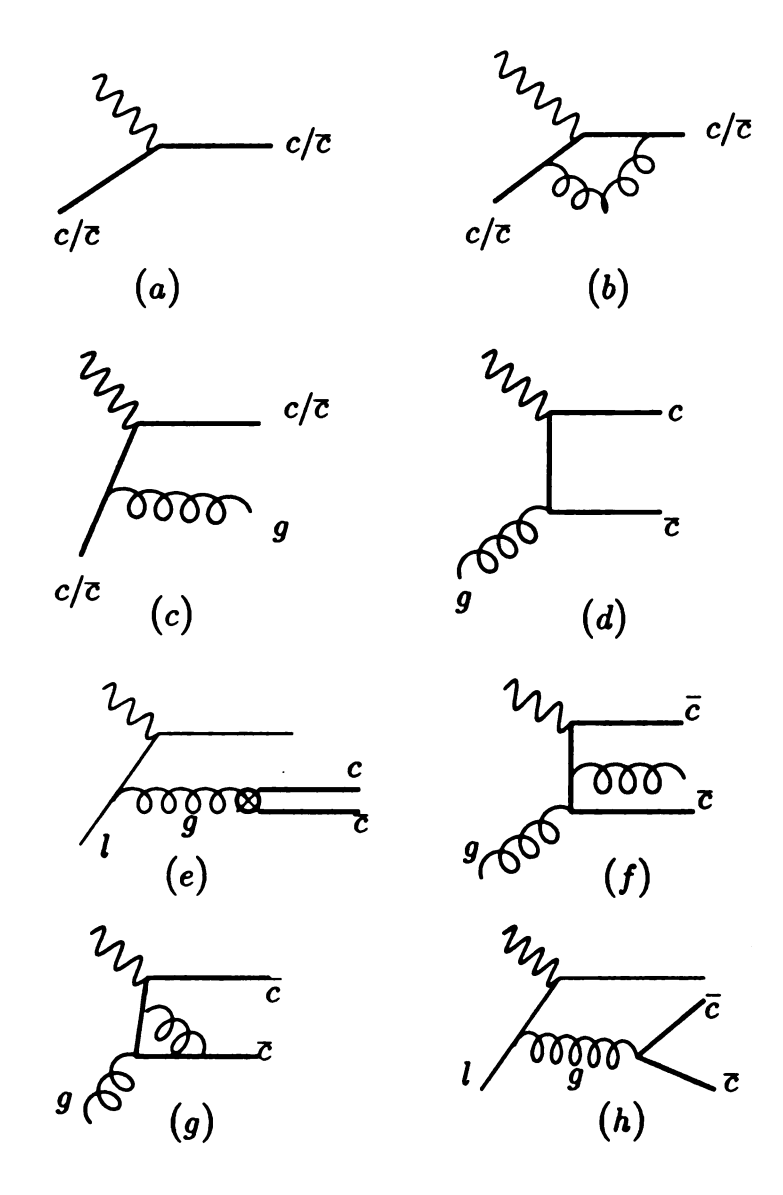


Figure 4.4: Processes contributing to the leading ACOT scheme calculation. (a), (b), (c) only present in the 4-flavor region, (d), (e), (f), (g), (h) presents in both the 3-flavor scheme region and the 4-flavor scheme region. HC1:(d), HE1:(a), HE2:(b),(c), GF2:(e), HC2:(f),(g),(h). Only one diagram for each process is plotted.

The order of magnitude of the various process contributions depends on how the parton distribution functions, especially the heavy quark parton density, are treated. In conventional applications of perturbative QCD with light partons, the parton distributions ϕ_N^a at some relatively low scale $\mu = Q_0$ are regarded as non-perturbative input; they are assumed to be of order unity. In practice, it is found that the gluon distribution dominates at small x and the valence u and d distributions dominate at large x. When a charm quark participates in the interaction, $\phi_N^c(x,\mu)$ is usually assumed to be generated through PQCD evolution. This is called "radiatively generated" charm. The parton distribution function $\phi_N^c(x,\mu)$ should therefore be of order α_s in the region immediately above charm threshold. As mentioned in the last chapter, it is possible, however, that a non-perturbative component of charm also exists inside the hadron at the scale $\mu = m_c$, both on general grounds (since m_c is not so much larger than the QCD scale) and from the point of view of specific model calculations [59]. This is another advantage of the ACOT scheme over the current routinely used three-flavor scheme. Since the three-flavor scheme assumes from the very beginning that there is no heavy quark distribution inside the proton at any energy scale, there is no way for it to accommodate a non-perturbative heavy quark distribution. On the contrary, the ACOT scheme can naturally accommodate a nonperturbative charm parton distribution $\phi_N^c(x, \mu = m_c) \neq 0$ and allow the size and shape of this component of hadron structure to be determined phenomenologically.

As a rough guide to the order of magnitude of the various factors which enter into the master equation, Equation. 4.38, we shall assume $\phi_N^c(x,\mu)$ to be of order α_s compared to the dominant parton distributions, whether the non-perturbative component is present or not:

$$\phi_N^c \sim \mathcal{O}(\alpha_s). \tag{4.41}$$

Although this assumption could fail in the case of a large non-perturbative component

of charm, it appears to be an extremely reasonable and safe starting point to take. This is because even if a truly quantitative comparison between theory and experiment has yet to be carried out, the fact that current three-flavor calculations are in qualitative agreement with the first measurements of the charm structure function F_2^c makes it unlikely that the non-perturbative component could be anomalously large. Reasonable dynamic models also suggest that the non-perturbative charm component is not more than a few percent. Similar considerations suggest for the fragmentation functions:

$$d_{c}^{H} \sim \mathcal{O}(1)$$

$$d_{G}^{H} \sim \mathcal{O}(\alpha_{s})$$

$$d_{a}^{H} \sim \mathcal{O}(\alpha_{s}^{2})$$

$$(4.42)$$

The numerical suffix in Equation 4.40 to the label of each term corresponds to the estimated order of magnitude of the term in powers of effective α_s , counting all the factors in the convolution $\phi \otimes \widehat{\sigma} \otimes d$.

As previous claimed, the ACOT scheme formalism contains the conventional parton model approach as a special case. This can be seen as follows: From the traditional zero-mass parton point of view, HE1 process represents the LO $O(\alpha_s^0)$ contribution. HC1, HE2 and GF2 represent the NLO $O(\alpha_s^1)$ contribution. The only difference is that the mass singularities associated with charm are subtracted by mass-subtraction term in this scheme instead of the $\overline{\rm MS}$ subtraction in the parton model approach. In the ACOT scheme, the mass dependence is kept without taking $m_c \to 0$. Appropriate choices of the finite terms in the mass-subtraction enable the hard cross section $\hat{\sigma}(m_c,\cdots)$ in this scheme to agree with the standard zero-mass results when $m \to 0$.

In the following sections, we will discuss the neutral current charm production in deep inelastic scattering based on Equation 4.23 and 4.22:

$$d\sigma = \frac{e^2 y}{8\pi Q^2} dx dy \frac{d\phi}{2\pi} \int_0^1 \frac{d\xi}{\xi} \phi_N^a(\xi, \mu^2) \left(D_i^L D_j^L w_{L,a}^{ij} + D_i^R D_j^R w_{R,a}^{ij} \right)$$

$$F_{\lambda}(x,Q^{2}) = \frac{1}{2} \int_{0}^{1} \frac{d\xi}{\xi} \phi(\xi,\mu^{2}) \left(f_{\lambda}^{L}(\xi,\mu^{2},Q^{2},\alpha_{s}) + f_{\lambda}^{R}(\xi,\mu^{2},Q^{2},\alpha_{s}) \right)$$
(4.43)

Helicity current J^i results for the each contributing process will be presented¹.

4.4 Leading Order Calculations

The ACOT scheme leading order processes include the leading order flavor excitation process (HE1), leading order flavor creation process (HC1) and the double counting term (HC1_{sub}). The leading order heavy quark structure functions in this scheme were calculated by M. Aivazis *el. al.*[56, 41, 58]. However, that calculation was limited to the inclusive structure functions only and did not provide any information about the final state particle differential distributions.

The leading order $\gamma^*/Z + c \to c$ is very simple and its contribution to the cross section is infra-red safe. There are only four non-vanishing helicity amplitudes: $\gamma^*_-/Z_- + c_L \to c_R$, $\gamma^*_+/Z_+ + c_R \to c_L$, $\gamma^*_0/Z_0 + c_L \to c_L$ and $\gamma^*_0/Z_0 + c_R \to c_R$ in this process. The latter two are proportional to the quark mass and will disappear when quark mass becomes zero because of the helicity conservation in the massless limit. The explicit expressions of the helicity amplitudes are listed in Appendix A. Since this process is a $2 \to 2$ lepton hadron scattering process, the azimuthal angle $\tilde{\phi}$ between the lepton sector and hadron sector dependence in Equation 4.17 is trivial, and the parton momentum ξ integration in Equation 4.22 and 4.23 for this process shrinks into a δ function with parton momentum fraction $\xi_0 = \frac{\eta}{2} \left(1 + \sqrt{(1 + \frac{4m_c^2}{Q^2})}\right)$.

The helicity amplitudes for the partonic process $\gamma^*/Z+g \to c+\bar{c}$ can be calculated in the $c\bar{c}$ center-of-mass frame. For helicity structure functions, this gives

$$w^{ij} = \frac{1}{32\pi^2} \int J^i J^{j*} \beta \frac{d\cos\tilde{\theta}}{2} \frac{d\tilde{\phi}}{2\pi}, \tag{4.44}$$

¹The author thanks Carl Schmidt for making the results available.

where $\beta = \sqrt{1 - \frac{4m_c^2}{\hat{s}}}$ with $\hat{s} = Q^2 \left(\frac{\xi}{\eta} - 1\right)$, $\tilde{\theta}$ is the scattering angle and $\tilde{\phi}$ is the angle between the lepton plane and the hadron plane. The lower limit ξ_{th} on the convolution variable ξ is $\eta(1 + \frac{4m_c^2}{Q^2})$ due to the mass effects. The helicity amplitudes from this process are also listed in Appendix A.

Although the partonic helicity structure function w^{ij} for $\gamma^*/Z + g \to c + \bar{c}$ process in Equation 4.44 is finite after integrating over the phase space, it contains terms proportional to $\ln(\mu^2/m_c^2)$. As we pointed out before, these terms are already factored into the charm distribution function ϕ_N^c of the 4-flavor scheme and their contributions have been resummed into the flavor excitation processes HE1. To correct the double counting between process HE1 and HC1, we must subtract off the gluon-to-charm splitting term in the evolution of the charm parton density, and this leads to the subtraction term HC1_{sub}:

$$w_{HC1_{\text{sub}}}^{ij} = w_0^{ij} \times \frac{\alpha_s}{2\pi} \ln \frac{\mu^2}{m_c^2} \int \frac{d\xi}{\xi} \phi_N^g(\xi, \mu^2) P_{cg}(\frac{\xi_0}{\xi}), \tag{4.45}$$

where w_0^{ij} is the leading order HE1 helicity structure function and splitting function $P_{cg}(z) = \frac{1}{2}(z^2 + (1-z)^2)$. Essentially, the charm distribution function resums the collinear logarithmic terms to all orders and the subtraction term is used to correct the double counting of the first leg in the resummation.

4.5 Next-to-Leading Order Calculations

The next-to-leading order contributions to the heavy quark deep inelastic scattering include the one loop level flavor excitation process (HE2_v), the next-to-leading order flavor excitation process (HE2), the double counting term (HE2_{sub}), the gluon fragmentation process (GF2) and the next-to-leading order flavor excitation processes (HC2).

The virtual corrections to $\gamma^*/Z + c \to c$ can be summarized in the vertex function. If the lowest order vertex is $-ie\gamma^{\mu}(f_V + f_A\gamma^5)$, then the one loop order corrections would have a general form of $-ie\left(\gamma^{\mu}(F_{1V} + F_{1A}\gamma^5) + \frac{i\sigma^{\mu\nu}q_{\nu}}{2m_c}F_{2V}\right)$. Calculating both wave function renormalizations and vertex loop corrections in the CWZ scheme, one obtains

$$F_{1V} = \frac{\alpha_s}{2\pi} C_q f_V (I_1 + I_2) \tag{4.46}$$

$$F_{1A} = \frac{\alpha_s}{2\pi} C_q f_A (I_1 - I_2) \tag{4.47}$$

$$F_{2V} = \frac{\alpha_s}{2\pi} C_q f_V(2I_2) \tag{4.48}$$

where

$$I_{1} = \left(\frac{4\pi\mu^{2}}{m_{C}^{2}}\right)^{\epsilon} \Gamma(1+\epsilon) \left\{ \frac{1}{\epsilon} \left[-1 - \left(\frac{1+\beta^{2}}{2\beta}\right) \ln\left(\frac{\beta-1}{\beta+1}\right) \right] - 2 + \left(\frac{1+\beta^{2}}{2\beta}\right) \left[-\frac{3}{2} \ln\left(\frac{\beta-1}{\beta+1}\right) - \frac{1}{2} \ln\left(\frac{\beta-1}{\beta+1}\right) \ln\left(\frac{\beta^{2}-1}{4\beta^{2}}\right) + Li_{2}\left(\frac{\beta+1}{2\beta}\right) - Li_{2}\left(\frac{\beta-1}{2\beta}\right) \right] \right\}$$

$$(4.49)$$

$$I_2 = \frac{m_c^2}{q^2 \beta} \ln(\frac{\beta - 1}{\beta + 1}) \tag{4.50}$$

The separation of I_1 and I_2 terms is due to the reason that I_1 term is proportional to the leading order vertex $-ie\gamma^{\mu}(f_V+f_A\gamma^5)$ while I_2 term is not. In Equation 4.46, C_q is 4/3 for QCD and f_V and f_A are the vector and axial vector couplings of the vector boson with the quark. In Equation 4.49, $\beta = \sqrt{1 - \frac{4m_c^2}{q^2}}$, and $Li_2(x)$ is the usual Spence function defined by

$$Li_2(x) = -\int_0^x \frac{\ln(1-z)}{z} dz. \tag{4.51}$$

The $\frac{1}{\epsilon}$ term in Equation 4.49 is the infrared unsafe piece, and it will cancel against the soft gluon contributions from HE2 process.

With the renormalized vertex coupling coefficients F_{1V} , F_{1A} and F_{2V} available, the helicity amplitudes can be easily calculated as in HE1 process.

The helicity amplitudes for partonic process $\gamma^*/Z + c \to c + g$ can be calculated similar to the $\gamma^*/Z + g \to c + \bar{c}$ process. Actually, due to the crossing symmetry between the outgoing and incoming momenta, the calculation can be simplified by using results from $\gamma^*/Z + g \to c + \bar{c}$ process. The final results are also listed in Appendix A.

After integrating over the final state phase space, the $\gamma^*/Z + c \rightarrow c + g$ partonic helicity structure function w^{ij} in Equation 4.44 has a $\frac{1}{\epsilon}$ term. This term comes from the part of the phase space where a very soft gluon g is emitted. This infrared divergence is proportional to helicity structure function for the leading order process HE1 w_0^{ij} and cancels against the $\frac{1}{\epsilon}$ term in the HE2_v loop diagram. Because the integration diverges when the gluon is soft, the Monte Carlo method cannot be applied to the whole phase space region. In our implementation we use the phase space splicing method [60] which allows us to isolate the soft singular poles. In the soft gluon phase space region, eikonal approximations for the amplitudes and analytical integration using dimensional regularization are used to perform the integration. For all the other phase space region, normal Monte Carlo method is used. The cancellation of soft singularities takes place when the contributions from the renormalized virtual diagrams are added. This structure function for the soft integration region is

$$w_{soft} = w_0 * 2 \frac{\alpha_s C_q}{2\pi} \Gamma(1+\epsilon) (\frac{4\pi\mu^2}{m_c^2})^{\epsilon} (\frac{m^2}{Q^2 \beta \delta})^{2\epsilon} \left\{ \frac{1}{\epsilon} \left[1 - \frac{1+\beta^2}{2\beta} \ln(\frac{\beta+1}{\beta-1}) \right] + \left[1 + \frac{1+\beta^2}{2\beta} \left(\ln(\frac{\beta+1}{\beta-1}) - \frac{\pi^2}{6} + Li((\frac{\beta-1}{\beta+1})^2) + 2\ln(\frac{\beta^2-1}{4\beta}) \ln(\frac{\beta+1}{\beta-1}) + \ln^2(\frac{\beta+1}{\beta-1}) \right) \right] \right\},$$

$$(4.52)$$

where ω_0 is the leading order HE1 process helicity structure function and δ is a

parameter used to separate the soft region from the phase space. To obtain a correct and stable result, δ must be small enough so that the eikonal approximations are valid for the analytical integration, and it also must be large enough so that the Monte Carlo integration will not be trapped in the divergence region. Although both soft and non-soft region integrations could strongly depend on δ , the sum of the two should not depend on δ . This can be used as a self consistence test.

Similar to the HC1 case, there is also a double counting between the HE1 and HE2. As expected, to correct the double counting between process HE2 and HE1, we must subtract off the charm-to-gluon splitting term in the evolution of the charm parton density, and this leads to a subtraction term HC1_{sub}:

$$w_{HE2_{\text{sub}}}^{ij} = w_0^{ij} \times \frac{\alpha_s}{2\pi} \int \frac{d\xi}{\xi} \phi_N^g(\xi, \mu^2) \tilde{\phi}_{cc}(\frac{\xi_0}{\xi}). \tag{4.53}$$

where $ilde{\phi}_{cc}$ is the splitting function defined by

$$\tilde{\phi}_{cc}(z) = \frac{4}{3} \left[\left(\frac{1+z^2}{1-z} \right) \left(\ln \frac{\mu^2}{m_c^2} - 1 - 2 \ln(1-x) \right) \right]_+ \tag{4.54}$$

The $\gamma^* + q \to q + g$ vector boson and light parton scattering process is similar to HE2 process except the q quark mass is zero. So its helicity amplitudes can be obtained by simply setting the quark mass to zero in the helicity amplitudes for HE2 process. The gluon fragmentation term $d_g^c(z, \mu^2)$ is defined by

$$d_g^c(z,\mu^2) = \frac{\alpha_s}{2\pi} P_{cg}(z) \ln(\frac{\mu^2}{m_c^2}), \tag{4.55}$$

and it should be evolved through the GLAP equation in order to resum the logarithmic terms to all orders. Then the evolved fragmentation function is convoluted with the $\gamma^* + q \rightarrow q + g$ two-to-two parton process to obtain its contributions to the charm quark production cross section.

In this work, we have not included the HC2 processes $\gamma^* + g \to c + \bar{c} + g$ and $\gamma^* + q \to c + \bar{c} + q$. The logarithmic contributions for the inclusive cross section from

these processes have been resummed in the flavor excitation processes. When the energy scale is much larger than the charm mass threshold, total HC2 contributions are well represented in our HE1, HE2 terms. However, when the energy scale is around the threshold, the logarithmic terms are small and we have left out some important contributions from the non-logarithmic terms. Also, for differential distributions, the HC2 processes have additional kinematic configurations that are not available to the lower order processes, and thus have a more accurate description to the exclusive states of the final state hadrons.

Our eventual goal is to achieve next-to-leading order accuracy throughout the whole energy scale range by including the HC2 processes in our ACOT scheme calculation. However, our results in this work show that both the inclusive results and differential distributions agree well with experiments. This implies that although HC2 contributions can be important in some cases, our present calculation already captures most of the important physics needed to interpret current data. In the next chapter, we will present our results and compare with other calculations and experiment data.

Chapter 5

Results of Inclusive and Differential Distributions of Charm Quark Production at HERA

In this chapter, we will use the ACOT scheme formalism we described before to calculate inclusive F_2^c and differential distributions for charm productions at HERA.

HERA(Hadron-Elektron-Ring-Anlage) is the world's first electron (positron)-proton collider. It can operate with either electron or positron beams. The current beam energies are $E_e = 27.6$ GeV for electrons and $E_P = 820$ GeV for protons. The center of mass energy $\sqrt{s} = \sqrt{4E_eE_P} = 301$ GeV. The H1 [61, 62] and ZEUS [63] detectors in the ep interaction regions detect the the scattered electron and the emerging hadrons. Recently, charm quark production data from neutral current deep inelastic scattering became available from H1 [64] and ZEUS [65]. In particular, substantial samples of $D^{*\pm}(2010)$ and $D^0(1864)$ mesons have been obtained. In this chapter, we will present the ACOT scheme results for charm quark and D^* meson production in the x and Q^2 region covered by the HERA collider.

First, we will discuss some issues related the actual programming implementation.

The choice of parton distributions is determined by the renormalization scheme. For
the ACOT calculations, we use CTEQ4M parton distributions. Our actual program-

ming implementation uses the phase space splicing method to separate infrared divergences from other finite pieces and use the Monte Carlo method [66] to numerically carry out the phase space integration. Following the introduction of the implementation, we will present the inclusive F_2^c results. Our results agree well with experiments and are much more efficient than the conventional three-flavor scheme calculation. Since we use a Monte Carlo method to integrate the final state phase space, we can easily incorporate experimental cuts. We will show results of differential distributions $\frac{d\sigma}{dp_T}$, $\frac{d\sigma}{dQ^2}$, $\frac{d\sigma}{dW}$, $\frac{d\sigma}{d\eta}$ for the D^* meson with appropriate experimental cuts. These results also agree well with experimental data.

5.1 Implementation of the Calculation

To calculate inclusive structure functions, we need to sum all the subprocess contributions we discussed in the last chapter. Thus, we get

$$F_{\lambda}^{c}(Q^{2}, x, ..) = \phi^{g} \otimes {}^{1}f_{g,\lambda}^{c\bar{c}} + (\phi^{c} - \phi^{g} \otimes {}^{1}\tilde{\phi}_{g}^{c} - \phi^{c} \otimes {}^{1}\tilde{\phi}_{c}^{c}) \otimes {}^{0}f_{c,\lambda}^{c} + \phi^{c} \otimes {}^{1}f_{c,\lambda}^{cg} + \phi^{g} \otimes {}^{1}f_{q,\lambda}^{qg} \otimes d_{g}^{c}$$

$$(5.1)$$

where the $\ln\left(\frac{\mu}{m_c}\right)$ terms in the $f_{a,\lambda}$ factors are kept intact, and the needed subtraction terms are explicitly grouped with the leading $2\rightarrow 1$ term with the same kinematics. In Equation 5.1,

$${}^{1}\tilde{\phi}_{c}^{c} = \frac{\alpha_{s}}{2\pi} \frac{4}{3} \left[\left(\frac{1+x^{2}}{1-x} \right) \left(\ln \frac{\mu^{2}}{m_{c}^{2}} - 1 - 2\ln(1-x) \right) \right]_{+}$$
 (5.2)

$${}^{1}\tilde{\phi}_{g}^{c} = (\alpha_{s}/2\pi)^{2}P_{g\to q}(x)\ln\frac{\mu^{2}}{m_{c}^{2}}$$
 (5.3)

$${}^{1}\mathrm{d}_{g}^{c} = \frac{\alpha_{s}(\mu_{0})T_{F}}{2\pi}(x^{2} + (1-x)^{2})\ln\frac{\mu^{2}}{m_{c}^{2}}.$$
 (5.4)

Note that in this chapter, we will use c to denote the heavy quark, *i.e.*, charm quark, and use H to denote charm hadrons, such as D^* .

Parton distribution functions are scheme-dependent quantities. Appropriate choices of parton distribution functions are crucial to the implementation of ACOT scheme calculation and meaningful comparisons between physical predictions from different schemes. The collinear divergences appearing in a particular factorization scheme must be canceled by properly defined parton distribution functions (and, in general, fragmentation functions). The parton distribution functions $\phi_N^a(x,\mu)$ needed for this work can be found from the CTEQ [29, 31] distributions. For all the numerical results from ACOT scheme calculations presented below, we use the CTEQ4M distributions. In order to compare results from LO and NLO three-flavor scheme, we use the CTEQ4F3 distributions for the latter calculations. The CTEQ4M and CTEQ4F3 distributions are obtained from global analysis of the same data sets, using the same procedure, but in the two distinct renormalization and factorization schemes respectively [31]: CTEQ4M is defined in the CWZ scheme and CTEQ4F3 is defined in the three-flavor scheme.

The fragmentation functions $d_a^H(x,\mu)$ describe the process in which a final state parton a fragments into a charm hadron H. These functions are needed for the calculation of the differential distributions because it is the cross sections of D meson that are measured in the experiments. The fragmentation functions are similar to the parton distribution functions, and they need to be evolved from suitable initial functions at some scale μ_0 according to the GLAP equations We will use the fragmentation functions obtained Cacciari and Greco el/al. [67] in our calculation. For a given hadronic charm final state H, we have

$$d_a^H(x,\mu_0) = d_a^c(x,\mu_0) \otimes D_c^H(x,\mu_0)$$
 (5.5)

where the partonic charm fragmentation functions $\{d_a^c; a = u, d, s, g, c\}$ are considered perturbatively calculable, and $D_c^H(x, \mu_0)$ is a nonperturbative function that could be extracted from experiments similar to the global analysis for parton distribution functions. In particular, Reference [67] gives, to order α_s :

$$d_c^c(x,\mu_0) = \delta(1-x) + \frac{\alpha_s(\mu_0)C_F}{2\pi} \left[\frac{1+x^2}{1-x} \left(\ln \frac{\mu_0^2}{m_c^2} - 2\ln(1-x) - 1 \right) \right]_{\perp} (5.6)$$

$$d_{\mathbf{g}}^{c}(x,\mu_{0}) = \frac{\alpha_{s}(\mu_{0})T_{F}}{2\pi}(x^{2} + (1-x)^{2})\ln\frac{\mu_{0}^{2}}{m_{s}^{2}}$$
(5.7)

$$d_q^c(x,\mu_0) = d_{\bar{q}}^c(x,\mu_0) = d_{\bar{c}}^c(x,\mu_0) = 0$$
 (5.8)

where $T_F = 1/2$ and $C_F = 4/3$. Note that, although $d_c^c(x, \mu_0)$ contains a delta function, Equation 5.5 makes $d_a^H(x, \mu_0)$ a well-defined function for any H. The total inclusive cross section represented by F_2^c is obtained, in principle, by summing over all $H: \sum_H d_a^H(x, \mu_0) = d_a^c(x, \mu_0)$. For our numerical calculation of F_2^c , we only need to convolute GLAP evolved $d_g^c(z, \mu^2)$ with $\gamma^*/Z + q \rightarrow q + g$ process because F_2^c is totally inclusive in the final charm state hadrons. Since D_c^H does not affect the inclusive structure functions, we will discuss it later in the next section when we discuss differential distributions.

In the implementation of the parton distribution functions, we have to satisfy the matching conditions 3.3 and 3.4 when the number of flavors switches between 3 and 4. It was pointed out in Reference [68] that, at order α_s , the finite renormalization of both $\alpha_s(\mu)$ and $\phi^a(x,\mu)$ of Equation 3.3 and 3.4 vanish if the matching scale is chosen to be $\mu_c = m_c$. Thus, it is tempting to introduce a single coupling function $\alpha_s(\mu)$, coinciding with ${}^3\alpha_s(\mu)$ for $\mu < m_c$ and with ${}^4\alpha_s(\mu)$ for $\mu > m_c$, which would then be continuous across the transition point. The same applies to the parton distribution functions $\phi^a(x,\mu)$. In spite of this convenience, however, there are good reasons to perhaps consider choosing a transition scale other than $\mu_c = m_c$. First, the continuity

of $\alpha_s(\mu)$ and $\phi^a(x,\mu)$ across the point $\mu_c = m_c$ does not hold beyond leading order, as shown by recent explicit NLO calculation [50, 55]. Secondly, intuitive considerations indicate that the physical threshold for charm production should be at a higher scale, say $2m_c$. Furthermore, unless there is really a non-perturbative component of charm inside the nucleon, the partonic interpretation of charm, built into the 4-flavor scheme, becomes a physically natural picture only at a scale higher than m_c . However, no matter what the choice of μ_0 is, to have a smooth transition across the threshold and effective applicability at all energy level for the ACOT scheme calculation, μ_0 should always be the same order of magnitude as the charm mass. Following the ACOT leading order calculation, we also choose μ_0 to be m_c in this work. In keeping with the choice of the matching point in our overall calculation, we also choose $\mu_0 = m_c$ for the fragmentation functions.

We now consider the calculation of F_2^c due to the individual subprocesses in Equation 5.1. Only γ^* is explicitly used in the process descriptions although the descriptions apply to both γ^* and Z.

- ${}^{0}(\gamma^{*}c \to c) + (\gamma^{*}g \to c\bar{c}) Subtraction$: These terms comprise the original ACOT calculation [56, 41]. With non-zero m_c , they are all finite. The helicity amplitudes are listed in the Appendix A. The implementation of the new Monte Carlo calculation is straightforward. We have verified that the new Monte Carlo program reproduces the original ACOT results in detail.
- $^{1}(\gamma^{*}c \to c) + (\gamma^{*}c \to gc) Subtraction$: The relevant helicity amplitudes for these processes are listed in Appendix A. Individual terms in these $\mathcal{O}(\alpha_{s})$ virtual and real corrections to the LO $\gamma^{*}c \to c$ process contain soft divergences after the renormalization. In the Monte Carlo implementation, we use the phase-space splicing [60] method to achieve the proper cancellation of the soft divergences

between the real and virtual parts. First, the d-dimensional, two-body phase space of the $\gamma^*c \to gc$ process is divided into two domains according to the softness of the emitted gluon. A theoretical parameter δ is introduced in the programming for this purpose. Second, the $2 \rightarrow 2$ matrix matrix element in the soft gluon domain is approximated by a simpler form through the eikonal approximation, and then the approximated matrix element is integrated over the soft gluon phase space analytically. Finally, the partially integrated result from the soft gluon phase space region is added to the renormalized virtual $\gamma^*c \to c$ contributions to explicitly cancel the soft $\frac{1}{\epsilon}$ pole. Both the reminder left after the cancellation of the $\frac{1}{\epsilon}$ pole and the matrix element from the non-soft gluon region of the $\gamma^*c \to gc$ phase space are finite. The two separate contributions can be integrated numerically through the normal Monte Carlo method. While individually, each of the two contributions depends on the arbitrary theoretical parameter δ , the sum of them should be independent of δ . This has been used as a self consistency test for our programming. An appropriate choice of δ is important. If δ is too small, then the numerical Monte Carlo integration would be trapped in the singularity region of the phase space. On the other hand, if δ is too large, then the eikonal approximation used to simplify the computation would be invalid. Our extensive tests show our results are flat in an appropriate range of δ we haven chosen.

For double-checking, we also implemented an analytic calculation based on the formulas by Hoffmann and Moore [69]. The total F_2^c of $\gamma^*c \to gc$ and one loop level $\gamma^*c \to c$ processes are compared.

As shown in Figure 5.1 and 5.2, the two calculations agree quite well with each other over the full x and Q range, with the exception of small values of Q/m_c and Bjorken x. This is more evident in Figure 5.3. The difference can be

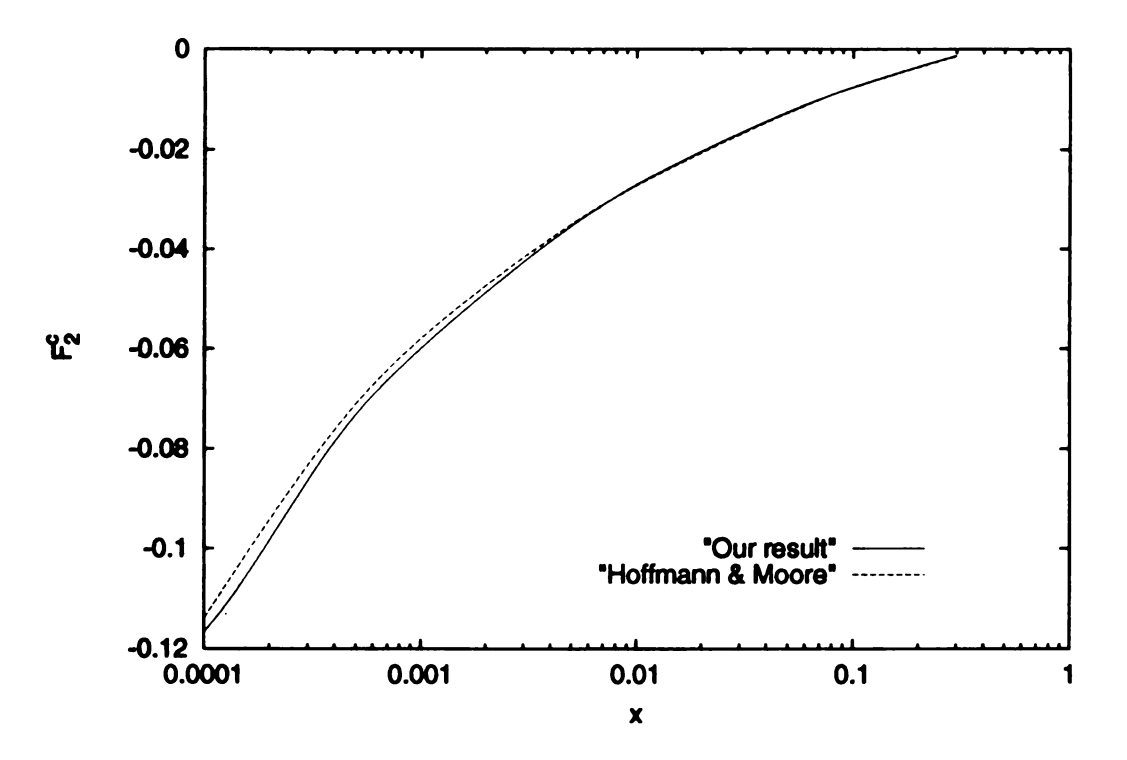


Figure 5.1: F_2^c for $Q^2 = 100$ and $m_c = 1.5$ GeV from $^1(\gamma^*c \to c) + (\gamma^*c \to gc)$ processes. Solid line is this work's result. Dashed line is the calculation of Reference [69]

understood as due a different treatment of the charm quark kinematics adopted by Reference [69] in deriving their formulas. When m_c is small compared to Q, this effect is expected to go away. This is exactly what we see in Figure 5.4 where m_c is set to smaller value — 0.3 GeV.

 $(\gamma^* q \to gq) \cdot (g \to c\bar{c})$: The treatment of the gluon-fragmentation term requires some care due to kinematics of zero-mass partons. The integrated cross section of $\gamma^* + q \to q + g$ process would have an infrared singularity arising from the integration in the region $\hat{t} = (p_{\gamma} - p_q^{\text{final}})^2 \to 0$. But this potential singularity is outside the physical region when the proper kinematic limit for the entire process, $t > t_{\min} = 4m_c^2$, is applied. The resulting finite expression, however, will have a logarithm factor $\ln \frac{Q}{m_c}$ due to the m_c cutoff of the phase space integration. This appears, on the surface, to contradict our claim of infra-red

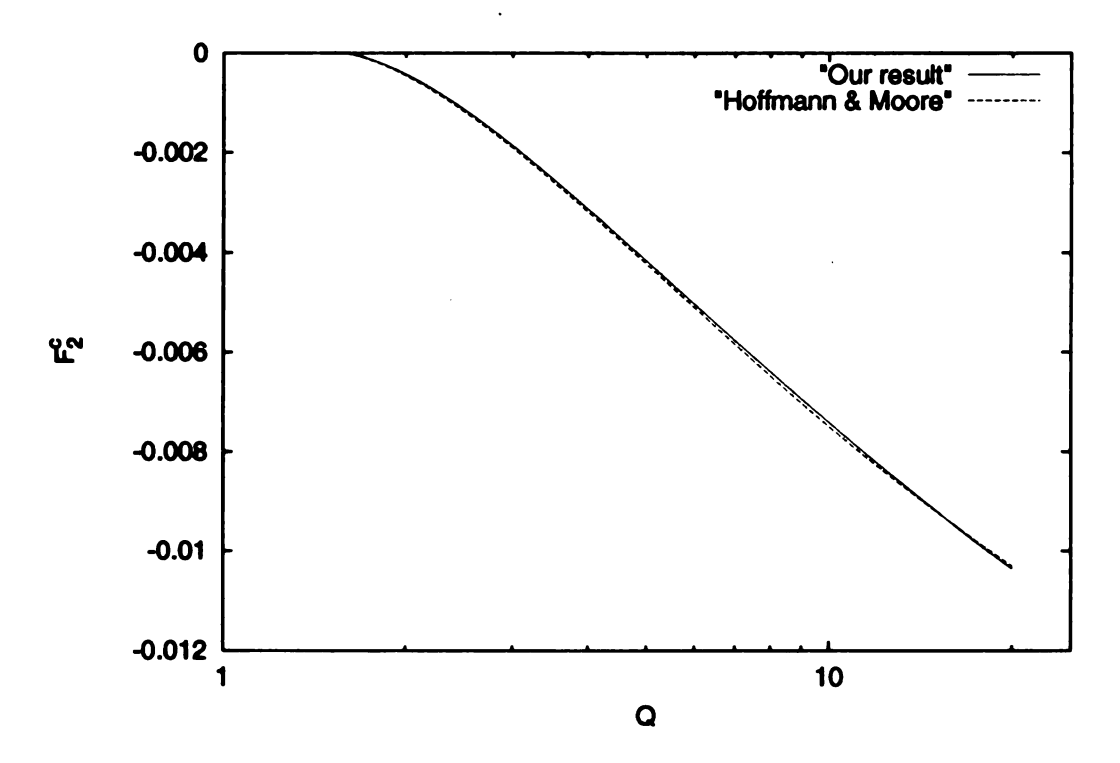


Figure 5.2: F_2^c for x = 0.1 and $m_c = 1.5$ GeV from $^1(\gamma^*c \to c) + (\gamma^*c \to gc)$ processes. Solid line is this work's result. Dashed line is the calculation of Reference [69]

safety of the ACOT scheme calculation. The resolution of this dilemma lies in the observation that the c-quark dynamically mixes with all the others as an active quark flavor in the ACOT scheme. The particular $\ln(\frac{Q}{m_c})$ factors seen here cancel with corresponding ones appearing in charm-loop contributions to light quark final state contributions to the total F_2 . The total structure function F_2 is well defined to all orders. However, because the charm-loop diagram contribution to light quark final states does not contribute to F_2^c , the charm contribution to F_2 , i.e., F_2^c , is not well defined at high orders in the ACOT scheme. In practice, for this order of α_s calculation, the entire contribution due to the gluon fragmentation subprocess is so small in the current HERA kinematic range, we do not need to worry about this problem. However, it will become a relevant issue when the calculation is extended to order α_s^2 , since this term is intimately related to the resummation of final-state collinear logarithms

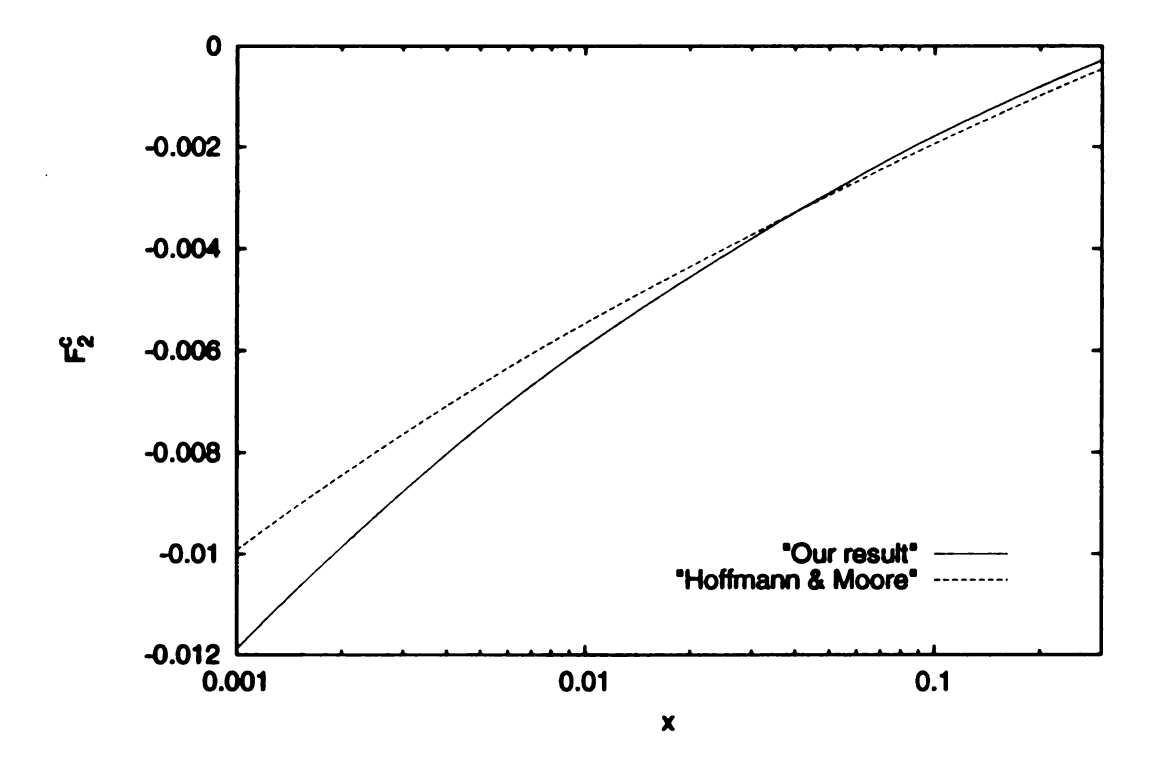


Figure 5.3: F_2^c for $Q^2 = 10$ and $m_c = 1.5$ GeV from $^1(\gamma^*c \to c) + (\gamma^*c \to gc)$ processes. Solid line is this work's result. Dashed line is the calculation of Reference [69]

in the NLO calculation.

5.2 Inclusive Charm Structure Function

We start by considering inclusive measurements, i.e., the inclusive structure function, F_2^c , and the total cross section for the production of charm quarks, e.g., σ^c .

In principle, the calculation contains three scale choices: the renormalization scale, the parton distribution factorization scale and the fragmentation scale. As is customary, we set the three to be equal. The scale should be dominated by the heavy quark mass for small values of Q but insensitive the heavy quark mass at large Q. We make the scale ansatz

$$\mu_0^2 = \begin{cases} \frac{1}{2} (Q^2 + \frac{m_c^4}{Q^2}) & \text{for } Q > m_c \\ m_c^2 & \text{for } Q \le m_c \end{cases}$$
 (5.9)

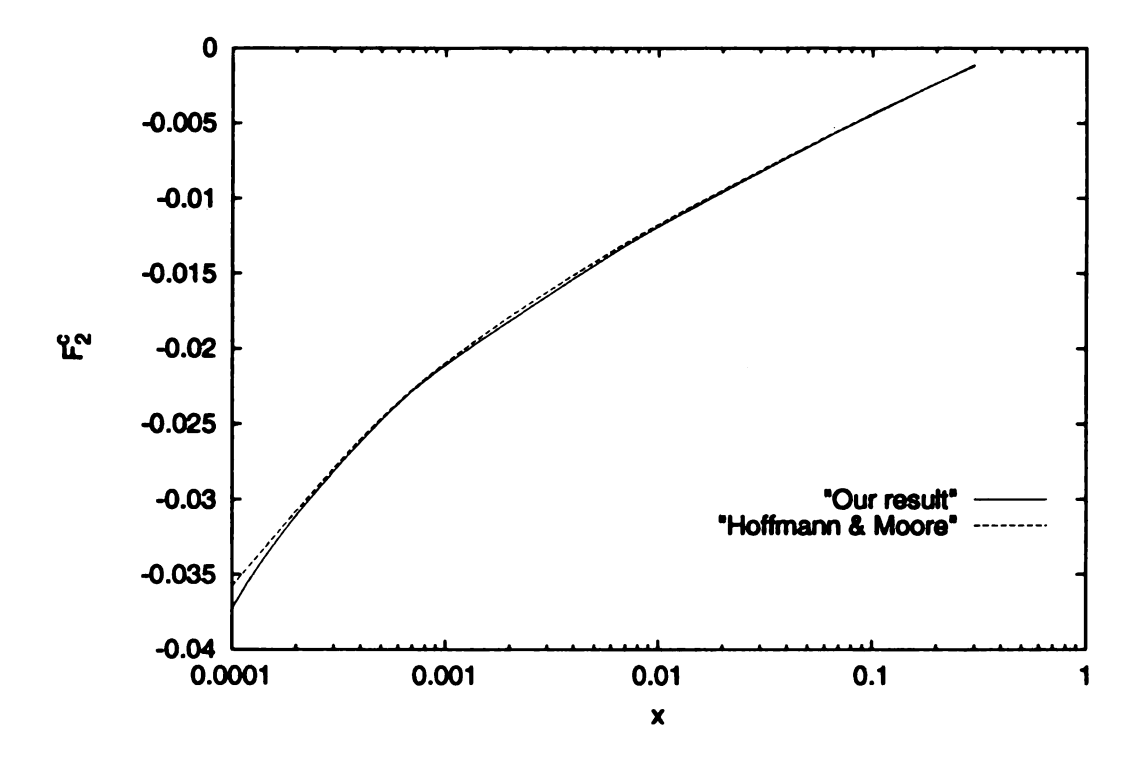


Figure 5.4: F_2^c for $Q^2 = 10$ and $m_c = 0.3$ GeV from $^1(\gamma^*c \to c) + (\gamma^*c \to gc)$ processes. Solid line is this work's result. Dashed line is the calculation of Reference [69]

In Figure 5.5 we display the μ -dependence of F_2^c at x=0.01, Q=10 GeV, using μ_0 as the reference value. Adding the higher-order terms to the leading ACOT results increases the cross section without substantially changing the μ -dependence. In either the LO ACOT or the NLO ACOT result case the μ dependence is weaker than the LO three-flavor calculation; it is approximately the same as the NLO three-flavor calculation. We expect that the full $\mathcal{O}(\alpha_s^2)$ calculation will improve the μ -dependence after the contributions from the higher order flavor creation processes with experimental cuts are added.

Once we have made a scale choice, the only parameters in the calculation are $\Lambda_{\rm QCD}$ and the charm quark pole mass, m_c . For the former, we use $\Lambda_{\overline{\rm MS}}^{(5)}=0.202$ GeV. However, the charm quark mass is not as well determined. In Figure 5.6 we show the dependence of the D^* cross section on the charm quark mass m_c . The shaded band

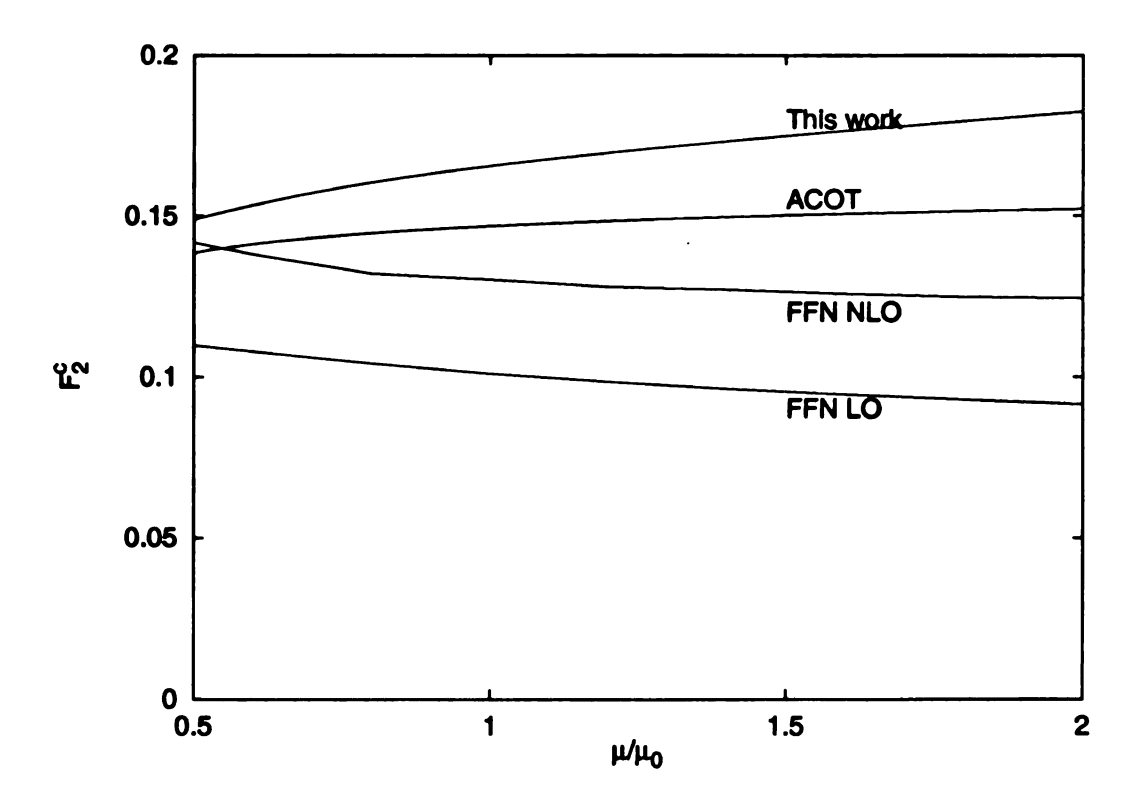


Figure 5.5: μ -dependence of $F_2^c(x=0.01,Q=10~{\rm GeV})$ in various calculational schemes. μ_0 is defined by Equation. 5.9.

represents measured cross section from ZEUS [63] within 1- σ experimental errors. The cross section is measured in the region 1 GeV² $\leq Q^2 \leq$ 600 GeV², 0.04 $\leq y \leq$ 0.7, 1.5 GeV $\leq p_t^D \leq$ 10 GeV, and $|\eta^D| \leq$ 1.5. These cuts are easily applied to our Monte Carlo implementation. The total integrated D^* cross section is related to the charm cross section by a fragmentation probability constant, which we take to be 0.26 [70]. Once the cuts are applied, however, there will be some residual dependence on the D^* fragmentation function in the result.

The measured cross section is consistent with the typical range of estimates of the charm quark pole mass within the 1- σ range, although lower values of m_c are disfavored. Based on this analysis we use $m_c = 1.5$ GeV for our other calculations. For consistent implementation of this comparison, we have used parton distribution functions fit for each individual value of m_c .

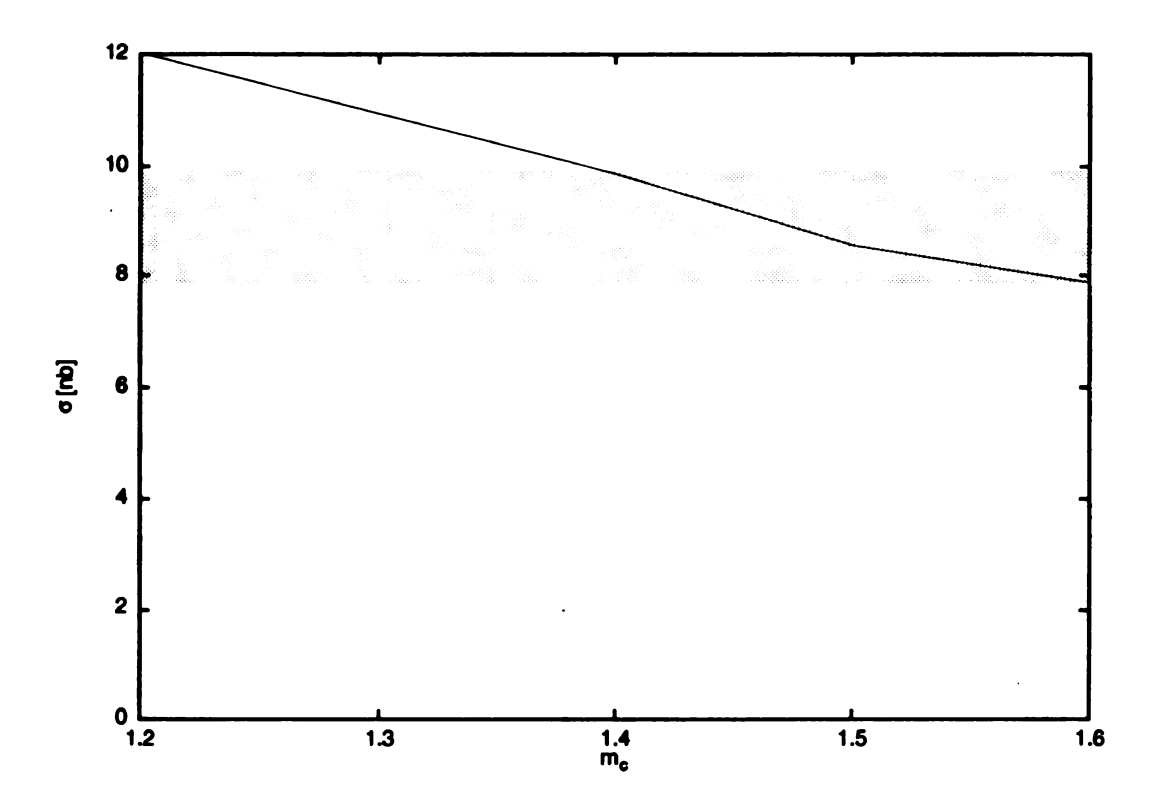


Figure 5.6: Measured D^* cross section at Zeus [63] with experimental cuts (described in the text) compared with our calculation as a function of the pole mass m_c . The shaded band represents the $1-\sigma$ experimental errors.

Figure 5.7 shows our results for F_2^c for various values of Q^2 . Our calculation is in good agreement with the data, as is the three-flavor NLO calculation. The differences between the two calculations are well within the experimental uncertainties. Since our calculation only involves order α_s terms, this means the same result is obtained with significant efficiency and economy compared to the conventional order α_s^2 three-flavor NLO calculation. The CPU time required by our calculation is nearly an order of magnitude smaller than required by the three-flavor NLO calculation. The efficiency is due to the fact that the major contributions of the complicated NLO three-flavor formula are from those large logarithmic terms which have been neatly resumed into the flavor excitation processes in our formalism.

Notice that while the simple three-flavor LO is substantially smaller than either the three-flavor NLO calculation or ours, our results are very similar to the three-

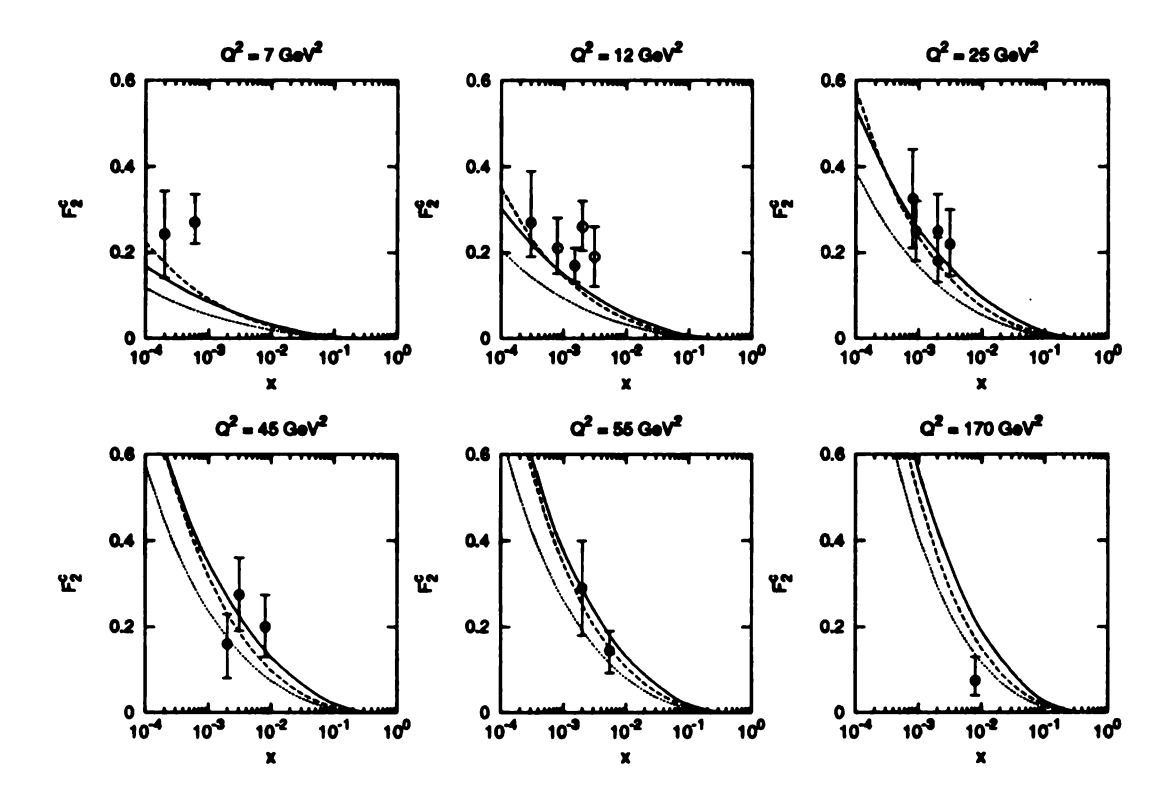


Figure 5.7: Total F_2^c for various values of Q^2 . Solid lines: ACOT. Dashed lines: three-flavor NLO calculation of Reference [38]. Dotted lines: three-flavor LO calculation. Solid points: Zeus 95 preliminary [65]. Open points: H1 [64].

flavor NLO results throughout most of the available range of Q^2 . This also implies that the flavor excitation processes where charm c is treated as an active parton effectively resums the most important contributions from the higher order processes. The small differences between our calculation and the three-flavor NLO calculation are illustrative and easily understood. The largest difference between the two calculations occurs at the smallest values of Q^2 . The logarithms resumed by our calculation are not so large in this region and the three-flavor NLO calculation is superior because it includes the contributions from the $O(\alpha_s^2)$ HC2 processes $\gamma^* + g \to c + \bar{c} + g$ and $\gamma^* + q \to c + \bar{c} + q$. We can see, however, for the majority of the parameter space explored at HERA energies the two calculations are practically indistinguishable. At the highest measured energies the two calculations begin to diverge. Here the logarithms begin to dominate the calculation. In this case our calculation is the

most reliable, although more experimental data and smaller error bars are needed to practically distinguish the two calculations.

Figure 5.8 shows the comparison between the LO ACOT F_2^c and F_2^c from this work at x = 0.1. The small correction that the NLO ACOT processes has in the whole energy range indicates the ACOT scheme perturbative expansion is well behaved. Notice the relatively large correction from the LO three-flavor result which indicates that the ACOT scheme calculation resums all the important contributions from the higher order, more complicated three-flavor heavy quark creation HC2 processes.

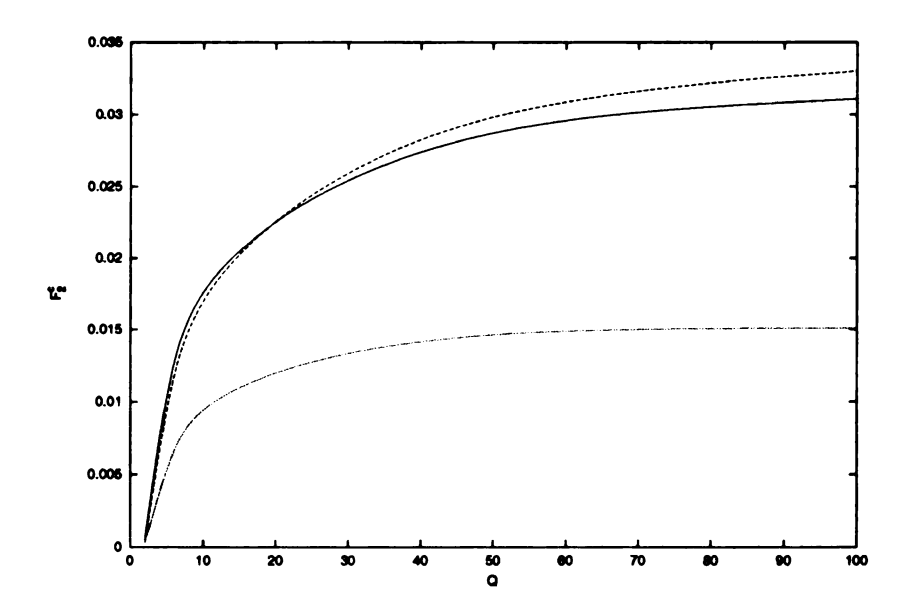


Figure 5.8: F_2^c at x = 0.1, solid line: This work, dashed line: LO ACOT calculation, dotted line: LO three-flavor calculation

Figure 5.9 shows the results of our calculation for $F_2^c(x,Q)$ for fixed x=0.01. Near threshold the HC1 (photon-gluon fusion) piece dominates. In this region the leading-order subtraction piece tends to cancel the contribution of the HE1 (heavy-flavor excitation) piece. As Q increases, so do the $log\left(\frac{m_c}{Q}\right)$ terms. The effect is that the HE1 piece quickly starts to dominate the cross section. The logarithmic term is present in the HC1 piece also, so the HC1 piece also grows rapidly. However, the subtraction term, which removes the would-be doubly-counted logarithm cancels the

majority of the HC1 term. The net effect is that the cross section is completely dominated by the HE1 term at large Q.

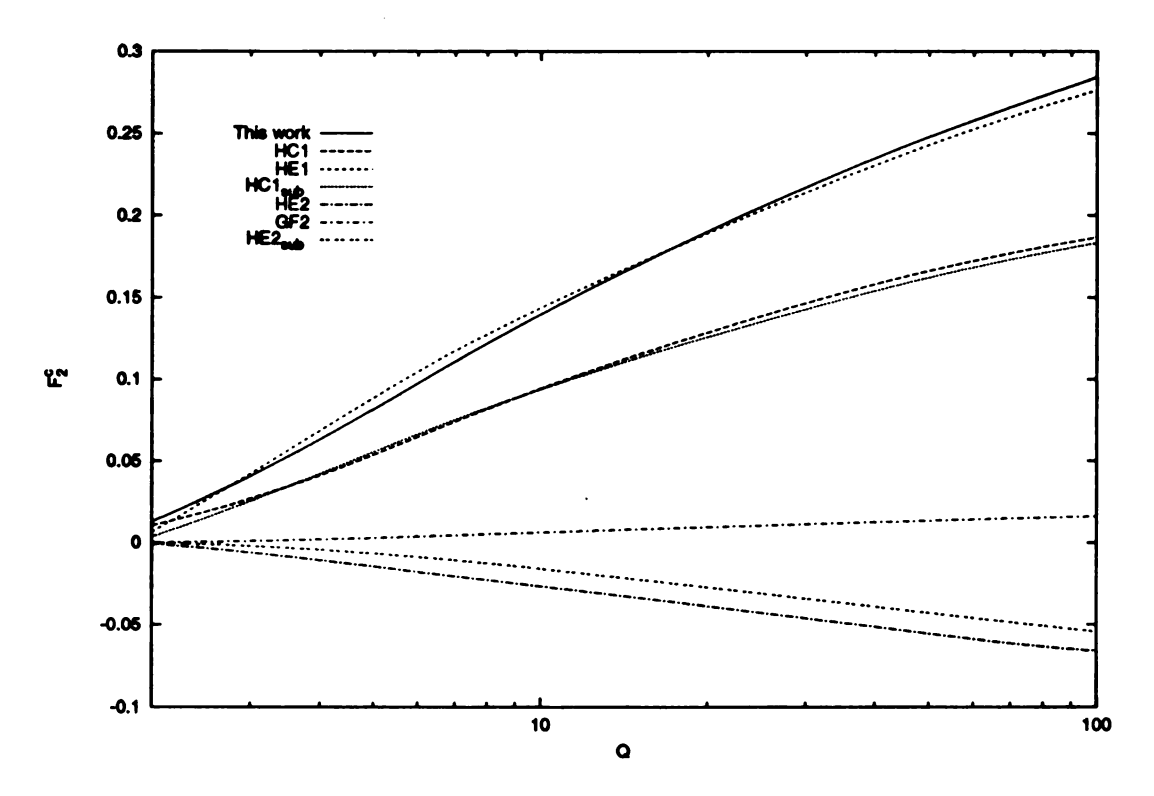


Figure 5.9: Contributions of the various subprocesses to $F_2^c(x,Q)$ at fixed x=0.01. The sign convention is such that the total cross section is HE1 + HC1 - HC1_{sub} + HE2 - HE2_{sub} + GF2

The new features of this calculation (compared with Reference [56]) are the GF2 and HE2 contributions, along with the corresponding subtraction. The new contributions are considerably smaller than the lower-order HE1 and HC1 pieces, indicating that the perturbation series is converging as it should. At this (relatively large) value of x the fragmentation (GF2) contribution is the most important factor for large Q. The net effect of the HE2 contribution is very small after the subtraction is included. Be aware that the relative sizes of the contributions are strongly x-dependent. However, it is a general feature that the HE2 and GF2 contributions are small corrections to the HE1 and HC1 contributions for reasonable values of x and Q.

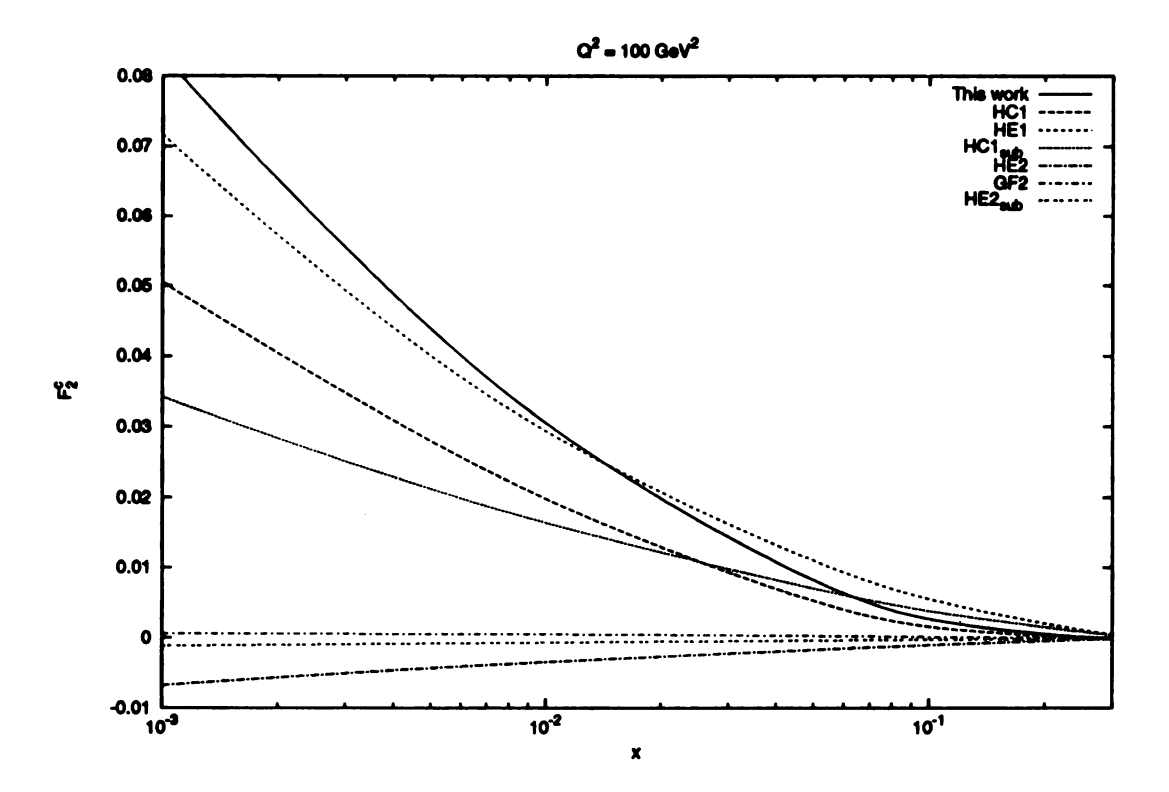


Figure 5.10: Contributions of the various subprocesses to $F_2^c(x,Q)$ at fixed $Q^2=7$ GeV. The sign convention is such that the total cross section is HE1 + HC1 - HC1_{sub} + HE2 - HE2_{sub} + GF2

In Figure 5.10, we see the same interplays between various subprocesses. For fixed Q, the large x limit correspond to the partonic hard scattering energy approaches to the final state threshold and every contribution becomes small. For $x \to 0$, the structure function rises significantly.

5.3 Differential Distributions

Because we have a Monte Carlo implementation of our calculation we are able to generate predictions for differential distributions involving final-state charm mesons. We are also able to directly incorporate experimental cuts into our calculation. This is an important advantage. Our calculation produces somewhat different results from three-flavor calculations in the small p_t region. If the experiments have to extrapolate

their data over the typically unobserved small p_t region, the results may depend more on differences between our calculations and another calculation than on the observed data. It is much better to directly compare the unextrapolated data with the appropriate theory.

In order to make predictions for mesons, as opposed to quarks, we need to incorporate the fragmentation of charmed quarks into charmed mesons. We have used the Peterson [71] form for the fragmentation of the charm quark into charmed mesons,

$$d_{c,np}^{D^{(\bullet)}}(z) = \frac{A}{z[1 - 1/z - \epsilon/(1 - x)]^2},$$
 (5.10)

with $\epsilon = 0.02$ [72, 73, 74] and A such that the branching fraction $B(c \to D^*) = 0.26$ [70]. The "np" in Equation 5.10 reflects non-perturbative nature of the fragmentation function. The Peterson form has the advantage of being widely used. Unfortunately, it violates the scaling behavior of QCD as found by heavy quark effective theory. However, inasmuch as it is merely a functional form fit to experimental data, it is perfectly satisfactory for our purposes.

The fit to Equation 5.10 in Reference [73] includes a convolution with the $c \to c$ fragmentation function in Equation 5.6, i.e.,

$$d_c^{D^{(\bullet)}}(z,\mu) = d_c^c(z,\mu) \otimes d_{c,np}^{D^{(\bullet)}}(z)$$
(5.11)

The fit includes data from $\sqrt{s} = 10.6$ GeV and $\sqrt{s} = 91.2$ GeV, so the perturbative evolution is substantial. The perturbative evolution only has a small effect on our calculation for HERA energies. Nonetheless, we include it for consistency.

There is an ambiguity in defining the momentum fraction of a heavy quark meson, z, for heavy quark fragmentation. We use the light-cone coordinate scaling variable, $p_D^+ = \xi p_c^+$, to scale the momenta for fragmentation kinematics in the lab frame. Harris and Smith [51] use a different prescription for fragmentation in their 3-flavor scheme

NLO calculation. In their prescription the 3-momenta scale such that $\vec{p}_D = \xi \vec{p}_c$. They then adjust the energy such that $p_D^2 = m_D^2$. We have verified that our results are insensitive to the differences between the two prescriptions. It is may be possible, however, to come up with an observable which depends more strongly on the exact prescription, so one must be careful when comparing results of different calculations.

Although the Monte Carlo approach allows us to plot arbitrary distributions, some care is required in choosing and interpreting them. First, the factorization scheme upon which we rely has been proven only for total cross sections. Differential distributions may still require other resummation in some kinematic regions. Second, our results for differential distributions at the quark level are singular in some regions. The simplest example is the p_t -distribution due to the leading order flavor excitation process HE1 $\gamma^* + c \rightarrow c$. The quark p_t is described by a Dirac delta function at zero. The same problem also happens in jet calculations. In hadron-hadron collisions this is rarely noticed because the singular region is experimentally inaccessible. In ep collisions, however, the singular region is visible in the lab frame. Fortunately, experiments measure mesons, not quarks. Once our quark-level calculation is convoluted with meson fragmentation, all our distributions are physically smooth. Actually, the presence of such effects probably indicates a need for a small- p_t resummation at some level.

To compare to our calculations of differential distributions, we have used preliminary data from Zeus 95 [75] for experimental data because it is substantially more detailed than similar previously published distributions from Zeus and H1. We expect similarly detailed data from H1 in the near future. In Figure 5.11 we compare our predicted p_t distribution with the Zeus 95 preliminary data. Notice that this and the following differential distributions in this chapter are subject to experimental cuts $\text{GeV}^2 \leq Q^2 \leq 600 \text{ GeV}^2$, $0.04 \leq y \leq 0.7$, $1.5 \text{ GeV} \leq p_t^{D^*} \leq 10 \text{ GeV}$, and $|\eta^{D^*}| \leq 1.5$.

The distribution in Q^2 is free from the potential problems in the p_t distribution. We

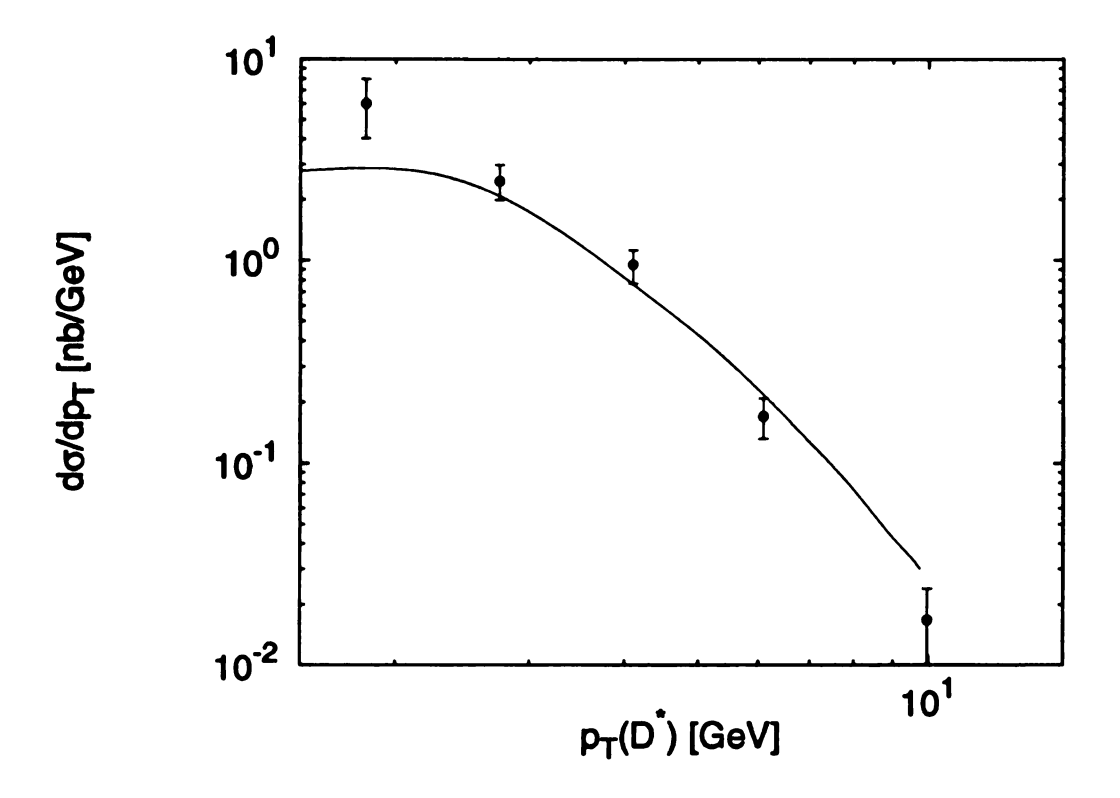


Figure 5.11: p_t distribution compared with data from Zeus 95. The experimental cuts are described in the text.

compare our results with the Zeus results in Figure 5.12. We also compare our predictions with experimental results for the distributions in η^{D^*} and W in Figure 5.14 and 5.13, respectively. The center-of-mass energy of the virtual photon-proton system, W, is given by

$$W^2 = m_P^2 + Q^2(\frac{1}{r} - 1). (5.12)$$

These distributions do not involve any further subtleties in the calculation. Unfortunately, the shape of the distributions is more a function of cuts than physics, so they serve primarily as a demonstration that our calculation is consistent with the experimental results under the appropriate cuts.

More differential distributions are possible, but they may involve further subtleties. For example, the evolution included in the GLAP equations involves an

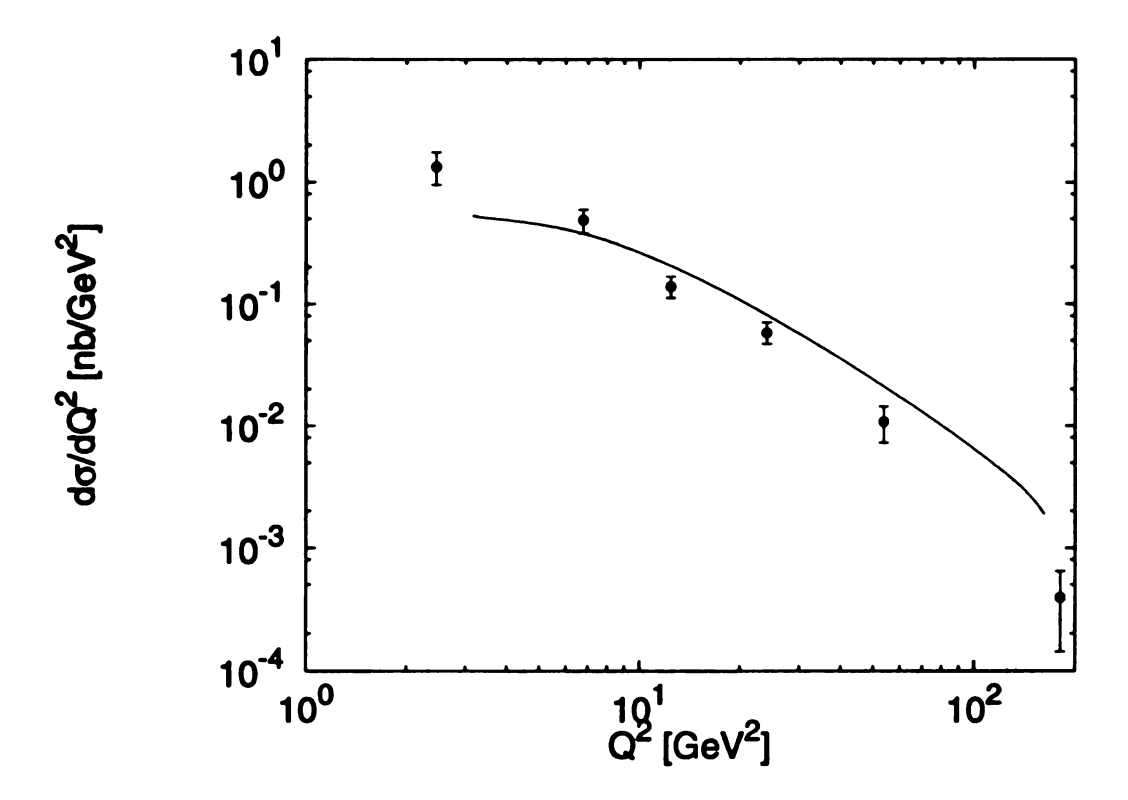


Figure 5.12: Q^2 distribution compared with data from Zeus 95. The experimental cuts are described in the text.

integration over the remaining final state particles. For this reason we are unable to extract charm-charm correlations, such as the azimuthal angle distribution, in the final state. Measuring the longitudinal momentum distribution of the charmed particles in the final state presents another problem. While the distributions are not singular, they depend strongly on the assumptions that go into our definition of the momentum fraction, the light-cone scaling prescriptions, and the frame in which the momentum scaling is implemented. These problems leave us without a definitive prediction for the longitudinal momentum distribution.

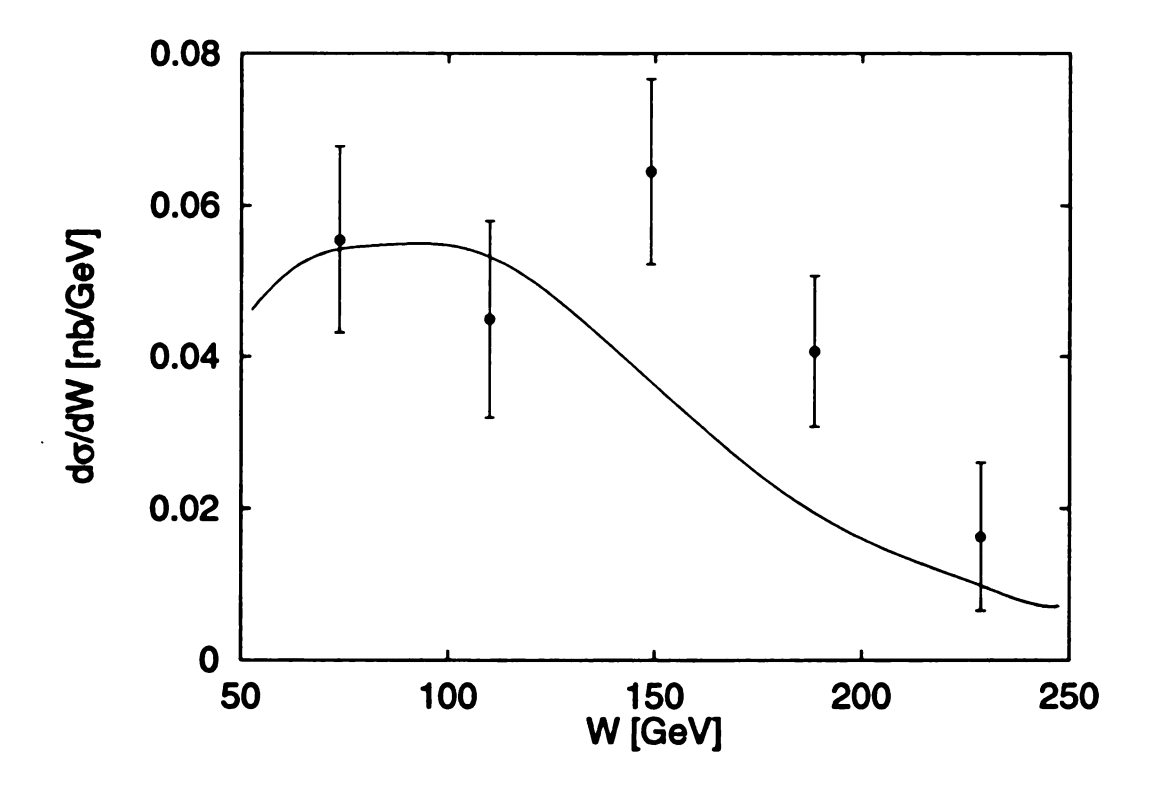


Figure 5.13: W distribution compared with data from Zeus 95. The experimental cuts are described in the text.

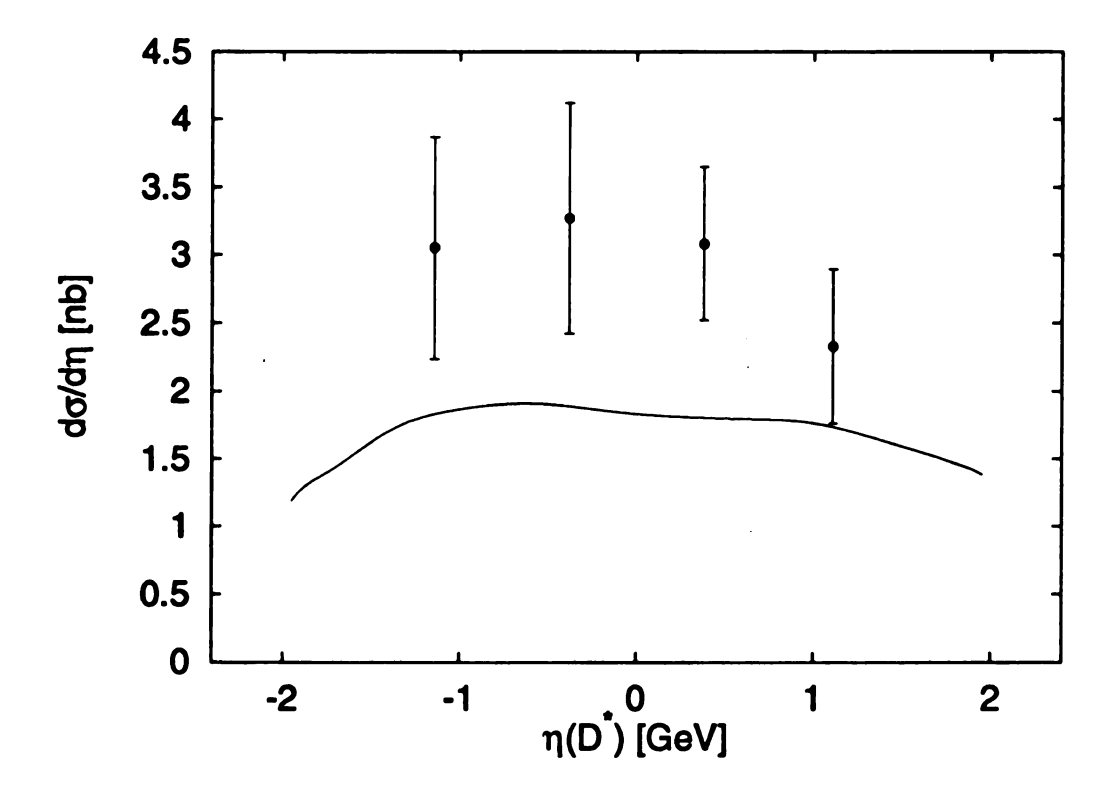


Figure 5.14: η distribution compared with data from Zeus 95. The experimental cuts are described in the text.

Chapter 6

Summary and Outlook

We discussed the physics of heavy quark production at deep inelastic scattering. First, we introduced the ACOT scheme and pointed out that the three-flavor scheme calculation, which has been widely used for recent heavy quark production phenomenological study, can not be reliably applied when the relevant energy scale is far larger than the heavy quark mass. Then, we demonstrated our formalism by calculating the inclusive F_2^c and various charm meson distribution functions at HERA using the helicity method and the Monte Carlo integration. Our results agree well with experiments.

This work extends the original ACOT leading order calculation by adding the terms which are required to give a full NLO calculation at high energies and implementing our calculation in a Monte Carlo analysis which allows to calculate differential distributions and incorporate experimental cuts.

Extending our work to the full NLO at high energies brings our calculation to the level of accuracy of the other theoretical inputs to the CTEQ global QCD analysis, and unlike the three-flavor NLO calculations, ours is valid to arbitrarily high energies. At HERA energies our calculation gives similar results to the NLO three-flavor calculation for inclusive quantities, but much more efficiently. The calculation is much simpler and the resulting program runs faster. This will useful for future global QCD

analysis where efficient computation is very important. At the theoretical level, we point out that we have identified the numerically most important contributions to heavy quark production. We also point out that the smallness of the corrections included in this work indicates that our perturbation series is in fact well-behaved. One might worry that the fairly large NLO/LO ratio seen in the three-flavor scheme indicates significant corrections from even higher order processes. However, the ACOT scheme does not have this problem.

By generating results for differential distributions we have shown that our calculation also does a reasonable job of predicting the details of heavy quark production. In this case we do expect the three-flavor NLO to have something of an edge. That calculation includes $2 \rightarrow 3$ kinematics; ours does not. Nonetheless, our predictions are in reasonable agreement with data from HERA. By incorporating experimental cuts in the Monte Carlo we are able to ensure that we are comparing our calculation directly with the data and not with the details of a different calculation needed to extrapolate the experimental data to all of phase space.

Having established that our calculation does a reasonable job in describing the existing HERA data, we are now in a position to explore further in several directions. We can extend the ACOT results to include all $O(\alpha_s^2)$ terms. Such a calculation would include all the advantages of both the current ACOT calculation and the three-flavor NLO calculation, especially, for the differential distributions. With more data available in the future, we will be able to use ACOT calculations to extract parton informations in the global analysis of the parton distribution functions. Another especially interesting question is whether the proton contains a non-perturbative charm component or not. The ACOT scheme is the only existing scheme which can address this problem in a self-consistent way.

Appendix A

Helicity Amplitudes of Heavy Quark Deep Inelastic Scattering Productions Via Neutral Current Interactions

In this appendix, we list the helicity amplitudes of the contributing processes¹. The notation is as following:

C denotes a heavy quark with mass m_c , i.e. charm quark, and $Q = \sqrt{-q^2}$ where q is the γ^*/Z momentum.

A.1
$$\gamma^*/Z + C \rightarrow C$$

For the $\gamma^*/Z + C \to C$ process with arbitrary vector boson and quark couplings $-ie\left[(F_{1V} + F_{1A}\gamma^5)\gamma^{\mu} + \frac{i\sigma^{\mu\nu}q^{\nu}}{2m_c}F_{2V} + \frac{i\sigma^{\mu\nu}q^{\nu}}{2m_c}F_{2A}\right]$, the helicity amplitude $J^i(q_j, q'_k)$, where i, j, k are the helicities of the vector boson, the initial state quark, the final state quark respectively, are:

$$J^{-}(q_{L}, q'_{R}) = -ie\sqrt{2}Q(F_{1V} + F_{2V} - \beta F_{1A})$$

$$J^{+}(q_{R}, q'_{L}) = -ie\sqrt{2}Q(-F_{1V} - F_{2V} - \beta F_{1A})$$

¹The author thanks Carl Schmidt for making the results available.

$$J^{0}(q_{L}, q'_{L}) = -ieQ \left(\frac{2m_{c}}{Q} F_{1V} - \frac{Q}{2m_{c}} F_{2V} - \frac{Q}{2m_{c}} \beta F_{2A} \right)$$

$$J^{0}(q_{R}, q'_{R}) = -ieQ \left(\frac{2m_{c}}{Q} F_{1V} - \frac{Q}{2m_{c}} F_{2V} + \frac{Q}{2m_{c}} \beta F_{2A} \right), \tag{A.1}$$

In the equations, $\beta = \sqrt{1 + \frac{4m_c^2}{Q^2}}$.

A.2 $\gamma^*/Z + g \rightarrow C + \bar{C}$, **HC1**

The helicity amplitudes $J^i(g_j, q_k, \bar{q}_l) = g_{qL}J^i(L, g_j, q_k, \bar{q}_l) + g_{qR}J^i(R, g_j, q_k, \bar{q}_l)$ listed below are calculated in the $c\bar{c}$ center of mass frame, as plotted in Figure A.1. The L, R indicate the chirality of the current and g_{qL}, g_{qR} are defined in 4.14 with electron helicity implicitly included. i, j, k, l are the helicities of the vector boson, the gluon, the final state quark, and the final state antiquark, respectively.

$$J^{+}(L, g_{+}, q_{L}, \bar{q}_{L}) = A_{-+}(-Bsc + C_{+}s^{2})$$

$$J^{+}(L, g_{+}, q_{L}, \bar{q}_{R}) = A_{++}(-Bc^{2} + C_{+}sc)$$

$$J^{+}(L, g_{+}, q_{R}, \bar{q}_{L}) = A_{--}(-Bs^{2} - C_{+}sc)$$

$$J^{+}(L, g_{+}, q_{R}, \bar{q}_{R}) = A_{-+}(-Bsc + C_{+}c^{2})$$

$$J^{+}(R, g_{+}, q_{L}, \bar{q}_{L}) = A_{-+}(-Bsc + C_{-}c^{2})$$

$$J^{+}(R, g_{+}, q_{L}, \bar{q}_{R}) = A_{--}(-Bc^{2} - C_{-}sc)$$

$$J^{+}(R, g_{+}, q_{R}, \bar{q}_{L}) = A_{++}(-Bs^{2} + C_{-}sc)$$

$$J^{+}(R, g_{+}, q_{R}, \bar{q}_{R}) = A_{-+}(-Bsc - C_{-}s^{2})$$

$$J^{-}(L, g_{+}, q_{L}, \bar{q}_{L}) = A_{-+}(-Bsc)$$

$$J^{-}(L, g_{+}, q_{L}, \bar{q}_{R}) = A_{++}(+Bs^{2})$$

$$J^{-}(L, g_{+}, q_{R}, \bar{q}_{L}) = A_{--}(+Bc^{2})$$

$$J^{-}(L, g_{+}, q_{R}, \bar{q}_{R}) = A_{-+}(-Bsc)$$

$$J^{-}(R, g_{+}, q_{L}, \bar{q}_{L}) = A_{-+}(-Bsc)$$

$$J^{-}(R, g_{+}, q_{L}, \bar{q}_{R}) = A_{--}(+Bs^{2})$$

$$J^{-}(R, g_{+}, q_{R}, \bar{q}_{L}) = A_{++}(+Bc^{2})$$

$$J^{-}(R, g_{+}, q_{R}, \bar{q}_{R}) = A_{-+}(-Bsc)$$

$$J^{0}(L, g_{+}, q_{L}, \bar{q}_{L}) = 2^{-1/2}A_{-+}[B(+s^{2}/D + Dc^{2}) - DC_{+}sc]$$

$$J^{0}(L, g_{+}, q_{L}, \bar{q}_{R}) = 2^{-1/2}A_{++}[B(+sc/D - Dsc) + DC_{+}s^{2}]$$

$$J^{0}(L, g_{+}, q_{R}, \bar{q}_{L}) = 2^{-1/2}A_{--}[B(-sc/D + Dsc) + DC_{+}c^{2}]$$

$$J^{0}(L, g_{+}, q_{R}, \bar{q}_{R}) = 2^{-1/2}A_{-+}[B(-c^{2}/D - Ds^{2}) - DC_{+}sc]$$

$$J^{0}(R, g_{+}, q_{L}, \bar{q}_{L}) = 2^{-1/2}A_{-+}[B(-c^{2}/D - Dsc) - DC_{-}s^{2}]$$

$$J^{0}(R, g_{+}, q_{L}, \bar{q}_{R}) = 2^{-1/2}A_{--}[B(+sc/D - Dsc) - DC_{-}c^{2}]$$

$$J^{0}(R, g_{+}, q_{R}, \bar{q}_{L}) = 2^{-1/2}A_{-+}[B(-sc/D + Dsc) - DC_{-}c^{2}]$$

$$J^{0}(R, g_{+}, q_{R}, \bar{q}_{R}) = 2^{-1/2}A_{-+}[B(+s^{2}/D + Dc^{2}) + DC_{-}sc],$$

where

$$A_{\pm\pm} = \frac{-2ieg_s T^a [(1 \pm \beta)(1 \pm \beta)]^{1/2}}{(1 - \beta^2 \cos^2 \theta')},$$

$$B = (E_{\text{charm}}/E_{gluon})\beta \sin \theta' = (1 - \eta/\xi)\beta \sin \theta',$$

$$C_{\pm} = 1 \pm \beta \cos \theta',$$

$$D = \sqrt{\hat{s}}/Q = \sqrt{\xi/\eta - 1},$$

$$\hat{s} = Q^2(\frac{\xi}{\eta} - 1),$$

$$\beta = \sqrt{1 - \frac{4m_c^2}{\hat{s}}}$$
(A.3)

and $s = \sin(\theta'/2)$, $c = \cos(\theta'/2)$. θ' is the scattering angle as plotted in Figure A.1.

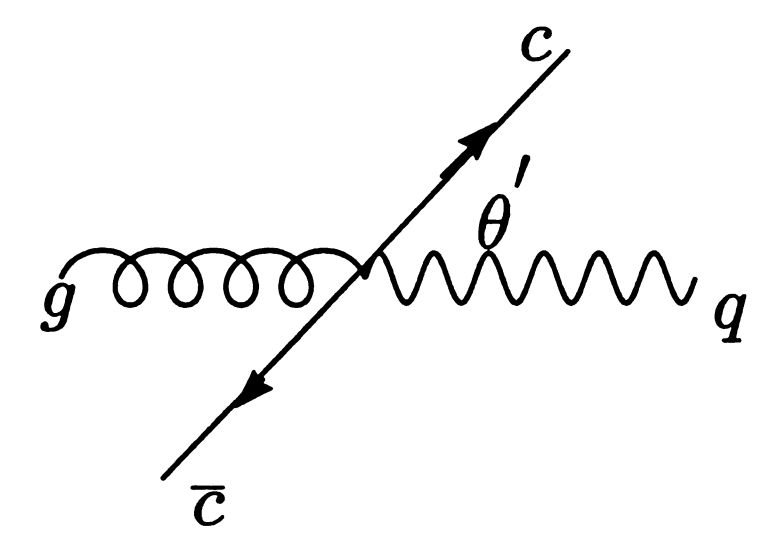


Figure A.1: $\gamma^*/Z + g \rightarrow c + \overline{c}$ in the $c\overline{c}$ center of mass frame.

The remaining processes can be obtained by

$$J^{i}([L,R],g_{j},q_{L},\bar{q}_{L}) = J^{-i}([R,L],g_{-j},q_{R},\bar{q}_{R})$$

$$J^{i}([L,R],g_{j},q_{L},\bar{q}_{R}) = -J^{-i}([R,L],g_{-j},q_{R},\bar{q}_{L}) . \tag{A.4}$$

A.3 $\gamma^*/Z + C \rightarrow C + g$, **HE2**

The helicity amplitude $J^i(g_j, q_k, q'_l) = g_L J^i(L, g_j, q_k, q'_l) + g_R J^i(R, g_j, q_k, q'_l)$ listed below are calculated in the gc center of mass frame, as plotted in Figure A.2. The L, R indicate the chirality of the current and g_{qL}, g_{qR} are defined in 4.14 with the electron helicity implicitly included. i, j, k, l are the helicities of the vector boson, the gluon, the initial state quark, and the final state quark, respectively.

$$J^{+}(L, g_{+}, q_{L}, q'_{L}) = -A_{++}(s^{3})$$

$$J^{+}(L, g_{+}, q_{R}, q'_{L}) = -A_{+-}(s^{2}c)(1 + B)$$

$$J^{+}(L, g_{+}, q_{L}, q'_{R}) = A_{-+}(cs^{2})$$

$$J^{+}(L, g_{+}, q_{R}, q'_{R}) = A_{--}(cs^{2})(1 + B)$$

$$J^{+}(R, g_{+}, q_{L}, q'_{L}) = 0$$

$$J^{+}(R, g_{+}, q_{R}, q'_{L}) = A_{-+}(2cs^{2})B$$

$$J^{+}(R, g_{+}, q_{L}, q'_{R}) = 0$$

$$J^{+}(R, g_{+}, q_{R}, q'_{R}) = -A_{++}(s)(Bc^{2} + D)$$

$$J^{-}(L, g_{+}, q_{L}, q'_{L}) = A_{++}(c^{3})$$

$$J^{-}(L, g_{+}, q_{L}, q'_{L}) = A_{+-}(c^{3})$$

$$J^{-}(L, g_{+}, q_{L}, q'_{R}) = A_{-+}(s^{2}c)(1 - B)$$

$$J^{-}(L, g_{+}, q_{L}, q'_{L}) = A_{--}(sc^{2})$$

$$J^{-}(R, g_{+}, q_{L}, q'_{L}) = A_{--}(sc^{2})B$$

$$J^{-}(R, g_{+}, q_{L}, q'_{L}) = 0$$

$$J^{-}(R, g_{+}, q_{L}, q'_{R}) = -A_{+-}(c)(-Bs^{2} + D)$$

$$J^{-}(R, g_{+}, q_{L}, q'_{L}) = -2^{-1/2}A_{++}cs^{2}(-2q_{0} + B(q_{0} + p))/Q$$

$$J^{0}(L, g_{+}, q_{L}, q'_{L}) = 2^{-1/2}A_{-+}s(q_{0}(s^{2} - c^{2}) - p + B(q_{0} + p)c^{2})/Q$$

$$J^{0}(L, g_{+}, q_{L}, q'_{L}) = 2^{-1/2}A_{--}c(q_{0}(s^{2} - c^{2}) - p + B(q_{0} - p)s^{2})/Q$$

$$J^{0}(R, g_{+}, q_{L}, q'_{L}) = 2^{-1/2}A_{--}s^{2}cB(q_{0} - p)/Q$$

$$J^{0}(R, g_{+}, q_{L}, q'_{L}) = -2^{-1/2}A_{-+}s^{2}cB(q_{0} + p)/Q$$

$$J^{0}(R, g_{+}, q_{L}, q'_{L}) = -2^{-1/2}A_{-+}s^{2}cB(q_{0} + p)/Q$$

$$J^{0}(R, g_{+}, q_{L}, q'_{R}) = 2^{-1/2}A_{-+}s(q_{0} - p)(Bc^{2} + D)$$

$$J^{0}(R, g_{+}, q_{L}, q'_{R}) = 2^{-1/2}A_{++}s(q_{0} + p)(-Bs^{2} + D),$$
(A.6)

where

$$A_{\pm\pm} = \frac{-2ieg_s T^a [(E'_p/E_p)(1 \pm \beta')(1 \pm \beta)]^{1/2}}{(1 - \beta \cos \theta')} ,$$

$$B = p/E_l,$$

$$D = \frac{p^{\mu} \cdot l_{\mu}}{p'^{\mu} \cdot l_{\mu}},$$

$$\hat{s} = (\frac{\xi}{\eta} - 1)Q^{2} + (1 - \frac{\xi}{\eta})m^{2},$$

$$E_{l} = \frac{\hat{s} - m^{2}}{2\sqrt{\hat{s}}},$$

$$E'_{p} = \frac{\hat{s} + m^{2}}{2\sqrt{\hat{s}}},$$

$$E_{p} = \frac{\hat{s} + Q^{2} + m^{2}}{2\sqrt{\hat{s}}},$$

$$q_{0} = \frac{\hat{s} - Q^{2} - m^{2}}{2\sqrt{\hat{s}}},$$
(A.7)

and $s=\sin(\theta'/2)$, $c=\cos(\theta'/2)$. θ' is the $\gamma^*/Z(q)+c/\bar{c}(p)\to g(l)+c/\bar{c}(p')$ scattering angle, p^μ is the 4-momentum of the initial state quark, p'^μ is the 4-momentum of the final state quark and l^μ is the 4-momentum of the gluon, The meanings of q_0, p, p', E_p, E_p' can be read from Figure A.2.

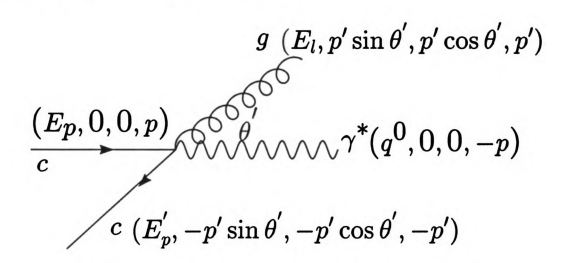


Figure A.2: $\gamma^*/Z + c \rightarrow g + c$ in the gc center of mass frame.

The remaining processes can be obtained by

$$J^{i}([L, R], g_{j}, q_{L}, q'_{L}) = J^{-i}([R, L], g_{-j}, q_{R}, q'_{R})$$

$$J^{i}([L,R],g_{j},q_{L},q'_{R}) = -J^{-i}([R,L],g_{-j},q_{R},q'_{L})$$
 (A.8)

Appendix B

From Helicity Amplitudes to Cross Sections

In this appendix, we derive the cross section formula we used for this work. Most of the equations are already presented in the main text, but here we collect these scattered formulas together for easier reference.

From the factorization theorem, the cross section for deep inelastic scattering $l_1(k) + N(P) \rightarrow l_2(k') + H(p') + X(p_x)$ is

$$d\sigma^{l_1 N \to l_2 HX} = \frac{1}{2\Delta(s, M_N^2, 0)} \int \frac{d\xi}{\xi} \phi_N^a(\xi, \mu^2) |M_a|^2 d\Gamma,$$
 (B.1)

with phase space factor $D\Gamma$ as

$$d\Gamma = (2\pi)^4 \delta^4(p + k - k' - p' - \sum p'_x) \frac{d^3k'}{(2\pi)^3 2k'_0} \frac{d^3p'}{(2\pi)^3 2E'} \Pi \frac{d^3p'_x}{(2\pi)^3 2E'_a} . \tag{B.2}$$

Simplifying Equation B.1 by using the standard variables used in DIS,

$$\frac{d^3k'}{(2\pi)^3 2k'_0} = \frac{ME_{l_1}y}{8\pi^2} dx dy \frac{d\phi}{2\pi},$$

$$\Delta(s, M_N^2, 0) = 2M_N E_{l_1},$$

we obtain

$$d\sigma = \frac{y}{32\pi^2} dx dy \frac{d\phi}{2\pi} \int \frac{d\xi}{\xi} \phi_N^a(\xi) |M_a|^2 d\Gamma', \tag{B.3}$$

with

$$d\Gamma' = (2\pi)^4 \delta^4(p + q - p' - \sum p'_x) \frac{d^3 p'}{(2\pi)^3 2E'} \Pi \frac{d^3 p'_x}{(2\pi)^3 2E'_x}$$
(B.4)

for the hadronic final state.

Using the helicity method, we can write the cross section as

$$d\sigma = \frac{y}{32\pi^2} dx dy \frac{d\phi}{2\pi} \int \frac{d\xi}{\xi} \phi_N^a(\xi)$$

$$\left(p_{eL} * |j_{eL}^{\mu} J_{a\mu}^{eL}|^2 + p_{eR} * |j_{eR}^{\mu} J_{a\mu}^{eR}|^2 \right) d\Gamma',$$
(B.5)

where eL, eR represent the left-handed lepton and the right-handed lepton respectively. The sum of p_{eL} and p_{eR} , which represent a polarized lepton beam, is obvious 1. For neutral current interaction, we can extract a factor $\frac{e^2}{Q^4}$ from the matrix element squared. The vector boson and quark coupling can then be written as $-ie\gamma^{\mu}g_a^b$ where a=qL, qR labels the left and right chiral couplings of the quark to the neutral bosons and b=eL, eR labels the left and right handed incoming lepton currents. g_a^b can be obtained as the following:

$$g_{qL}^{eL} = Q_q - \left(\frac{-\frac{1}{2} + \sin^2 \theta_W}{\sin \theta_W \cos \theta_W}\right) \left(\frac{Q^2}{Q^2 + M_Z^2}\right) \left(\frac{T_{3q} - Q_q \sin^2 \theta_W}{\sin \theta_W \cos \theta_W}\right)$$

$$g_{qR}^{eL} = Q_q - \left(\frac{-\frac{1}{2} + \sin^2 \theta_W}{\sin \theta_W \cos \theta_W}\right) \left(\frac{Q^2}{Q^2 + M_Z^2}\right) \left(\frac{-Q_q \sin^2 \theta_W}{\sin \theta_W \cos \theta_W}\right)$$

$$g_{qL}^{eR} = Q_q - \left(\frac{\sin^2 \theta_W}{\sin \theta_W \cos \theta_W}\right) \left(\frac{Q^2}{Q^2 + M_Z^2}\right) \left(\frac{T_{3q} - Q_q \sin^2 \theta_W}{\sin \theta_W \cos \theta_W}\right)$$

$$g_{qR}^{eR} = Q_q - \left(\frac{\sin^2 \theta_W}{\sin \theta_W \cos \theta_W}\right) \left(\frac{Q^2}{Q^2 + M_Z^2}\right) \left(\frac{-Q_q \sin^2 \theta_W}{\sin \theta_W \cos \theta_W}\right). \tag{B.6}$$

In Equation B.6, Q_q is the fraction charge of the quark, T_{3q} is the quark's third component of the weak isospin, and θ_W is the weak angle. The coupling g_a^b effectively adds the photon and Z boson contributions to the hadron current at the amplitude level after the lepton currents are factored out.

Defining the vector boson polarization vectors ϵ_i^{μ} as

$$\epsilon_0^{\mu}(P,q) = \frac{(-q^2)P^{\mu} + (P \cdot q)q^{\mu}}{\sqrt{(-q^2)\left[(P \cdot q)^2 - q^2P^2\right]}}$$

$$\epsilon_q^{\mu}(P,q) = \frac{q^{\mu}}{\sqrt{-q^2}}$$

$$\epsilon_+^{\mu}(P,q) = \frac{e^{-i\tilde{\phi}}}{\sqrt{2}}(0,+1,-i,0)$$

$$\epsilon_-^{\mu}(P,q) = \frac{e^{+i\tilde{\phi}}}{\sqrt{2}}(0,+1,+i,0).$$
(B.7)

The lepton currents can be expanded as

$$j_{eL}^{\mu} = \sqrt{2Q^2} \left[\frac{\sinh \psi}{\sqrt{2}} \epsilon_0^{\mu} - (\frac{\cosh \psi - 1}{\sqrt{2}}) \epsilon_+^{\mu} - (\frac{\cosh \psi + 1}{\sqrt{2}}) \epsilon_-^{\mu} \right]$$

$$= \sqrt{2Q^2} D_i^L \epsilon_i^{\mu}, \quad i = +, -, 0$$

$$j_{eR}^{\mu} = \sqrt{2Q^2} \left[\frac{\sinh \psi}{\sqrt{2}} \epsilon_0^{\mu} - (\frac{\cosh \psi + 1}{\sqrt{2}}) \epsilon_+^{\mu} - (\frac{\cosh \psi - 1}{\sqrt{2}}) \epsilon_-^{\mu} \right]$$

$$= \sqrt{2Q^2} D_i^R \epsilon_i^{\mu}, \quad i = +, -, 0$$
(B.8)

Then, the cross section can be written as

$$d\sigma = \frac{ye^{2}}{16\pi^{2}Q^{2}}dxdy\frac{d\phi}{2\pi}\int \frac{d\xi}{\xi}\phi_{N}^{a}(\xi,\mu^{2})$$

$$\left(p_{eL}*D_{i}^{eL}D_{j}^{eL}J_{eL,a}^{i}J_{eL,a}^{j*}+p_{eR}*D_{i}^{eR}D_{j}^{eR}J_{eR,a}^{i}J_{eR,a}^{j*}\right)d\Gamma'$$
(B.9)

where $J^i = \epsilon^i_\mu J^\mu$. For heavy quark production at HERA where unpolarized electron beam scattering with proton, $p_L = p_R = \frac{1}{2}$, so the cross section and the structure functions simplify to

$$d\sigma = \frac{ye^2}{32\pi^2 Q^2} dx dy \frac{d\phi}{2\pi} \int_0^1 \frac{d\xi}{\xi} \phi_N^a(\xi, \mu^2) \left(D_i^{eL} D_j^{eL} J_{eL,a}^i J_{eL,a}^{j*} + D_i^{eR} D_j^{eR} J_{eR,a}^i J_{eR,a}^{j*} \right) d\Gamma'$$
(B.10)

and

$$F_{\lambda}(x,Q^2) = \frac{1}{8\pi} \int_0^1 \frac{d\xi}{\xi} \phi(\xi,\mu^2) \left(D_{\lambda}^{eL} D_{\lambda}^{eL} J_{eL,a}^{\lambda} J_{eL,a}^{\lambda*} + D_{\lambda}^{eR} D_{\lambda}^{eR} J_{eR,a}^{\lambda} J_{eR,a}^{\lambda*} \right) d\Gamma' . \quad (B.11)$$

Now, we will present the more detailed cross section formulas for different processes. We use L and R to represent the left and right handed chiral couplings respectively. The hadronic currents will be expanded with the hadronic amplitudes listed in Appendix A. The phase space factor $d\Gamma'$ will also be presented in terms of the kinematic variables introduced in Appendix A.

B.1
$$\gamma^*/Z + C \rightarrow C$$
, **HE1**

$$d\sigma = \frac{ye^2}{32\pi^2Q^2}dxdy\frac{d\phi}{2\pi} \int_0^1 \frac{d\xi}{\xi} \phi_N^C(\xi,\mu^2) \left(D_i^{eL} D_j^{eL} J_{eL,C}^i J_{eL,C}^{j*} + D_i^{eR} D_j^{eR} J_{eR,C}^i J_{eR,C}^{j*} \right) d\Gamma'$$

$$= \frac{ye^2}{8\pi Q^2}dxdy\frac{d\phi}{2\pi} \int_0^1 \frac{d\xi}{\xi} \phi_N^C(\xi,\mu^2) * \frac{\xi\delta(\xi-\xi_0)}{2\sqrt{1+4m^2/Q^2}} * \frac{1}{2} *$$

$$\left((D_0^{eL} * (g_L^{eL} J^0(L,q_L,q_L) + g_R^{eL} J^0(R,q_L,q_L)))^2 + (D_0^{eL} * (g_L^{eL} J^0(L,q_R,q_R) + g_R^{eL} J^0(R,q_R,q_R)))^2 + (D_0^{eL} * (g_L^{eL} J^-(L,q_L,q_R) + g_R^{eL} J^-(R,q_L,q_R)))^2 + (D_+^{eL} * (g_L^{eL} J^+(L,q_R,q_L) + g_R^{eL} J^+(R,q_R,q_L)))^2 + (D_0^{eR} * (g_L^{eR} J^0(L,q_L,q_L) + g_R^{eR} J^0(R,q_L,q_L)))^2 + (D_0^{eR} * (g_L^{eR} J^0(L,q_R,q_R) + g_R^{eR} J^0(R,q_R,q_R)))^2 + (D_-^{eR} * (g_L^{eR} J^-(L,q_L,q_R) + g_R^{eR} J^-(R,q_L,q_R)))^2 + (D_-^{eR} * (g_L^{eR} J^-(L,q_L,q_R) + g_R^{eR} J^-(R,q_L,q_R)))^2 + (D_-^{eR} * (g_L^{eR} J^+(L,q_R,q_L) + g_R^{eR} J^-(R,q_L,q_R)))^2 + (D_-^{eR} * (g_L^{eR} J^+(L,q_R,q_L) + g_R^{eR} J^-(R,q_L,q_R)))^2 \right).$$
(B.12)

The helicity amplitude Js are defined as in Appendix A with

$$J^{i}(q_{j}, q_{k}) = g_{L}J^{i}(L, q_{j}, q_{k}') + g_{R}J^{i}(R, q_{j}, q_{k}'),$$
(B.13)

where L,R represent the left and right chiral couplings respectively. Changing the V-A coupling to chiral couplings in Equation A.1 gives the appropriate helicity amplitudes used in Equation B.12. In Equation refapp1X1, $\xi_0 = \frac{\eta}{2} \left(1 + \sqrt{(1 + \frac{4m_c^2}{Q^2})} \right)$ with

$$\frac{1}{\eta} = \frac{1}{2x} + \sqrt{\frac{1}{4x^2} + \frac{M_N^2}{Q^2}}$$

B.2 $\gamma^*/Z + C \rightarrow C$, **HE2**

This one is similar to the above one, except Js, defined in Appendix A.1, are calculated using renormalized couplings:

$$-ie\left[(F_{1V} + F_{1A}\gamma^5)\gamma^{\mu} + \frac{i\sigma^{\mu\nu}q^{\nu}}{2m_c}F_{2V} + \frac{i\sigma^{\mu\nu}q^{\nu}}{2m_c}F_{2A}\right]$$
(B.14)

with

$$F_{1V} = \frac{\alpha_s}{2\pi} C_q f_V (I_1 + I_2)$$
 (B.15)

$$F_{1A} = \frac{\alpha_s}{2\pi} C_q f_A (I_1 - I_2) \tag{B.16}$$

$$F_{2V} = \frac{\alpha_s}{2\pi} C_q f_V(2I_2) \tag{B.17}$$

where

$$I_{1} = \left(\frac{4\pi\mu^{2}}{m_{c}^{2}}\right)^{\epsilon} \Gamma(1+\epsilon) \left\{ \frac{1}{\epsilon} \left[-1 - \left(\frac{1+\beta^{2}}{2\beta}\right) \ln\left(\frac{\beta-1}{\beta+1}\right) \right] - 2 + \left(\frac{1+\beta^{2}}{2\beta}\right) \left[-\frac{3}{2} \ln\left(\frac{\beta-1}{\beta+1}\right) - \frac{1}{2} \ln\left(\frac{\beta-1}{\beta+1}\right) \ln\left(\frac{\beta^{2}-1}{4\beta^{2}}\right) + Li_{2}\left(\frac{\beta+1}{2\beta}\right) - Li_{2}\left(\frac{\beta-1}{2\beta}\right) \right] \right\},$$

$$(B.18)$$

$$I_2 = \frac{m_c^2}{q^2 \beta} \ln(\frac{\beta - 1}{\beta + 1}).$$
 (B.19)

 $Li_2(x)$ is the usual Spence function defined by

$$Li_2(x) = -\int_0^x \frac{\ln(1-z)}{z} dz$$
, (B.20)

and
$$\beta = \sqrt{1 + \frac{4m^2}{Q^2}}$$
.

B.3 $\gamma^*/Z + g \rightarrow C + \overline{C}$, **HC1**

In Equation B.21, $\beta = \sqrt{1 - \frac{4m^2}{\hat{s}}}$, as defined in Appendix A.2.

$$\begin{split} d\sigma &= \frac{ye^2}{32\pi^2Q^2} dx dy \frac{d\phi}{2\pi} \int_0^1 \frac{d\xi}{\xi} \phi_N^g(\xi,\mu^2) \left(D_i^{eL} D_j^{eL} J_{eL,g}^i J_{eL,g}^{i*} + D_i^{eR} D_j^{eR} J_{eR,g}^i J_{eR,g}^{j*} \right) d\Gamma' \\ &= \frac{ye^2}{8\pi Q^2} dx dy \frac{d\phi}{2\pi} \int_0^1 \frac{d\xi}{\xi} \phi_N^g(\xi,\mu^2) * \frac{\beta}{32\pi^2} * 4\pi \alpha_s * \frac{Tr[T^a T^a]}{8} * \frac{1}{2} * \frac{d\cos\theta'}{2} \frac{d\tilde{\phi}}{2\pi} * \\ & \left[\left(D_0^{eL} * (g_L^{eL} J^0(L,g_+,q_L,\bar{q}_L) + g_R^{eL} J^0(R,g_+,q_L,\bar{q}_L) \right) \right. \\ &+ D_+^{eL} * (g_L^{eL} J^+(L,g_+,q_L,\bar{q}_L) + g_R^{eL} J^+(R,g_+,q_L,\bar{q}_L)) * e^{-i\phi} \\ &+ D_-^{eL} * (g_L^{eL} J^-(L,g_+,q_L,\bar{q}_L) + g_R^{eL} J^-(R,g_+,q_L,\bar{q}_L)) * e^{+i\phi} \right)^2 \\ &+ \left(D_0^{eL} * (g_L^{eL} J^0(L,g_+,q_L,\bar{q}_R) + g_R^{eL} J^0(R,g_+,q_L,\bar{q}_R)) * e^{-i\phi} \right. \\ &+ D_-^{eL} * (g_L^{eL} J^0(L,g_+,q_L,\bar{q}_R) + g_R^{eL} J^+(R,g_+,q_L,\bar{q}_R)) * e^{-i\phi} \\ &+ D_-^{eL} * (g_L^{eL} J^-(L,g_+,q_L,\bar{q}_R) + g_R^{eL} J^0(R,g_+,q_R,\bar{q}_L)) * e^{-i\phi} \\ &+ D_-^{eL} * (g_L^{eL} J^0(L,g_+,q_R,\bar{q}_L) + g_R^{eL} J^+(R,g_+,q_R,\bar{q}_L)) * e^{-i\phi} \\ &+ D_-^{eL} * (g_L^{eL} J^0(L,g_+,q_R,\bar{q}_L) + g_R^{eL} J^-(R,g_+,q_R,\bar{q}_L)) * e^{-i\phi} \\ &+ D_-^{eL} * (g_L^{eL} J^-(L,g_+,q_R,\bar{q}_L) + g_R^{eL} J^-(R,g_+,q_R,\bar{q}_R)) * e^{-i\phi} \\ &+ \left(D_0^{eL} * (g_L^{eL} J^0(L,g_+,q_R,\bar{q}_R) + g_R^{eL} J^-(R,g_+,q_R,\bar{q}_R)) * e^{-i\phi} \right)^2 \\ &+ \left(D_0^{eL} * (g_L^{eL} J^0(L,g_+,q_R,\bar{q}_R) + g_R^{eL} J^0(R,g_+,q_R,\bar{q}_R)) * e^{-i\phi} \right)^2 \end{aligned}$$

$$+ D_{-}^{L} * (g_{L}^{eL} J^{-}(L, g_{+}, q_{R}, \bar{q}_{R}) + g_{R}^{eL} J^{-}(R, g_{+}, q_{R}, \bar{q}_{R})) * e^{+i\phi})^{2}$$

$$+ \left(D_{0}^{eL} * (g_{L}^{eL} J^{0}(L, g_{-}, q_{L}, \bar{q}_{L}) + g_{R}^{eL} J^{0}(R, g_{-}, q_{L}, \bar{q}_{L})) * e^{-i\phi} \right)$$

$$+ D_{+}^{eL} * (g_{L}^{eL} J^{+}(L, g_{-}, q_{L}, \bar{q}_{L}) + g_{R}^{eL} J^{+}(R, g_{-}, q_{L}, \bar{q}_{L})) * e^{-i\phi}$$

$$+ D_{-}^{eL} * (g_{L}^{eL} J^{-}(L, g_{-}, q_{L}, \bar{q}_{L}) + g_{R}^{eL} J^{-}(R, g_{-}, q_{L}, \bar{q}_{R})) * e^{+i\phi})^{2}$$

$$+ \left(D_{0}^{eL} * (g_{L}^{eL} J^{0}(L, g_{-}, q_{L}, \bar{q}_{R}) + g_{R}^{eL} J^{0}(R, g_{-}, q_{L}, \bar{q}_{R})) * e^{+i\phi}\right)^{2}$$

$$+ \left(D_{0}^{eL} * (g_{L}^{eL} J^{-}(L, g_{-}, q_{L}, \bar{q}_{R}) + g_{R}^{eL} J^{-}(R, g_{-}, q_{L}, \bar{q}_{R})) * e^{-i\phi} \right)$$

$$+ D_{-}^{eL} * (g_{L}^{eL} J^{-}(L, g_{-}, q_{R}, \bar{q}_{L}) + g_{R}^{eL} J^{-}(R, g_{-}, q_{L}, \bar{q}_{R})) * e^{-i\phi}$$

$$+ D_{-}^{eL} * (g_{L}^{eL} J^{0}(L, g_{-}, q_{R}, \bar{q}_{L}) + g_{R}^{eL} J^{-}(R, g_{-}, q_{R}, \bar{q}_{L})) * e^{-i\phi}$$

$$+ D_{-}^{eL} * (g_{L}^{eL} J^{-}(L, g_{-}, q_{R}, \bar{q}_{L}) + g_{R}^{eL} J^{-}(R, g_{-}, q_{R}, \bar{q}_{L})) * e^{-i\phi}$$

$$+ D_{-}^{eL} * (g_{L}^{eL} J^{-}(L, g_{-}, q_{R}, \bar{q}_{R}) + g_{R}^{eL} J^{-}(R, g_{-}, q_{R}, \bar{q}_{R})) * e^{+i\phi}$$

$$+ D_{-}^{eL} * (g_{L}^{eL} J^{-}(L, g_{-}, q_{R}, \bar{q}_{R}) + g_{R}^{eL} J^{-}(R, g_{-}, q_{R}, \bar{q}_{R})) * e^{+i\phi}$$

$$+ D_{-}^{eL} * (g_{L}^{eL} J^{-}(L, g_{-}, q_{R}, \bar{q}_{R}) + g_{R}^{eL} J^{-}(R, g_{-}, q_{R}, \bar{q}_{R})) * e^{+i\phi}$$

$$+ D_{-}^{eL} * (g_{L}^{eL} J^{-}(L, g_{-}, q_{R}, \bar{q}_{R}) + g_{R}^{eL} J^{-}(R, g_{-}, q_{R}, \bar{q}_{R})) * e^{+i\phi}$$

$$+ D_{-}^{eL} * (g_{L}^{eR} J^{-}(L, g_{+}, q_{L}, \bar{q}_{L}) + g_{R}^{eR} J^{-}(R, g_{+}, q_{L}, \bar{q}_{L})) * e^{-i\phi}$$

$$+ D_{-}^{eR} * (g_{L}^{eR} J^{-}(L, g_{+}, q_{L}, \bar{q}_{R}) + g_{R}^{eR} J^{-}(R, g_{+}, q_{L}, \bar{q}_{R})) * e^{-i\phi}$$

$$+ D_{-}^{eR} * (g_{L}^{eR} J^{-}(L, g_{+}, q_{L}, \bar{q}_{R}) + g_{R}^{eR} J^{-}(R, g_{+}, q_{L}, \bar{q}_{R})) * e^{-i\phi}$$

$$+ D_{-}^{eR} * (g_{L}^{eR} J^{-}(L, g_{+}, q_{L}, \bar{q}_{L}) + g_{R}^{eR} J^{-}(R$$

$$+ D_{+}^{eR} * (g_{L}^{eR} J^{+}(L, g_{+}, q_{R}, \bar{q}_{R}) + g_{R}^{eR} J^{+}(R, g_{+}, q_{R}, \bar{q}_{R})) * e^{-i\phi}$$

$$+ D_{-}^{eR} * (g_{L}^{eR} J^{-}(L, g_{+}, q_{R}, \bar{q}_{R}) + g_{R}^{eR} J^{-}(R, g_{+}, q_{R}, \bar{q}_{R})) * e^{+i\phi})^{2}$$

$$+ \left(D_{0}^{eR} * (g_{L}^{eR} J^{0}(L, g_{-}, q_{L}, \bar{q}_{L}) + g_{R}^{eR} J^{0}(R, g_{-}, q_{L}, \bar{q}_{L})) \right)$$

$$+ D_{+}^{eR} * (g_{L}^{eR} J^{+}(L, g_{-}, q_{L}, \bar{q}_{L}) + g_{R}^{eR} J^{+}(R, g_{-}, q_{L}, \bar{q}_{L})) * e^{-i\phi}$$

$$+ D_{-}^{eR} * (g_{L}^{eR} J^{-}(L, g_{-}, q_{L}, \bar{q}_{L}) + g_{R}^{eR} J^{-}(R, g_{-}, q_{L}, \bar{q}_{L})) * e^{+i\phi})^{2}$$

$$+ \left(D_{0}^{eR} * (g_{L}^{eR} J^{0}(L, g_{-}, q_{L}, \bar{q}_{R}) + g_{R}^{eR} J^{0}(R, g_{-}, q_{L}, \bar{q}_{R})) * e^{+i\phi} \right)^{2}$$

$$+ \left(D_{0}^{eR} * (g_{L}^{eR} J^{+}(L, g_{-}, q_{L}, \bar{q}_{R}) + g_{R}^{eR} J^{+}(R, g_{-}, q_{L}, \bar{q}_{R})) * e^{-i\phi} \right)$$

$$+ D_{-}^{eR} * (g_{L}^{eR} J^{-}(L, g_{-}, q_{L}, \bar{q}_{R}) + g_{R}^{eR} J^{-}(R, g_{-}, q_{L}, \bar{q}_{R})) * e^{+i\phi})^{2}$$

$$+ \left(D_{0}^{eR} * (g_{L}^{eR} J^{+}(L, g_{-}, q_{R}, \bar{q}_{L}) + g_{R}^{eR} J^{+}(R, g_{-}, q_{R}, \bar{q}_{L})) * e^{-i\phi} \right)$$

$$+ D_{-}^{eR} * (g_{L}^{eR} J^{-}(L, g_{-}, q_{R}, \bar{q}_{L}) + g_{R}^{eR} J^{-}(R, g_{-}, q_{R}, \bar{q}_{L})) * e^{+i\phi})^{2}$$

$$+ \left(D_{0}^{eR} * (g_{L}^{eR} J^{-}(L, g_{-}, q_{R}, \bar{q}_{L}) + g_{R}^{eR} J^{-}(R, g_{-}, q_{R}, \bar{q}_{L})) * e^{+i\phi} \right)^{2}$$

$$+ \left(D_{0}^{eR} * (g_{L}^{eR} J^{-}(L, g_{-}, q_{R}, \bar{q}_{R}) + g_{R}^{eR} J^{-}(R, g_{-}, q_{R}, \bar{q}_{R})) * e^{+i\phi} \right)^{2}$$

$$+ \left(D_{0}^{eR} * (g_{L}^{eR} J^{-}(L, g_{-}, q_{R}, \bar{q}_{R}) + g_{R}^{eR} J^{-}(R, g_{-}, q_{R}, \bar{q}_{R})) * e^{+i\phi} \right)^{2}$$

$$+ \left(D_{0}^{eR} * (g_{L}^{eR} J^{-}(L, g_{-}, q_{R}, \bar{q}_{R}) + g_{R}^{eR} J^{-}(R, g_{-}, q_{R}, \bar{q}_{R})) * e^{-i\phi} \right)$$

$$+ \left(D_{0}^{eR} * (g_{L}^{eR} J^{-}(L, g_{-}, q_{R}, \bar{q}_{R}) + g_{R}^{eR} J^{-}(R, g_{-}, q_{R}, \bar{q}_{R})) * e^{-i\phi} \right)$$

$$+ \left(D_{0}^{eR} * (g_{L}^{eR} J^{-}(L, g_{-}, q_{R}, \bar{q}_{R}) + g_{R}^{eR} J^{-}(R, g_{-}, q_{R}, \bar{q}_{R})) * e^{-i\phi} \right)$$

$$+ \left(D_{0}^{eR} * (g_$$

B.4 $\gamma^*/Z + C \rightarrow C + g$, **HE2**

The definitions of $\sqrt{\hat{s}}$ and E_l in Equation B.22 are in Appendix A.3.

$$\begin{split} d\sigma &= \frac{ye^2}{32\pi^2Q^2}dxdy\frac{d\phi}{2\pi}\int_0^1\frac{d\xi}{\xi}\phi_N^C(\xi,\mu^2)\left(D_i^{eL}D_j^{eL}J_{eL,g}^iJ_{eL,g}^{j*} + D_i^{eR}D_j^{eR}J_{eR,g}^iJ_{eR,g}^{j*}\right)d\Gamma' \\ &= \frac{ye^2}{8\pi Q^2}dxdy\frac{d\phi}{2\pi}\int_0^1\frac{d\xi}{\xi}\phi_N^C(\xi,\mu^2)*\frac{2E_l}{\sqrt{\hat{s}}}\frac{1}{32\pi^2}*4\pi\alpha_s*\frac{Tr[T^aT^a]}{3}*\frac{1}{2}*\frac{d\cos\theta'}{2}\frac{d\tilde{\phi}}{2\pi}*\\ &\left[\left(D_0^{eL}*(g_L^{eL}J^0(L,g_+,q_L,\bar{q}_L)+g_R^{eL}J^0(R,g_+,q_L,\bar{q}_L)\right)\right.\\ &+ D_+^{eL}*(g_L^{eL}J^+(L,g_+,q_L,\bar{q}_L)+g_R^{eL}J^+(R,g_+,q_L,\bar{q}_L))*e^{-i\phi} \end{split}$$

$$+ D_{-}^{eL} * (g_L^{eL} J^{-}(L, g_+, q_L, \bar{q}_L) + g_R^{eL} J^{-}(R, g_+, q_L, \bar{q}_L)) * e^{+i\phi})^2$$

$$+ \left(D_0^{eL} * (g_L^{eL} J^{0}(L, g_+, q_L, \bar{q}_R) + g_R^{eL} J^{0}(R, g_+, q_L, \bar{q}_R)) \right)$$

$$+ D_{+}^{eL} * (g_L^{eL} J^{+}(L, g_+, q_L, \bar{q}_R) + g_R^{eL} J^{+}(R, g_+, q_L, \bar{q}_R)) * e^{-i\phi}$$

$$+ D_{-}^{eL} * (g_L^{eL} J^{-}(L, g_+, q_L, \bar{q}_R) + g_R^{eL} J^{-}(R, g_+, q_L, \bar{q}_R)) * e^{-i\phi}$$

$$+ D_0^{eL} * (g_L^{eL} J^{0}(L, g_+, q_R, \bar{q}_L) + g_R^{eL} J^{-}(R, g_+, q_R, \bar{q}_L))$$

$$+ D_0^{eL} * (g_L^{eL} J^{-}(L, g_+, q_R, \bar{q}_L) + g_R^{eL} J^{-}(R, g_+, q_R, \bar{q}_L)) * e^{-i\phi}$$

$$+ D_{-}^{eL} * (g_L^{eL} J^{-}(L, g_+, q_R, \bar{q}_L) + g_R^{eL} J^{-}(R, g_+, q_R, \bar{q}_L)) * e^{-i\phi}$$

$$+ D_{-}^{eL} * (g_L^{eL} J^{-}(L, g_+, q_R, \bar{q}_R) + g_R^{eL} J^{-}(R, g_+, q_R, \bar{q}_R)) * e^{-i\phi}$$

$$+ D_{-}^{eL} * (g_L^{eL} J^{-}(L, g_+, q_R, \bar{q}_R) + g_R^{eL} J^{-}(R, g_+, q_R, \bar{q}_R)) * e^{-i\phi}$$

$$+ D_{+}^{eL} * (g_L^{eL} J^{-}(L, g_+, q_R, \bar{q}_R) + g_R^{eL} J^{-}(R, g_+, q_R, \bar{q}_R)) * e^{-i\phi}$$

$$+ D_{-}^{eL} * (g_L^{eL} J^{-}(L, g_+, q_R, \bar{q}_R) + g_R^{eL} J^{-}(R, g_+, q_L, \bar{q}_L)) * e^{-i\phi}$$

$$+ D_{-}^{eL} * (g_L^{eL} J^{-}(L, g_-, q_L, \bar{q}_L) + g_R^{eL} J^{-}(R, g_-, q_L, \bar{q}_L)) * e^{-i\phi}$$

$$+ D_{-}^{eL} * (g_L^{eL} J^{-}(L, g_-, q_L, \bar{q}_L) + g_R^{eL} J^{-}(R, g_-, q_L, \bar{q}_R)) * e^{-i\phi}$$

$$+ D_{-}^{eL} * (g_L^{eL} J^{-}(L, g_-, q_L, \bar{q}_R) + g_R^{eL} J^{-}(R, g_-, q_L, \bar{q}_R)) * e^{-i\phi}$$

$$+ D_{-}^{eL} * (g_L^{eL} J^{-}(L, g_-, q_L, \bar{q}_R) + g_R^{eL} J^{-}(R, g_-, q_L, \bar{q}_R)) * e^{-i\phi}$$

$$+ D_{-}^{eL} * (g_L^{eL} J^{-}(L, g_-, q_R, \bar{q}_L) + g_R^{eL} J^{-}(R, g_-, q_R, \bar{q}_L)) * e^{-i\phi}$$

$$+ D_{-}^{eL} * (g_L^{eL} J^{-}(L, g_-, q_R, \bar{q}_L) + g_R^{eL} J^{-}(R, g_-, q_R, \bar{q}_L)) * e^{-i\phi}$$

$$+ D_{-}^{eL} * (g_L^{eL} J^{-}(L, g_-, q_R, \bar{q}_L) + g_R^{eL} J^{-}(R, g_-, q_R, \bar{q}_L)) * e^{-i\phi}$$

$$+ D_{-}^{eL} * (g_L^{eL} J^{-}(L, g_-, q_R, \bar{q}_R) + g_R^{eL} J^{-}(R, g_-, q_R, \bar{q}_R)) * e^{-i\phi}$$

$$+ D_{-}^{eL} * (g_L^{eL} J^{-}(L, g_-, q_R, \bar{q}_R) + g_R^{eL} J^$$

$$+ D_{-}^{fR} * (g_{L}^{eR} J^{+}(L, g_{+}, q_{L}, \bar{q}_{L}) + g_{R}^{eR} J^{+}(R, g_{+}, q_{L}, \bar{q}_{L})) * e^{-i\phi}$$

$$+ D_{-}^{eR} * (g_{L}^{eR} J^{-}(L, g_{+}, q_{L}, \bar{q}_{L}) + g_{R}^{eR} J^{-}(R, g_{+}, q_{L}, \bar{q}_{L})) * e^{-i\phi}$$

$$+ D_{-}^{eR} * (g_{L}^{eR} J^{0}(L, g_{+}, q_{L}, \bar{q}_{R}) + g_{R}^{eR} J^{0}(R, g_{+}, q_{L}, \bar{q}_{R})) * e^{-i\phi}$$

$$+ D_{+}^{eR} * (g_{L}^{eR} J^{+}(L, g_{+}, q_{L}, \bar{q}_{R}) + g_{R}^{eR} J^{+}(R, g_{+}, q_{L}, \bar{q}_{R})) * e^{-i\phi}$$

$$+ D_{+}^{eR} * (g_{L}^{eR} J^{+}(L, g_{+}, q_{L}, \bar{q}_{R}) + g_{R}^{eR} J^{-}(R, g_{+}, q_{L}, \bar{q}_{R})) * e^{-i\phi}$$

$$+ D_{-}^{eR} * (g_{L}^{eR} J^{-}(L, g_{+}, q_{R}, \bar{q}_{L}) + g_{R}^{eR} J^{-}(R, g_{+}, q_{R}, \bar{q}_{L})) * e^{-i\phi}$$

$$+ D_{+}^{eR} * (g_{L}^{eR} J^{+}(L, g_{+}, q_{R}, \bar{q}_{L}) + g_{R}^{eR} J^{+}(R, g_{+}, q_{R}, \bar{q}_{L})) * e^{-i\phi}$$

$$+ D_{+}^{eR} * (g_{L}^{eR} J^{-}(L, g_{+}, q_{R}, \bar{q}_{L}) + g_{R}^{eR} J^{-}(R, g_{+}, q_{R}, \bar{q}_{L})) * e^{-i\phi}$$

$$+ D_{-}^{eR} * (g_{L}^{eR} J^{-}(L, g_{+}, q_{R}, \bar{q}_{R}) + g_{R}^{eR} J^{-}(R, g_{+}, q_{R}, \bar{q}_{R})) * e^{-i\phi}$$

$$+ D_{-}^{eR} * (g_{L}^{eR} J^{-}(L, g_{+}, q_{R}, \bar{q}_{R}) + g_{R}^{eR} J^{-}(R, g_{+}, q_{R}, \bar{q}_{R})) * e^{-i\phi}$$

$$+ D_{-}^{eR} * (g_{L}^{eR} J^{-}(L, g_{+}, q_{R}, \bar{q}_{R}) + g_{R}^{eR} J^{-}(R, g_{+}, q_{R}, \bar{q}_{R})) * e^{-i\phi}$$

$$+ D_{-}^{eR} * (g_{L}^{eR} J^{-}(L, g_{-}, q_{L}, \bar{q}_{L}) + g_{R}^{eR} J^{-}(R, g_{-}, q_{L}, \bar{q}_{L})) * e^{-i\phi}$$

$$+ D_{-}^{eR} * (g_{L}^{eR} J^{-}(L, g_{-}, q_{L}, \bar{q}_{L}) + g_{R}^{eR} J^{-}(R, g_{-}, q_{L}, \bar{q}_{L})) * e^{-i\phi}$$

$$+ D_{-}^{eR} * (g_{L}^{eR} J^{-}(L, g_{-}, q_{L}, \bar{q}_{R}) + g_{R}^{eR} J^{-}(R, g_{-}, q_{L}, \bar{q}_{R})) * e^{-i\phi}$$

$$+ D_{-}^{eR} * (g_{L}^{eR} J^{-}(L, g_{-}, q_{L}, \bar{q}_{R}) + g_{R}^{eR} J^{-}(R, g_{-}, q_{L}, \bar{q}_{R})) * e^{-i\phi}$$

$$+ D_{-}^{eR} * (g_{L}^{eR} J^{-}(L, g_{-}, q_{L}, \bar{q}_{R}) + g_{R}^{eR} J^{-}(R, g_{-}, q_{L}, \bar{q}_{R})) * e^{-i\phi}$$

$$+ D_{-}^{eR} * (g_{L}^{eR} J^{-}(L, g_{-}, q_{R}, \bar{q}_{L}) + g_{R}^{eR} J^{-}(R, g_{-}, q_{R}, \bar{q}_{L}))$$

Bibliography

- [1] John F. Donoghue, Eugene Golowich, Barry R. Holstein, Dynamics of The Standard Model, Cambridge University Press, 1992.
- [2] Paul Langacker in Proceedings of the Theoretical Advanced Study Institute in Elementary Particle Physics, TASI'95, World Scientific, 1996
- [3] S. L. Glashow, Nucl. Phys. 22, 579 (1961); S. Weinberg, Phys. Rev. Lett. 19, 1264 (1967); A. Salam in Elementary Particle Theory, ed. N. Svartholm, (Almqvist and Wiksells, Stockholm, 1969) p. 367
- [4] Taizo Muta, Foundations of Quantum Chromodynamics., World Scientific, 1987
- [5] C. N. Yang and R. Mills, Phys. Rev. 96, 191 (1954);
- [6] Review of Particle Properties, Phys. Rev. D54, 1 (1996).
- [7] UA1: G. Arnison et al., Phys. Lett. B166, 484 (1986);
- [8] UA2: R. Ansari et al., Phys. Lett. B186, 440 (1987); J. Alitti et al., Phys. Lett. B276, 354 (1992)
- [9] N. Cabibbo, Phys. Rev. Lett. 10, 531 (1963).
- [10] S.L. Glashow, J.Iliopoulos & L. Maiani, Phys. Rev. D2, 1585 (1970).
- [11] M. Kobayashi and K. Maskawa, Prog. Theor. Phys. 49, 652 (1973).
- [12] Shasha, Dennis Elliott, Out of Their Minds: the Lives and Discoveries of 15 Great Computer scientists, New York: Copernicus, c1995.
- [13] E. D. Bloom et al., Phys. Rev. Lett. 23, 930 (1969); M. Brieidenbach et al., Phys. Rev. Lett. 23, 935 (1969); J. I. Friedman, H.W. Kendall, Ann. Rev. Nucl. Part. Sci. 22, 203 (1972)
- [14] J. D. Bjorken, Phys. Rev. 185, 1975 (1969)
- [15] G. Sterman, An Introduction to Quantum Field Theory, Cambridge University Press, 1993
- [16] J. C. COllins, Renormalization, Cambridge University Press, 1984
- [17] J. D. Bjorken, E.A. Paschos, Phys. Rev. D2, 1585 (1797);

- [18] R. P. Feynman, Phys. Rev. Lett. 23, 1415 (1969)
- [19] M. Gell-Mann, Phys. Lett. 8, 214 (1964)
- [20] F. Halzen, A.D. Martin, Quarks and Leptons: An introductory Course in Modern Particle Physics, John Wiley & Sons, Inc. 1984
- [21] D. Amati, R. Petronzio & G. Veneziano, Nucl. Phys. B140, 54; B146, 29 (1978); R.K. Ellis, H. Georgi, M. Machacek, H.D. Politzer & G.G. Ross, Nucl. Phys. B152, 285 (1979); S.B. Libby & G. Sterman, Phys. Rev. D18, 3252 (1978); J.C. Collins, D.E. Soper & G. Sterman, in Perturbative Quantum Chromodynamics, ed. A.H. Mueller, World Scientific (1989).
- [22] V.N. Gribov and L.N. Lipotov, Yad. Fiz. 15, 781 Sov. J. Nucl. Phys. 15, 438 (1972).
- [23] L.N. Lipotov, Yad. Fiz. 20, 181 Sov. J. Nucl. Phys. 20, 94 (1975)
- [24] G. Altarelli and G. Parisi Nucl. Phys. B126, 298 (1977).
- [25] S.D. Drell, D.J. Levy, and T.M. Yan, Phys. Rev. Lett. 22, 744 (1969); Phys. Rev. 187, 2159 (1969); Phys. Rev. D1, 1035 (1970); S.D. Drell and T.M. Yan, Phys. Rev. Lett. 25, 316 (1970); T.M. Yan and S.D. Drell, Phys. Rev. D1, 2402 (1970).
- [26] C. Balazs, C.P. Yuan, Phys. Rev. **D56**, 5558 (1997)
- [27] R. K. Ellis, W. G. Scoot in *Proton-Antiproton Collider Physics* World Scientific, 1998
- [28] F. Abe et al., Phys. Rev. Lett. 62, 613 (1989); ibid 62, 3020(1989)
- [29] J. Botts, J.G. Morfin, J.F. Owens, Jianwei Qiu, Wu-Ki Tung, and H. Weerts, Phys. Lett. B304, 159 (1993).
- [30] CTEQ Collaboration (H.L. Lai et al.), Phys. Rev. D51, 4763 (1995).
- [31] CTEQ Collaboration (H.L. Lai et al.), Phys. Rev. D55, 1280 (1997).
- [32] A.D. Martin, W.J. Stirling, and R.G. Roberts, Phys. Rev. D50, 6734 (1994); Phys. Lett. B354, 155 (1995).
- [33] A.D. Martin, R.G. Roberts, and W.J. Stirling, Phys. Lett. B387, 419 (1996).
- [34] G. Sterman in Proceedings of the Theoretical Advanced Study Institute in Elementary Particle Physics, TASI'95, World Scientific, 1996
- [35] CDF Collaboration, F. Abe et al., Phys. Rev. Lett. 74, 2626 (1995).
- [36] DØ Collaboration, S. Abachi et al., Phys. Rev. Lett. 74, 2632 (1995).
- [37] S. Frixione, M. Mangano, P. Nason, G. Ridolfi in *Heavy Flavours II* World Scientific, to be published.
- [38] E. Laenen, S. Riemersma, J. Smith and W.L. van Neerven, Phys. Lett. B291, 325 (1992)

- [39] E. Laenen, S. Riemersma, J. Smith and W.L. van Neerven, *Nucl. Phys.* **B392**, 162 (1993)
- [40] E. Laenen, S. Riemersma, J. Smith and W.L. van Neerven, Nucl. Phys. B392, 229 (1993)
- [41] M. Aivazis, J. Collins, F. Olness, W.K. Tung, Phys. Rev. D50, 3102 (1994)
- [42] A. D. Martin, R.G. Roberts, M.G. Ryskin, W.J. Stirling, Eur. Phys. J C2, 287 (1998)
- [43] H1 collaboration: S. Aid et. al., Nucl. Phys. B472, 32 (1996). ZEUS collaboration: M. Derrick et al., DESY 96-076 (to appear in Z. Phys.)
- [44] H1 collaboration: C. Adloff etal., DESY-96-138, hep-ex/9607012.
- [45] A.D. Martin, R.G. Roberts, W.J. Stirling, Phys. Rev. D50, 6734 (1994).
- [46] E. Eichten et al., Rev. Mod. Phys. 56, 579 (1984), Erratum 58, 1065 (1986).
- [47] P. Nason, S. Dawson, R. K. Ellis Nucl. Phys. B327, 49(1989), Erratum: B335, 260 (1990)
- [48] W. Beenakker, W.L. van Neerven, R. Meng, G.A. Schuler, J. Smith Nucl. Phys. B351, 507 (1991); W. Beenakker, H. Kuijf, W.L. van Neerven, J. Smith Phys. Rev. D40, 54 (1989);
- [49] M. Buza, Y. Matiounine, J. Smith, W.L. van Neerven, Nucl. Phys. B472, 611 (1996)
- [50] M. Buza, Y. Matiounine, J. Smith, W.L. van Neerven, Eur. Phys. J. bf C1, 301 (1998)
- [51] B.W. Harris, J. Smith Nucl. Phys. **B452**, 109 (1995)
- [52] J.C. Collins, F. Wilczek, and A. Zee, Phys. Rev. D18, 242 (1978).
- [53] J.C. Collins, hep-ph/9806259
- [54] S. Qian, Argonne preprint, ANL-HEP-PR-84-72; PhD thesis, IIT(1985)
- [55] W. Bernreuther, PITHA-94-31; hep-ph/9409390; QCD at LEP, 39 (1994)
- [56] M. Aivazis, J. Collins, F. Olness, W.K. Tung, Phys. Rev. D50, 3085 (1994)
- [57] J. C. Collins, D. E. Soper, G. Sterman, Nucl. Phys. B261, 104 (1985), and Nucl. Phys. B308, 833 (1988); G. Bodwin, Phys. Rev. D31, 2616 (1985), and Phys. Rev. D34, 3932 (1986)
- [58] F. I. Olness, S. T. Riemersma Phys. Rev. **D51**, 4746 (1995)
- [59] S.J. Brodsky, P. Hoyer, C. Peterson and N. Sakai, Phys. Lett. B93, (451) 1980;
 S.J. Brodsky, C. Peterson and N. Sakai, Phys. Rev. D23, 2745 (1981).
- [60] H. Baer, J. Ohnemus, J.F. Owens, Phys. Rev. D46, 2844 (1989).

- [61] H1 Collab., I. Abt et al., Nucl. Instr. and Meth. A386, (310) 1997.
- [62] H1 Collab., I. Abt et al., Nucl. Instr. and Meth. A386, (348) 1997.
- [63] ZEUS Collab., M. Derrick et al., Phys. Lett. B293, 465 (1992); Z. Phys. C63, 391 (1994); A. Caldwell, Proc. ICHEP 92, Dallas 1992, ed. J. R. Sanford, vol. II, p. 1856.
- [64] C. Adloff et al. (H1 Collab.), Z.Phys. C72, 593 (1996).
- [65] M. Derrick et al. (ZEUS Collab.), Phys. Lett. B349, 225 (1995); M. Derrick et al. (ZEUS Collab.), XXVIII Int. Conf. on HEP '96, Warsaw (1996); J. Breitweg et al. (ZEUS Collab.), Phys. Lett. B407, 402 (1997).
- [66] W. Press, S. Teukolsky, W. Vetterling, B. Flannery, Numerical recipes in C, Cambridge University Press, 1992.
- [67] M. Cacciari and M. Greco, Phys. Rev. D55, 7134 (1997); M. Cacciari, M. Greco,
 S. Rolli, A.Tanzini, Phys. Rev. D55, 2736 (1997); M. Cacciari, M. Greco, Z.
 Phys. C69, 459 (1996).
- [68] J.C. Collins, Wu-Ki Tung, Nucl. Phys. B278, 934 (1986).
- [69] E. Hoffmann and R. Moore, Z. Phys. C20, 71 (1983).
- [70] R. Akers et al. (OPAL Collab.), Z. Phys. C67, 27 (1995).
- [71] C. Peterson, D. Schlatter, I. Schmitt, and P.M. Zerwas, *Phys. Rev.* **D27**, 105 (1983).
- [72] J. Chrin, Z. Phys. C36, 163 (1987).
- [73] M. Cacciari and M. Greco, Phys. Rev. D55, 7134 (1997).
- [74] J. Binnewies, B.A. Kniehl, and G. Kramer, Z. Phys. C76, 677 (1997).
- [75] A. Prinias, F_2^c , F_L and gluon determination at HERA, Talk given at International Europhysics Conference on High Energy Physics, 1997.